Fakultät für Medizin

II. Medizinische Klinik und Poliklinik

Klinikum rechts der Isar

Analysis of Ras effector pathways in pancreatic cancer progression and maintenance

Christian Veltkamp

Vollständiger Abdruck der von der Fakultät für Medizin der Technischen Universität München zur Erlangung des akademischen Grades eines

Doctor of Philosophy (Ph.D.)

genehmigten Dissertation.

Vorsitzende: Univ.-Prof. Agnes Görlach

Betreuer/in: apl. Prof. Dieter K. M. Saur

Prüfer der Dissertation:

1. Priv.-Doz. Dr. Günter Schneider

2. Priv.-Doz. Dr. Philipp J. Jost

3. Univ.-Prof. Rainer Glaß

Die Dissertation wurde am 11.07.2016 bei der Fakultät für Medizin der Technischen Universität München eingereicht und durch die Fakultät für Medizin am 20.09.2016 angenommen.

Table of contents

List of Tables

List of Figures

List of abbreviations

°C	degree Celsius
4-OHT	4-hydroxytamoxifen
AB	alcian blue
ADM	acinar-to-ductal-metaplasia
AFL	atypical flat lesion
AFN	atipamezole, flumazenil, naloxone
amp	ampicillin
ANOVA	analysis of variance
APS	ammonium persulphate
ATF	activating transcription factor
BLI	bioluminescence imaging
bp	base pair
BSA	bovine serum albumin
CDKN2A	cyclin-dependent kinase inhibitor 2A
cDNA	complementary deoxyribonucleic acid
Cers	ceramide synthase
CNV	copy number variation
COSMIC	catalogue of somatic mutations in cancer
CREB	cyclic AMP responsive element binding
CT	computed tomography
CypA	cyclophilin
Da	Dalton
DDR	DNA damage response
DMEM	Dulbecco´s modified Eagle medium
DMSO	dimethylsulfoxide
DNA	deoxyribonucleic acid
dNTP	deoxynucleoside triphosphate
DRS	dual-recombinase system
DTT	dithiothreitol
EDTA	ethylenediaminetetraacetic acid
Elas	elastase
ELISA	enzyme-linked immunosorbent assay
EMT	epithelial mesenchymal transition
ERK	extracellular signal-related kinase

EtOH	ethanol
EV	empty vector
F18-FDG	fluorine-18-2-fluoro-2-deoxy-D-glucose
Fbp2	fructose-1,6-bisphophatase isozyme 2
FCS	fetal calf serum
FDR	false discovery rate
FISH	fluorescence *in situ* hybridisation
FOLFIRINOX	folinic acid, fluorouracil, irinotecan, oxaliplatin
FOXO	forkhead box O protein
FSF	*frt*-stop-*frt*
FTI	farnesyltransferase inhibitor
g	gram
GAP	GTPase-activating protein
GEF	guanine nucleotide exchange factor
GEMM	genetically engineered mouse model
GSEA	gene set enrichment analysis
GSK3	glycogen synthase kinase 3
h	hour
H&E	hematoxylin and eosin
HDAC	histone deacetylase
HEK	human embryonic kidney
Hmgcr	3-hydroxy-3-methylglutaryl CoA reductase
i.p.	intraperitoneal
IAP	inhibitor of apoptosis protein
IHC	immunohistochemistry
IKKε	inhibitory κB kinase epsilon
IPMN	intraductal papillary mucinous neoplasm
kb	kilo base pair
KO	knock-out
Kras	v-Ki-ras2 Kirsten rat sarcoma viral oncogene homolog
L	liter
LB	Luria Broth Bertani
Ldha	lactate dehydrogenase A
LOH	loss of heterozygosity
LSL	*loxP*-stop-*loxP*
M	molar
MALDI	matrix-assisted laser desorption/ionization

MAPK	mitogen-activated protein kinase
MCN	mucinous cystic neoplasm
MDCT	multi-detector CT
mg	milligram
min	minute
mL	milliliter
mm	millimeter
mM	millimolar
MMF	midazolam, medetomidine, fentanyl
MRI	magnetic resonance imaging
mRNA	messenger ribonucleic acid
mTOR	mammalian target of rapamycin
MTT	3-(4,5-dimethyl-2-thiazolyl)-2,5-diphenyl-tetrazolium bromide
MW	molecular weight
nab	nanoparticle albumin-bound
ng	nanogram
NGS	next generation sequencing
nm	nanometer
nM	nanomolar
Nrf2	nuclear erythroid 2-related factor
NSCLC	non small cell lung cancer
OD	optical density
OXPHOS	oxidative phosphorylation
PAGE	polyacrylamide gel electrophoresis
PanIN	pancreatic intraepithelial neoplasia
Parp	poly (ADP-ribose)-polymerase
PBS	phosphate buffered saline
PCR	polymerase chain reaction
PDAC	pancreatic ductal adenocarcinoma
PDEδ	phosphodiesterase delta
PDK1	3-phosphoinositide-dependent protein kinase 1
Pdx1	pancreatic and duodenal homeobox 1
PET	positron emission tomography
Pfkl	phosphofructokinase, liver isoform
PH	pleckstrin homology
PI3K	phosphoinositide 3-kinase
PIP_2	phosphatidylinositol 4,5-bisphosphate

PIP_3	phosphatidylinositol 3,4,5-trisphosphate
PPP	pentose phosphate pathway
PTEN	phosphatase and tensin homolog
Ptf1a	pancreas transcription factor subunit alpha
PVDF	polyvinylidene fluoride
qRT-PCR	quantitative real time PCR
R26	*Rosa26*
RB	retinoblastoma
RNA	ribonucleic acid
ROI	region of interest
ROS	reactive oxygen species
rpm	revolutions per minute
rRNA	ribosomal ribonucleic acid
RT	room temperature
RTK	receptor tyrosine kinase
rtTA	reverse tetracycline transactivator
SEM	standard error of mean
SD	standard deviation
SDS	sodium dodecyl sulphate
SH2	Src homology 2
Skp2	S-phase kinase-associated protein 2
S.O.C.	Super Optimal Broth with catabolite repression
SUV	standardized uptake value
TAE	tris-acetate-EDTA
TAM	tamoxifen
TBST	tris-buffered saline tween-20
TCA	tricarboxylic acid
TE	tris-EDTA buffer
TEMED	N,N,N',N'-tetramethylethylenediamine, 1,2-bis(dimethylamino)-ethane
Tnc	tenascin C
TP53 / Trp53	transformation related protein 53
tTA	tetracycline transactivator
U	unit of enzyme activity
Ubr1	ubiquitin protein ligase E3 component N-recognin 1
UV	ultraviolet
V	volt
WB	western blot

WT	wild type
w/v	weight per volume
µg	microgram
µL	microliter
µm	micrometer
µM	micromolar

1 Abstract

Genetically engineered mouse models (GEMM) have dramatically improved our understanding of tumor evolution and therapeutic resistance. However, sequential genetic manipulation of gene expression is almost impossible using traditional Cre/*loxP*-based models. Our group has developed an inducible dual-recombinase system (DRS) by combining Flp/*frt* and Cre/*loxP* to improve GEMMs of pancreatic cancer. This enables investigation of multi-step carcinogenesis and genetic validation of therapeutic targets in autochthonous tumors on a genome-wide scale. Recently, we showed that cell-autonomous PI3K and Pdk1 are key effectors of oncogenic Kras in the pancreas, mediating formation of pancreatic intraepithelial neoplasia (PanIN) and pancreatic ductal adenocarcinoma (PDAC). *Pdk1* deletion blocked pancreatic carcinogenesis completely in a traditional Cre/*loxP*-based model, indicating its importance in tumor initiation. Here, I used the novel inducible DRS to investigate the role of Pdk1 during PDAC progression and maintenance *in vitro* and *in vivo*. I showed that secondary genetic targeting of *Pdk1* efficiently impaired PanIN progression *in vivo* and PDAC maintenance *in vitro* and *in vivo*, thereby validating Pdk1 as a promising target for therapeutic PDAC interventions. Transcriptomic and metabolic analyzes indicated that Pdk1 serves an important role in controlling tumor metabolism, at least partially through stimulation of glucose uptake. Although PDAC cells showed a marked response towards *Pdk1* deletion, a subpopulation of cancer cells survived *Pdk1* inactivation giving rise to resistant clones. My data thus indicate that a therapeutic strategy of optimized combination therapies is needed to combat pancreatic cancer.

The Raf/Mek/Erk signaling cascade presents another important Kras effector pathway, which is involved in pancreatic tumorigenesis. In this work, the role of the two Mek kinases Mek1 and Mek2 in PDAC formation and maintenance was studied using GEMMs. I demonstrated that *Mek1* deletion does not block PDAC initiation. Elimination of *Mek1* and *Mek2* inhibited growth of PDAC cell lines *in vitro*.

2 Zusammenfassung

Die Verwendung von genetisch veränderten Mausmodellen hat zu einem deutlich besseren Verständnis von Tumorentstehung und Therapieresistenz geführt. Allerdings sind sequentielle genetische Manipulationen von Genen in den klassischen Cre/*loxP*-basierten Systemen kaum möglich. Um dieses Problem zu umgehen, wurde in unserer Gruppe ein induzierbares Mausmodell zur Untersuchung des duktalen Adenokarzinoms des Pankreas (PDAC) entwickelt. Dabei wurden das Flp/*frt*- und das Cre/*loxP*-System kombiniert. Dies ermöglicht die Analyse der schrittweisen Karzinogenese und die genetische Validierung von therapeutischen Zielen in Tumoren auf genomweiter Ebene. Kürzlich konnten wir zeigen, dass zell-autonomes PI3K und Pdk1 wichtige Effektoren von onkogenem Kras im Pankreas darstellen, welche die Bildung von intraepithelialen Neoplasien (PanIN) und PDAC vermitteln. Die Deletion von *Pdk1* blockt die Karzinogenese im Pankreas in einem Cre/*loxP*-basierten Modell vollständig, wodurch die Bedeutung von Pdk1 für die Tumorinitiation unterstrichen wird. In dieser Arbeit wurde das neue induzierbare Rekombinationssystem verwendet, um die Rolle von Pdk1 in der PDAC-Progression und -Aufrechterhaltung *in vitro* und *in vivo* zu untersuchen. Ich konnte zeigen, dass eine sekundäre genetische Inaktivierung von *Pdk1* die PanIN-Progression *in vivo* blockt und die PDAC-Aufrechterhaltung *in vitro* und *in vivo* effizient hemmt und somit Pdk1 als aussichtsreiches Ziel für therapeutische Interventionen im PDAC validieren. Transkriptom-Untersuchungen und metabolische Analysen deuten darauf hin, dass Pdk1 eine wichtige Rolle in der Kontrolle des Tumormetabolismus spielt, indem es unter anderem die Aufnahme von Glukose stimuliert. Obwohl PDAC-Zellen eine deutliche Reaktion auf eine *Pdk1*-Deletion zeigten, konnte eine Subpopulation die *Pdk1*-Inaktivierung überleben und resistente Klone bilden. Meine Daten weisen somit darauf hin, dass eine therapeutische Strategie von optimierten Kombinationstherapien nötig sein wird, um das Pankreaskarzinom zu bekämpfen.

Die Raf/Mek/Erk-Signalkaskade stellt einen weiteren wichtigen Kras-Effektorsignalweg dar, der in der Tumorigenese des Pankreas von Bedeutung ist. In dieser Arbeit wurde die Rolle der beiden Mek-Kinasen Mek1 und Mek2 in der PDAC-Bildung und -Aufrechterhaltung mittels GEMMs untersucht. Ich zeigte, dass durch die Deletion von *Mek1* die Bildung von PDAC nicht gehemmt wird. Die gleichzeitige Eliminierung von *Mek1* und *Mek2* reduzierte das Wachstum von PDAC-Zelllinien *in vitro*.

3 Introduction

3.1 Pancreatic ductal adenocarcinoma (PDAC)

Pancreatic ductal adenocarcinoma (PDAC) is the predominant form of pancreatic cancer accounting for around 90% of all pancreatic tumors. The remaining cases comprise neuroendocrine tumors, which are derived from the hormone-producing cells of the pancreas, or rare exocrine tumors like acinar cell carcinoma. PDAC is mainly diagnosed at a late stage, because patients remain asymptomatic until tumors reach an advanced stage which is already characterized by distant metastases and resistance to chemotherapy and radiotherapy. Therefore, the prognosis for PDAC patients is devastating and has not changed significantly within the last 30 years with the 5-year survival remaining at only 6% in the United States (Siegel et al., 2014).

On the contrary, death rates of other solid tumor entities like colon cancer have declined due to improved screening and treatment regimens. For this reason, PDAC is predicted to be the second leading cause of cancer-related death in 2030 (Rahib et al., 2014). Established risk factors for PDAC are specific inherited disorders like Peutz-Jeghers syndrome (Giardiello et al., 2000; Iqbal et al., 2012; Jones et al., 2009; Kastrinos et al., 2009; Rebours et al., 2008; Vasen et al., 2000), chronic pancreatitis (Duell et al., 2012), smoking (Bosetti et al., 2012), diabetes mellitus (Ben et al., 2011) and obesity (Aune et al., 2012). However, no appropriate standard screening procedure for high risk patients is available nowadays.

Since 1997 gemcitabine has been the standard care for metastatic pancreatic cancer (Burris et al., 1997). Recently, single-agent gemcitabine treatment was replaced by combination chemotherapy. In one clinical study, FOLFIRINOX (folinic acid, fluorouracil, irinotecan, oxaliplatin) showed a significant prolongation of overall survival and improved quality of life compared to gemcitabine alone (Conroy et al., 2011). A second trial could demonstrate a similar advantage of combination of gemcitabine with nanoparticle albumin-bound paclitaxel (nab-paclitaxel) over single-agent gemcitabine (Von Hoff et al., 2013). However, the median survival in these studies was only prolonged for 4.3 and 1.8 months in the FOLFIRINOX and gemcitabine plus nab-paclitaxel, respectively. So there is an urgent need to find better treatment options.

3.2 Pancreatic cancer progression model

Different PDAC precursors have been described: pancreatic intraepithelial neoplasia (PanIN), mucinous cystic neoplasm (MCN) and intraductal papillary mucinous neoplasm (IPMN). The most common progression model is based on PanIN lesions graded 1A, 1B, 2

and 3 leading to invasive PDAC (Hruban et al., 2000). Activating mutations of the oncogene *KRAS* are the major genetic hallmark of PDAC. Recent genome sequencing studies have revealed that activating mutations of the *KRAS* oncogene are present in > 90% of low grade and high grade PanINs (Kanda et al., 2012) and invasive PDAC (Biankin et al., 2012; Jones et al., 2008) supporting the role of KRAS as an early and initiating event in PDAC formation. PanIN-1A lesions are ductal structures characterized by a flat epithelium consisting of columnar cells with basally located nuclei. In contrast, lesions of grade 1B display a papillary epithelium. *KRAS* mutations are followed by inactivating mutations of the tumor suppressor gene cyclin-dependent kinase inhibitor 2A (*CDKN2A*), encoding for $p16^{Ink4a}$ and $p14^{Arf}$ ($p19^{Arf}$ in mice), which can be detected already in these low-grade PanINs. Lesions harboring nuclear abnormalities like loss of polarity or enlarged nuclei are classified as PanIN-2. When increased cytologic disorganization and cribriforming luminal necrosis can be detected, lesions present as carcinoma *in situ* (grade 3) which can transform into invasive PDAC. In these stages inactivation of the tumor suppressor genes *TP53* and *SMAD4* is observed. Although most of the PanINs have *KRAS* mutations, only a small percentage of cells creating a lesion is mutated. The concentration of mutated *KRAS* per PanIN increases during PDAC progression (Kanda et al., 2012). PDAC is characterized by a strong degree of chromosomal instability (Harada et al., 2008; Jones et al., 2008; Kimmelman et al., 2008). Recent genome and whole-exome sequencing studies as well as transcriptomic analysis revealed that human PDAC specimens show a high heterogeneity and patients can be classified according to different molecular subtypes (Bailey et al., 2016; Biankin et al., 2012; Collisson et al., 2011). Identification of these groups provides fundamental implications for future PDAC treatments. In addition to the well-established genes *KRAS, CDKN2A*, *TP53*, SMAD4 and *TGFBR2*, the chromatin modifiers *EPC1* and *ARID2* and the DNA damage repair gene *ATM* were significantly mutated in human PDAC samples. Surprisingly, genes of the SLIT/ROBO signaling pathway involved in regulating axonal guidance play an important role in PDAC tumorigenesis (Bailey et al., 2016; Biankin et al., 2012).

More recently, new precursors for PDAC have been identified. Despite the ductal phenotype, there is evidence that pancreatic ducts are not the cells of origin for PDAC. In a process termed acinar-to-ductal-metaplasia (ADM), oncogenic Kras induces transdifferentiation of acinar cells to a ductal-like phenotype. ADM precedes PanIN formation, suggesting that it is an early event in PDAC development. Moreover, persistent ADM is a characteristic of chronic pancreatitis and is frequently associated with PanINs in PDAC patients. Therefore, acinar plasticity via ADM is considered as preneoplastic event in PDAC formation (Morris et al., 2010; Pinho et al., 2011; Shi et al., 2009). Atypical flat lesions (AFLs), tubular structures with enlarged nuclei arising in ADM regions, are proposed to present an additional precursor lesion for PDAC. AFLs are surrounded by a cellular and fibrous stroma and are found in

patients with familial history of PDAC and in mouse models with increasing occurrence in an age-dependent manner (Aichler et al., 2012).

3.3 Oncogenic KRAS

In humans, the three *RAS* genes *HRAS*, *KRAS* and *NRAS* encode four ~21 kDa small GTPases. KRAS4A and KRAS4B, the predominant variant in the pancreas, are derived from the *KRAS* gene by alternative splicing. RAS proteins cycle between an inactive GDP-bound state and an active GTP-bound state (Bourne et al., 1990; Field et al., 1987; Wittinghofer and Pai, 1991). The transition between these conformations is mediated by guanine nucleotide exchange factors (GEFs), which stimulate activation of RAS by facilitating the exchange from GDP to GTP (Wolfman and Macara, 1990), and by GTPase-activating proteins (GAPs), which promote RAS-mediated GTP hydrolysis and thus inactivation (Trahey and McCormick, 1987). The most commonly found *KRAS* mutations in human cancers are single point mutations at residues glycine 12 (G12), G13 and glutamine 61 (Q61) (Catalogue of Somatic Mutations in Cancer (COSMIC) database). 98% of *KRAS* mutations in PDAC occur at codon 12, leading to a G to aspartic acid (D) substitution ($Kras^{G12D}$) in the majority of cases, followed by a G to valine (V) exchange ($Kras^{G12V}$). Oncogenic substitutions of G12 or G13 compromise the ability of the RAS protein to hydrolyse GTP to GDP by preventing the formation of van der Waals interactions between RAS and GAPs through sterical hindrance (Scheffzek et al., 1997). Mutations of Q61 interfere with the coordination of a water molecule and thereby impair GTP hydrolysis and lock the RAS protein in an active state (Buhrman et al., 2010; Scheidig et al., 1999). Subsequently, a plethora of downstream signaling pathways is constitutively activated.

3.4 Kras-driven mouse models for pancreatic cancer

Since *KRAS* mutations occur in nearly all PanIN lesions and PDAC, genetically engineered mouse models (GEMMs) driven by oncogenic Kras have been created to mimic human pancreatic cancer. These GEMMs are based on a latent oncogenic $Kras^{G12D}$ allele silenced by a *loxP*-stop-*loxP* (*LSL*) cassette as a knock-in at the endogenous locus (*LSL-*$Kras^{G12D}$ mouse line) (Jackson et al., 2001). Pancreatic and duodenal homeobox 1-Cre (*Pdx1-Cre*) (Gannon et al., 2000) or Pancreas specific transcription factor, 1a-Cre (*Ptf1a-Cre*) (Nakhai et al., 2007) are used to achieve conditional activation of oncogenic Kras in the pancreas by Cre-mediated recombination of the *LSL* cassette. Pdx1 is expressed at embryonic day E8.5 (Offield et al., 1996), Ptf1a at E9.5 (Kawaguchi et al., 2002). Both Cre driver lines direct recombination in pancreatic acini, ducts and islets. However, *Pdx1-Cre* is also expressed in the bile duct, duodenum and stomach, while *Ptf1a-Cre* expression is also detectable in the

brain and the retina. *Pdx1-Cre;LSL-Kras$^{G12D/+}$* and *Ptf1a$^{Cre/+}$;LSL-Kras$^{G12D/+}$* mice develop PanINs as well as PDAC with a long latency and in 40% of tumor mice lung and liver metastasis are found. According to the PDAC progression model, the frequency and the grade of the lesions increase with aging (Eser et al., 2013; Hingorani et al., 2003; Schönhuber et al., 2014).

In order to address the effect of an additional *Trp53* mutation on PDAC progression, a conditionally expressed gain of function *Trp53^{R172H}* allele, the mouse ortholog of the *TP53^{R175H}* mutation in human Li-Fraumeni syndrome, was generated (Olive et al., 2004). *Pdx1-Cre;LSL-Kras$^{G12D/+}$;LSL-Trp53$^{R172H/+}$* mice display accelerated PanIN formation and invasive, metastatic PDAC with genomic instability (Hingorani et al., 2005). Other studies revealed that deficiencies of p53, Ink4a and Smad4 cooperate with oncogenic Kras to accelerate development of PDAC by using *Trp53$^{lox/lox}$*, *CDKN2A$^{lox/lox}$* and *Smad4$^{lox/lox}$* mice, respectively (Aguirre et al., 2003; Bardeesy et al., 2006a; Bardeesy et al., 2006b). Formation of IPMNs was observed in *Ptf1a$^{Cre/+}$;LSL-Kras$^{G12D/+}$;Smad4$^{lox/lox}$* mice.

To summarize, pancreas-specific expression of oncogenic Kras in GEMMs is sufficient to initiate murine PanIN and metastatic PDAC formation.

PDAC is not a paediatric disease and develops in adults due to sporadic mutations which occur rather in specific cell types than in the entire pancreas. To address these limitations of the described PDAC models, the group of Mariano Barbacid employed an inducible tet-off-system based on the *Elastase* (*Elas*) promoter which is specific for the pancreatic acinar lineage. Untreated *Elas-tTa;tetO-Cre;LSL-Kras$^{G12V/+}$* mice form PanIN lesions and PDAC confirming that acinar cell plasticity via ADM is involved in PDAC tumorigenesis. However, in the presence of doxycycline, binding of the tetracycline transactivator (*tTA*) to *tetO* sequences is inhibited and thus Kras^{G12V} expression is prevented. By feeding doxycycline to pregnant females and their new-born mice until day P60, Kras^{G12V} could be turned on in adult mice. Strikingly, only under conditions of chronic pancreatitis PanINs and PDAC are induced demonstrating that Kras alone is not capable of transforming adult acinar cells (Guerra et al., 2007). Recently, two groups analyzed the role of Kras oncogene addiction of PDAC cells by using a *Ptf1a$^{Cre/+}$;R26-LSL-rtTA-IRES-EGFP;tetO-LSL-Kras$^{G12D/+}$* mouse model. In the pancreas the *LSL* cassette preceding the reverse tetracycline transactivator (*rtTa*) *IRES-EGFP* construct is recombined (Belteki et al., 2005) leading to expression of rtTa and EGFP. Upon administration of doxycycline, rtTA is activated resulting in Kras^{G12D} induction which can be reverted by doxycycline withdrawal. Thereby, Kras^{G12D} can be turned off at different stages of tumorigenesis. Inactivation of oncogenic Kras resulted in cell death and redifferentiation of PanIN lesions into acinar cells and regression of established tumors (Collins et al., 2012a; Ying et al., 2012). These studies indicate that oncogenic Kras is

required for PDAC maintenance. Furthermore, sustained oncogenic Kras signaling was shown to be necessary for maintenance of metastases (Collins et al., 2012b).

Classical Cre/*loxP* based GEMMs of PDAC harbor the major limitation that they rely on a single Cre recombination step to activate or delete genes in the pancreas. Consequently, they do not allow modelling of multi-step PDAC tumorigenesis, manipulation of the tumor microenvironment and genetic validation of potential therapeutic drug targets in established tumors. For this reason, a dual-recombinase system (DRS) was created in our lab by combining both the Flp/*frt* and Cre/*loxP* recombination system. A transgenic *Pdx1-Flp* line was constructed to activate expression of an *frt*-stop-*frt* (*FSF*) silenced oncogenic $Kras^{G12D}$ allele ($FSF\text{-}Kras^{G12D/+}$) from its endogenous locus in the pancreas. $Pdx1\text{-}Flp;FSF\text{-}Kras^{G12D/+}$ mice form PanIN lesions which progress with long latencies to PDAC (Schönhuber et al., 2014), similarly to the established Cre/*loxP* based $Kras^{G12D}$-driven PDAC models (Hingorani et al., 2003). To subsequently manipulate Flp-recombined cells with the Cre/*loxP* system, a latent tamoxifen-inducible $CreER^{T2}$ allele, silenced by an *FSF* cassette, under the control of the strong *CAG* promoter was generated as a knock-in at the *Rosa26* locus ($FSF\text{-}R26^{CAG\text{-}CreERT2/+}$). By tamoxifen application the system allows time-specific genetic manipulation, which can be applied during PanIN progression or after invasive tumors have developed (Schönhuber et al., 2014).

GEMMs of PDAC phenocopy numerous aspects of human PDAC emphasising the role of oncogenic Kras for tumor initiation and maintenance and provide insights into the biology of this fatal disease and might decipher potential drug targets to combat PDAC.

3.5 KRAS downstream effector pathways

Its central role in PDAC places oncogenic KRAS at the top of the list of potential therapeutic targets. Since post-translational modifications promote membrane association of the KRAS protein and thus augment KRAS signaling, first attempts were focussed on inhibiting them leading to the development of farnesyltransferase inhibitors (FTIs). Despite promising results *in vitro* and in PDAC xenografts (Omer and Kohl, 1997), the FTI tipifarnib failed in a phase III clinical trial (Van Cutsem et al., 2004), probably due to compensation of geranylgeranyl transferases preserving Ras activity (Lerner et al., 1997). Although a plethora of approaches has been tested to pharmacologically block Kras, none of them could be successfully transitioned into the clinic, so that KRAS is widely considered as undruggable. However, in 2013 oncogenic Kras signaling was impaired by a small molecule inhibiting the interaction of KRAS and phosphodiesterase delta (PDEδ) which is required for enrichment of RAS at the cell membrane. The advantage over FTIs could be that the inhibition is not bypassed by

alternative lipidation mechanisms (Zimmermann et al., 2013). Future clinical studies have to address whether this approach can serve as effective treatment in human PDAC.
Instead of targeting Kras itself, another approach is to elucidate relevant signaling molecules mediating the oncogenic effects of KRAS in PDAC that might serve as targets for therapeutic interventions.
Numerous KRAS effector pathways have been described including RAF/MEK/extracellular signal-related kinase (ERK), phosphoinositide 3-kinase (PI3K)/3-phosphoinositide dependent protein kinase-1 (PDK1)/AKT, RalGEFs and the Rho-family GTPase Rac. Raf/Mek/Erk and PI3K signaling are the two pathways that have been studied most extensively in PDAC.

3.5.1 The RAF/MEK/ERK pathway

The Raf/MEK/ERK pathway, also known as mitogen-activated protein kinase (MAPK) pathway, was the first identified Ras effector cascade (Moodie et al., 1993; Vojtek et al., 1993; Warne et al., 1993; Zhang et al., 1993). Raf proteins (Araf, Braf, Craf) bind to Ras-GTP and thus they are recruited to the plasma membrane to be activated by different protein kinases (Marais et al., 1998; Marais et al., 1995). Subsequently, the serine/threonine kinase Raf phosphorylates and activates MEK1/2 which in turn activate ERK1/2 by phosphorylation (Crews and Erikson, 1993).
Ablation of both Mek or Erk kinases blocked formation of non small cell lung cancer (NSCLC) in a $Kras^{G12V}$-driven mouse model. Furthermore, it was shown that Craf was essential for NSCLC development (Blasco et al., 2011). In contrast to this finding, *Craf* elimination failed to block $Kras^{G12D}$-driven PDAC formation, rendering Craf dispensable for PDAC tumorigenesis (Eser et al., 2013). These observations emphasize the tissue specificity of Kras downstream signaling. PanIN lesions and PDAC are characterized by active MAPK signaling and it was demonstrated that maintenance of Erk activation is necessary for pancreatic tumorigenesis by Mek inhibition in $Ptf1a^{Cre/+};LSL\text{-}Kras^{G12D/+}$ mice (Ardito et al., 2012). Another group used an inducible $Pdx1\text{-}CreER^{T2}$ mouse model to express oncogenic $Braf^{V600E}$ in the pancreas upon tamoxifen administration leading to formation of PanIN lesions. Furthermore, $Braf^{V600E}$ was shown to cooperate with the oncogenic *Trp53* mutation $Trp53^{R270H}$ in the development of metastatic PDAC indicating the functional relevance of constitutive MAPK activation during PDAC tumorigenesis (Collisson et al., 2012).

3.5.2 The PI3K pathway

The PI3K family comprises heterodimeric lipid kinases containing catalytic and regulatory subunits. PI3K signaling is involved in a plethora of cellular processes like adhesion, apoptosis, cell growth, proliferation and survival. The catalytic subunits of the class I PI3Ks,

called p110α, p110β, p110γ and p110δ, are encoded by *PIK3CA*, *PIK3CB*, *PIK3CG* and *PIK3CD*, respectively. p110α, p110β are ubiquitously expressed, whereas the other two isoforms are mainly found in leukocytes.

PI3K can be activated by three different ways: Generally, a ligand binds to a receptor tyrosine kinase (RTK) which leads to dimerization of the receptor and autophosphorylation of the tyrosine residues. Thus, they can interact with Src homology 2 (SH2) domain containing molecules (Schlessinger, 2002).

1) In the first setting, the regulatory p85 subunit directly binds to a specific phospho-motif within the RTK (Domchek et al., 1992) to trigger activation of the catalytic p110 subunit.
2) In the second alternative, the adaptor protein Grb2 binds to another phospho-motif of the RTK (Pawson, 2004) and to the scaffolding protein Gab which consequently activates p85.
3) The third activation pathway occurs independently of p85 and involves RAS. Grb2 binds SOS which in turn activates RAS. Subsequently, p110 is activated by RAS (Ong et al., 2001).

Upon activation, PI3K converts phosphatidylinositol 4,5-bisphosphate (PIP_2) to phosphatidylinositol 3,4,5-triphosphate (PIP_3). This reaction is counteracted by the tumor suppressor phosphatase and tensin homolog (PTEN), which leads to termination of PI3K signaling. The second messenger PIP_3 binds to proteins containing pleckstrin homology (PH) domains (Cantley, 2002) and thereby recruits 3-phosphoinositide-dependent protein kinase 1 (PDK1) and AKT to the plasma membrane. Mammalian cells express three highly similar AKT isoforms (AKT1, AKT2 and AKT3). Located in close vicinity, PDK1 phosphorylates AKT at the residue threonine 308 resulting in AKT activation and downstream signaling (Alessi et al., 1997; Currie et al., 1999; Majumder and Sellers, 2005). PI3K-AKT signaling mediates survival, cell growth and metabolism by several mechanisms. Among others, AKT negatively regulates glycogen synthase kinase 3 (GSK3), the forkhead family of transcription factors (FOXOs) and TSC2 by phosphorylation. Furthermore, it inhibits the proapoptotic Bcl-2 family members BAD and BAX and NF-kB signaling resulting in upregulation of prosurvival inhibitor of apoptosis (IAP) genes (Cantley, 2002; Duronio, 2008; Engelman et al., 2006).

Mammalian target of rapamycin (mTOR) plays an essential role in regulating cell growth and metabolism by monitoring cellular energy levels and nutrient availability. mTOR exists in two distinct complexes: mTORC1 and mTORC2.

mTORC1 consists of mTOR, regulatory associated protein of mTOR (Raptor), proline-rich AKT substrate 40 kDa (PRAS40) and mLST8/GbL. mTORC2 is composed of mTOR, rapamycin insensitive companion of mTOR (Rictor), mammalian stress-activated protein kinase interacting protein 1 (mSIN1) and mLST8/GbL (Sabatini, 2006; Wullschleger et al.,

2006). Upon PI3K/AKT activation, mTORC1 signals via the downstream effectors p70 ribosomal S6 kinase (S6K) and 4E-binding protein 1 (4E-BP1) leading to increased protein synthesis, whereas in the mTORC2 complex, mTOR phosphorylates AKT at serine 473 (S473) (Sarbassov et al., 2005). Both phosphorylation events, T308 by PDK1 and S473 by mTOR, are required for complete AKT activation (Alessi et al., 1997; Stephens et al., 1998). Apart from AKT, PDK1 can activate p90 ribosomal S6 kinase (RSK), serum/glucocorticoid regulated kinase (SGK), protein kinase C (PKC) and S6K proteins by the PIF-pocket domain (Bayascas et al., 2008).

Aberrant PI3K signaling is a common feature of cancer (Engelman et al., 2006; Samuels et al., 2004; Thomas et al., 2007). Breast, endometrial, bladder and colorectal cancer present with high rates of PIK3CA mutations (COSMIC database) which are most frequently observed in three hotspots: H1047R in the kinase domain, E542K and E545 K in the helical domain (Samuels et al., 2004). Although PI3K mutations are only found in 8% of PDAC samples (COSMIC database), PI3K/AKT signaling was shown to be constitutively activated in PDAC cell lines and a significant fraction of human PDAC specimens, whereas PTEN expression was often lost or reduced (Asano et al., 2004; Ying et al., 2011). Ablation of Pten in *Pdx1-Cre;LSL-Kras*$^{G12D/+}$ mice resulted in formation of aggressive PDAC and dramatically shortened survival. Moreover, array comparative genome hybridization analysis revealed that *PTEN* deletions or *AKT2* amplifications occur in one third of the analysed human PDAC samples (Ying et al., 2011).

Oncogenic *PIK3CA*^{H1047R} mutation in a *Ptf1a*$^{Cre/+}$-based mouse model faithfully recapitulated ADM, PanIN, PDAC and metastasis formation as observed in the classical *Ptf1*$^{Cre/+}$*;LSL-Kras*$^{G12D/+}$ model. Histology and survival time were highly comparable between the two systems (Eser et al., 2013). However, *PIK3CA*^{H1047R} was not sufficient to induce PanINs in a *Pdx1-CreER*^{T2} model upon tamoxifen application at day P14 (Collisson et al., 2012). These contradictory findings could result from distinct recombination efficiencies of the Cre lines and different target cells or different time points of PIK3CA^{H1047R} activation (E8.5 versus P14). Moreover, p110α^{H1047R} expression levels can vary because PIK3CA^{H1047R} was expressed from the endogenous locus in the study of Collisson and colleagues (Kinross et al., 2012) whereas Eser and colleagues used a knock-in of *LSL-PIK3CA*^{H1047R} into the *Rosa26* locus. The importance of PI3K signaling for Kras^{G12D}-driven tumor initiation was further supported by experiments deleting the PI3K effector Pdk1. Strikingly, genetic *Pdk1* ablation blocked Kras^{G12D}-driven pancreatic carcinogenesis completely. PanINs were absent and only signs of fatty degeneration due to oncogenic stress were observed in older animals. *Ptf1a*$^{Cre/+}$*;LSL-Kras*$^{G12D/+}$*;Pdk1*$^{lox/lox}$ animals displayed the same survival as wild type controls whereas heterozygous *Pdk1* deletion neither changed survival time nor PanIN and PDAC formation significantly compared to *Ptf1a*$^{Cre/+}$*;LSL-Kras*$^{G12D/+}$ mice (Eser et al., 2013).

Pharmacologic inhibition of Mek in PDAC models *in vitro* and *in vivo* resulted in reduced phosphorylation of Erk and decreased proliferation, however, the effect was mainly cytostatic. Moreover, increased phosphorylation of Akt was observed. Upon combination with PI3K, AKT or EGFR inhibitors, cell death was induced and the treatment efficiency was improved leading to significantly enhanced tumor inhibition (Alagesan et al., 2015; Collisson et al., 2012; Walters et al., 2013).

In addition to the pathways discussed above, PI3K can activate the Rho family GTPase Rac1, which is involved in actin cytoskeleton organization (Cantley, 2002). This process is important for cancer cells to obtain a migratory phenotype. Ablation of *Rac1* in *Ptf1a*$^{Cre/+}$*;LSL-Kras*$^{G12D/+}$ mice resulted in reduced PanIN and PDAC formation (Heid et al., 2011). However, expression of constitutively active Rac1 (*Rac1*^{G12V}) in the pancreas (Srinivasan et al., 2009) was insufficient to form ADM and PanINs (Eser et al., 2013).

The Ral guanine nucleotide exchange factor (RalGEF) proteins (RalGDS, RGL, RGL2, RGL3) present another Ras effector pathway by linking Ras proteins to the activation of the small GTPases RalA and RalB (D'Adamo et al., 1997). RalGDS was shown to be required for Ras-induced transformation *in vitro* and for carcinogenesis in a skin cancer mouse model (Gonzalez-Garcia et al., 2005). High levels of GTP-bound RalA and RalB were detected in human PDAC and were shown to mediate tumor growth and metastasis in cell lines, respectively (Lim et al., 2006).

The question arises whether distinct Ras effectors are responsible for the different stages during tumor development. It has been demonstrated that MAPK, PI3K and RalGEF signaling are necessary for initiation of tumor growth. However, only PI3K was shown to be sufficient for tumor maintenance in the absence of Ras (Lim and Counter, 2005).

3.6 Oncogenic KRAS alters PDAC metabolism

In the presence of oxygen, cells metabolize glucose to carbon dioxide by the oxidation of pyruvate via the tricarboxylic acid (TCA) cycle in mitochondria. NADH which is generated by the TCA cycle fuels the oxidative phosphorylation to produce maximal amounts of ATP per glucose molecule with minimal lactate production. On the contrary, Otto Warburg and colleagues observed that cancer cells mainly metabolize glucose to lactate, even in the presence of oxygen (Warburg, 1956). This phenomenon is known as Warburg effect. Although aerobic glycolysis is inefficient regarding ATP production, it provides rapidly proliferating cells with numerous glycolytic intermediates which can be used for macromolecule biosynthesis to generate new cells (Vander Heiden et al., 2009).

The hypovascular and desmoplastic tumor microenvironment results in hypoxia and limited nutrient availability forcing PDAC cells to reprogram metabolism to improve their nutrient acquisition and use.

Oncogenic Kras increases aerobic glycolysis in PDAC cells by altering the expression of the glucose transporter (Glut1) and many other glycolytic enzymes like Hk1, Hk2, Pfkl as well as Ldha which converts pyruvate to lactate. Subsequently, $Kras^{G12D}$ channels glucose intermediates into the hexosamine biosynthesis pathway and the non-oxidative arm of the pentose phosphate pathway (PPP) for protein glycosylation and nucleotide biosynthesis, respectively (Ying et al., 2012).

In order to replenish the TCA cycle, most tumor cells depend on the conversion of glutamine (Gln)-derived glutamate into α-ketoglutarate in the mitochondria by glutamate dehydrogenase. In contrast, PDAC cells rely on a different glutamine pathway to fuel the TCA cycle. Gln-derived aspartate is transported in the cytoplasm where it is metabolized to oxaloacetate by aspartate transaminase leading to generation of NADPH, an antioxidant mitigating cytotoxic reactive oxygen species (ROS) (Son et al., 2013). Moreover, $Kras^{G12D}$ is capable of inducing the transcription of nuclear factor erythroid 2-related factor (Nrf2), which regulates antioxidant signaling and ROS detoxification, and thereby maintains the redox state of the cancer cell and promotes tumorigenesis (DeNicola et al., 2011).

PDAC cell lines and primary tumors exhibit activated autophagy and high levels of this process correlate with poor patient outcome. Intracellular components are engulfed in modified membranes (so-called autophagosomes) and degraded in lysosomes. Autophagy is useful for detoxification and provides the cancer cell with ATP and intermediary metabolites. By inhibiting this process with chloroquine, the survival in a $Kras^{G12D}$-driven PDAC mouse model was significantly increased (Fujii et al., 2008; Yang et al., 2011). In addition to autophagy, oncogenic Kras directs scavenging of serum lipids and proteins by an endocytic process called macropinocytosis to obtain needed metabolites (Commisso et al., 2013).

Recently, it was demonstrated that PDAC can be classified into three different groups (glycolytic, lipogenic, slow proliferative) by metabolite profiling (Daemen et al., 2015). Cell lines of the glycolytic subtype correlating with the quasi-mesenchymal subtype are sensitive to glycolytic and glutamine inhibitors of the glucose and glutamine pathway whereas cells of the lipogenic subtype were associated with the epithelial subtype and responded to lipid synthesis inhibition (Collisson et al., 2011; Daemen et al., 2015). In order to target PDAC metabolism therapeutically, it is necessary to successfully stratify subgroups by diagnostics first.

3.7 Resistance towards PI3K inhibition

PIK3CA gain-of-function mutations are frequent events in human cancer, rendering PI3K an interesting target for cancer therapy (Fruman and Rommel, 2014; Hennessy et al., 2005; Luo et al., 2003). However, a major drawback of tumor therapy is the acquisition of resistance towards a therapeutic agent and consequently tumor relapse. In a functional screen in *S. cerevisiae* using a plethora of PI3K inhibitors, a drug-sensitizing mutation (L814C) and a potential hotspot for resistance mutations (I800) were identified. Surprisingly, no resistance mutations at the gatekeeper residues were observed (Zunder et al., 2008). Engelman and colleagues showed that PI3K associates with HER3 in NSCLC cells sensitive to the EGFR inhibitor gefitinib to activate PI3K/AKT signaling (Engelman et al., 2005). In a following study they demonstrated that initially sensitive NSCLC cells acquire resistance towards gefinitib by focal amplification of the RTK c-MET leading to HER3-dependent PI3K activation (Engelman et al., 2007). By use of a tetracycline-inducible PIK3CA^{H1047R}-driven breast cancer mouse model, oncogenic PI3K was shown to be essential for tumor maintenance. However, tumor regression upon doxycycline removal was followed by tumor relapse some months later in around two-thirds of the animals. Focal amplifications of *c-MET* and *c-MYC* were detected. c-MET activated PI3K pathway via HER3, as observed in previous works, whereas resistance is independent of activation of PI3K in tumors with *c-MYC* amplifications. Moreover, Myc elevation and PI3K mutations coexist in a considerable fraction of human breast cancer patients (Liu et al., 2011b).

Recently, it has been shown that resistance of NSCLC cells towards EGFR inhibitor therapy can either be caused by a small subpopulation of pre-existing resistant cells or evolve during treatment from originally tolerant cells (Hata et al., 2016). Since the sensitivity to detect rare mutations by next generation sequencing is limited to allele frequencies of around 0.1% (Robasky et al., 2014), a high complexity DNA barcode library was used to find resistant clones in initial cell populations.

3.8 Aim of this work

Previous work in our group provided evidence that the PI3K/Pdk1 axis is essential for PDAC initiation (Eser et al., 2013). By using DRS-based GEMM of human PDAC, the role of Pdk1 signaling for tumor progression and maintenance was investigated in this study to validate Pdk1 as a potential target for therapeutic intervention. Therefore, the *Pdx1-Flp;FSF-Kras$^{G12D/+}$;FSF-R26$^{CAGCreERT2/+}$;Pdk1$^{lox/lox}$* mouse model was employed, which allowed to inactivate Pdk1 at any time point during PanIN progression or in established tumors *in vivo* by administration of tamoxifen. For the first setting, histological analyzes and quantification of PanIN lesions were performed. In the second approach, tumor volume and metabolism were

measured by magnetic resonance imaging and positron emission tomography, respectively. In addition, mouse-derived primary cancer cells were generated for *in vitro* studies. The effect of *Pdk1* deletion on growth and colony formation of cell lines was assessed and downstream effectors and mechanisms mediating the *Pdk1*-knock-out (KO) phenotype were studied by immunoblotting and RNA sequencing. Functional validation was carried out by metabolic assays. Moreover, Pdk1-independent clones were generated and whole exome sequencing of the first clones was conducted to decipher potential resistance mechanisms of PDAC cells towards *Pdk1* deletion.

Furthermore, the impact of the Ras effectors Mek1 and Mek2 will be studied in PDAC initiation and maintenance. The effect of *Mek1* deletion on PDAC initiation will be studied in *Ptf1a*$^{Cre/+}$;*LSL-Kras*$^{G12D/+}$;*Mek1*$^{lox/lox}$ and *Ptf1a*$^{Cre/+}$;*LSL-PIK3CA*$^{H1047R/+}$;*Mek1*$^{lox/lox}$ mice by histological and survival analysis. Primary cell lines derived from *Pdx1-Flp;FSF-Kras*$^{G12D/+}$;*FSF-R26*$^{CAGCreERT2/+}$;*Mek1*$^{lox/lox}$;*Mek2*$^{\Delta/\Delta}$ tumor mice were generated and the role of Mek1 and Mek2 on PDAC maintenance was analyzed by clonogenic and growth assays *in vitro*.

4 Materials

4.1 Technical equipment

Table 1. Technical equipment.

Device	Source
96-well magnetic ring-stand	Applied Biosystems, Inc., Carlsbad, CA, USA
Analytical balance A 120 S	Sartorius AG, Göttingen
Analytical balance BP 610	Sartorius AG, Göttingen
Autoclave 2540 EL	Tuttnauer Europe B.V., Breda, The Netherlands
AxioCam HRc	Carl Zeiss AG, Oberkochen
AxioCam MRc	Carl Zeiss AG, Oberkochen
Bag sealer Folio FS 3602	Severin Elektrogeräte GmbH, Sundern
Centrifuge Avanti® J25	Beckman Coulter GmbH, Krefeld
Centrifuge Rotina 46R	Andreas Hettich GmbH & Co. KG, Tuttlingen
Charge-coupled device camera equipped with an image intensifier OrcaII ER	Hamamatsu Photonics K.K., Herrsching
CO_2 incubator HERAcell®	Heraeus Holding GmbH, Hanau
CO_2 incubator MCO-5AC 17AI	Sanyo Sales & Marketing Europe GmbH, Munich
Cryostat Microm HM 560	Thermo Fisher Scientific, Inc., Waltham, MA, USA
Dewar carrying flask, type B	KGW-Isotherm, Karlsruhe
Discovery 901 7T MR System with a 205/120HD Gradient Coil	Agilent Technologies, Inc., Santa Clara, CA, USA
Electrophoresis power supply Power Pac 200	Bio-Rad Laboratories GmbH, Munich
Flexible receive array P-H02LE-070-01507-001 V01	Rapid Biomedical GmbH, Rimpar
Gamma counter 2480 Wizard 2	Perkin Elmer, Waltham, MA, USA
Gel Doc™ XR+ system	Bio-Rad Laboratories GmbH, Munich
Glass ware, Schott Duran®	Schott AG, Mainz
Heated paraffin embedding module EG1150 H	Leica Microsystems GmbH, Wetzlar
HERAsafe® biological safety cabinet	Thermo Fisher Scientific, Inc., Waltham, MA, USA
Hiseq2000 platform	Illumina, San Diego, CA, USA
Hiseq2500 platform	Illumina, San Diego, CA, USA
Homogenizer SilentCrusher M with tool 6F	Heidolph Instruments GmbH & Co. KG, Schwabach
Horizontal gel electrophoresis system	Biozym Scientific GmbH, Hessisch Oldenburg
Horizontal shaker	Titertek Instruments, Inc., Huntsville, AL, USA
Incubator shaker Thermoshake	C. Gerhardt GmbH & Co. KG, Königswinter
Laminar flow HERAsafe	Heraeus Holding GmbH, Hanau
Magnetic stirrer, Ikamag® RCT	IKA® Werke GmbH & Co. KG, Staufen

Microcentrifuge 5415 D	Eppendorf AG, Hamburg
Microcentrifuge 5417 R	Eppendorf AG, Hamburg
MicroPET 120	Siemens AG, Munich
Microplate reader Anthos 2001	Anthos Mikrosysteme GmbH, Krefeld
Microscope Axio Imager.A1	Carl Zeiss AG, Oberkochen
Microscope Axiovert 25	Carl Zeiss AG, Oberkochen
Microscope DM LB	Leica Microsystems GmbH, Wetzlar
Microtome Microm HM355S	Thermo Fisher Scientific, Inc., Waltham, MA, USA
Microwave	Siemens AG, Munich
Mini centrifuge MCF-2360	LMS Consult GmbH & Co. KG, Brigachtal
Mini-PROTEAN® Tetra Cell	Bio-Rad Laboratories GmbH, Munich
Multipette® stream	Eppendorf AG, Hamburg
Neubauer hemocytometer, improved	LO-Laboroptik GmbH, Bad Homburg
Odyssey® infrared imaging system	Li-Cor Biosciences, Lincoln, NE, USA
PALM laser-capture microdissection system	Carl Zeiss AG, Oberkochen
Paraffin tissue floating bath Microm SB80	Thermo Fisher Scientific, Inc., Waltham, MA, USA
pH meter 521	WTW Wissenschaftlich-Technische Werkstätten GmbH, Weilheim
Pipettes Reference®, Research®	Eppendorf AG, Hamburg
Pipetus®	Hirschmann Laborgeräte GmbH & Co. KG, Eberstadt
Power supplies E844, E822, EV243	Peqlab Biotechnologie GmbH, Erlangen
Qubit® 2.0 Fluorometer	Invitrogen GmbH, Karlsruhe
Spectrophotometer NanoDrop 1000	Peqlab Biotechnologie GmbH, Erlangen
StepOnePlus™ real time PCR system	Applied Biosystems, Inc., Carlsbad, CA, USA
Stereomicroscope Stemi SV 11	Carl Zeiss AG, Oberkochen
Surgical instruments	Thermo Fisher Scientific, Inc., Waltham, MA, USA
Thermocycler T1	Biometra GmbH, Göttingen
Thermocycler Tgradient	Biometra GmbH, Göttingen
Thermocycler Tpersonal	Biometra GmbH, Göttingen
Thermocycler UNO-Thermoblock	Biometra GmbH, Göttingen
Thermomixer compact	Eppendorf AG, Hamburg
Tissue processor ASP300	Leica Microsystems GmbH, Wetzlar
Tumbling Table WT 17	Biometra GmbH, Göttingen
Vortex Genius 3	IKA® Werke GmbH & Co. KG, Staufen
Water bath 1003	GFL Gesellschaft für Labortechnik mbH, Burgwedel

Western blot system SE 260 Mighty Small II	Hoefer, Inc., Holliston, MA, USA
YSI2950 Biochemistry Analyzer	YSI Inc. / Xylem Inc., Yellow Springs, Ohio, USA

4.2 Disposables

Table 2. Disposables.

Disposable	Source
Cell culture plastics	Becton Dickinson GmbH, Franklin Lakes, NJ, USA; Greiner Bio-One GmbH, Frickenhausen; TPP Techno Plastic Products AG, Trasadingen, Switzerland
Cell scrapers	TPP Techno Plastic Products AG, Trasadingen, Switzerland
Cell strainer, 100 µm, yellow	BD Biosciences, Franklin Lakes, NJ, USA
Chromatography paper, 3 mm	GE Healthcare Europe GmbH, Munich
Combitips BioPur®	Eppendorf AG, Hamburg
Conical tubes, 15 mL	TPP Techno Plastic Products AG, Trasadingen, Switzerland
Conical tubes, 50 mL	Sarstedt AG & Co., Nümbrecht
Cover slips	Gerhard Menzel, Glasbearbeitungswerk GmbH & Co. KG, Braunschweig
CryoPure tubes	Sarstedt AG & Co., Nümbrecht
Cuvettes	Greiner Bio-One GmbH, Frickenhausen
Disposable scalpels	Feather Safety Razor Co., Ltd., Osaka, Japan
Filtropur S 0.2	Sarstedt AG & Co., Nümbrecht
Filtropur S 0.45	Sarstedt AG & Co., Nümbrecht
Glass slides Superfrost® Plus	Gerhard Menzel, Glasbearbeitungswerk GmbH & Co. KG, Braunschweig
MicroAmp® optical 96-well reaction plate	Applied Biosystems, Inc., Carlsbad, CA, USA
Microtome blades S35 and C35	Feather Safety Razor Co., Ltd., Osaka, Japan
Pasteur pipettes	Hirschmann Laborgeräte GmbH & Co. KG, Eberstadt
PCR reaction tubes	Brand GmbH + Co. KG, Wertheim; Eppendorf AG, Hamburg
Petri dishes	Sarstedt AG & Co., Nümbrecht
Phase lock gel light tubes	5 Prime GmbH, Hamburg
Pipette tips	Sarstedt AG & Co., Nümbrecht
Reaction tubes, 0.5 mL, 1.5 mL and 2 mL	Eppendorf AG, Hamburg
Safe seal pipette tips, professional	Biozym Scientific GmbH, Hessisch Oldenburg
Safe-lock reaction tubes BioPur®	Eppendorf AG, Hamburg
Serological pipettes	Sarstedt AG & Co., Nümbrecht
Single use needles Sterican® 27 gauge	B. Braun Melsungen AG, Melsungen
Single use syringes Omnifix®	B. Braun Melsungen AG, Melsungen

Tissue embedding cassette system	Medite GmbH, Burgdorf
Transfer membrane Immobilon-P	Millipore GmbH, Schwalbach am Taunus

4.3 Reagents and enzymes

Table 3. Reagents and enzymes.

Reagent	Source
1 kb DNA extension ladder	Invitrogen GmbH, Karlsruhe
1,4-Dithiothreitol (DTT)	Carl Roth GmbH + Co. KG, Karlsruhe
2-Log DNA ladder (0.1–10.0 kb)	New England Biolabs GmbH, Frankfurt am Main
2-Mercaptoethanol, 98%	Sigma-Aldrich Chemie GmbH, Munich
2-Propanol (isopropanol)	Carl Roth GmbH + Co.
Agarose	Sigma-Aldrich Chemie GmbH, Munich
Agencourt AMPure XP Beads	Beckman Coulter GmbH, Krefeld
Ammonium persulfate	Sigma-Aldrich Chemie GmbH, Munich
Ampicillin sodium salt	Carl Roth GmbH + Co. KG, Karlsruhe
Blotting grade blocker non-fat dry milk	Bio-Rad Laboratories GmbH, Munich
Bovine serum albumin, fraction V	Sigma-Aldrich Chemie GmbH, Munich
Bradford reagent	Serva Electrophoresis GmbH, Heidelberg
Bromphenol blue	Sigma-Aldrich Chemie GmbH, Munich
Chloramphenicol	AppliChem GmbH, Darmstadt
Coelenterazine h	NanoLight Technologies, Pinetop, AZ, USA
Complete, EDTA-free, protease inhibitor cocktail Tablets	Roche Deutschland Holding GmbH, Grenzach-Wyhlen
D-Luciferin	Synchem UG + Co. KG, Kassel
Dimethylsulfoxide (DMSO)	Carl Roth GmbH + Co. KG, Karlsruhe
dNTP mix, 10mM each	Fermentas GmbH, St. Leon-Rot
Dodecylsulfate Na-salt in pellets (SDS)	Serva Electrophoresis GmbH, Heidelberg
Dulbecco's phosphate buffered saline, powder	Biochrom AG, Berlin
Ethanol (100%)	Merck KGaA, Darmstadt
Ethidium bromide	Sigma-Aldrich Chemie GmbH, Munich
Ethylenediaminetetraacetic acid (EDTA)	Invitrogen GmbH, Karlsruhe
Gel loading dye, blue	New England Biolabs GmbH, Frankfurt am Main
GeneRuler™ 100bp DNA ladder	Fermentas GmbH, St. Leon-Rot
Glycerol	Sigma-Aldrich Chemie GmbH, Munich
Glycin Pufferan®	Carl Roth GmbH + Co. KG, Karlsruhe
HEPES Pufferan®	Carl Roth GmbH + Co. KG, Karlsruhe
Histosec® pastilles (without DMSO)	Merck KGaA, Darmstadt
HotStarTaq DNA polymerase	Qiagen GmbH, Hilden
Hydrochloric acid (HCl)	Merck KGaA, Darmstadt

Isotonic sodium chloride solution	Braun Melsungen AG, Melsungen
LB agar (Luria/Miller)	Carl Roth GmbH + Co. KG, Karlsruhe
LB broth (Luria/Miller)	Carl Roth GmbH + Co. KG, Karlsruhe
Magnesium chloride	Carl Roth GmbH + Co. KG, Karlsruhe
Methanol	Merck KGaA, Darmstadt
Mouse diet LASCRdiet™ CreActive TAM400	LASvendi GmbH, Soest
N,N-dimethylformamide	Sigma-Aldrich Chemie GmbH, Munich
Nonidet P40	Roche Deutschland Holding GmbH, Grenzach-Wyhlen
Orange G	Carl Roth GmbH + Co. KG, Karlsruhe
Peanut oil	Sigma-Aldrich Chemie GmbH, Munich
PfuUltra™ high fidelity DNA polymerase	Agilent Technologies, Inc., Santa Clara, CA, USA
Phosphatase inhibitor mix I	Serva Electrophoresis GmbH, Heidelberg
Polyethylene glycol 4000	Merck KGaA, Darmstadt
Precision Plus Protein™ all blue standard	Bio-Rad Laboratories GmbH, Munich
Proteinase K, recombinant, PCR grade	Roche Deutschland Holding GmbH, Grenzach-Wyhlen
QuantiFast® SYBR® green PCR master mix	Qiagen GmbH, Hilden
REDTaq® ReadyMix™ PCR reaction mix	Sigma-Aldrich Chemie GmbH, Munich
Restriction endonucleases	New England Biolabs GmbH, Frankfurt am Main
RNase-free DNase set	Qiagen GmbH, Hilden
RnaseA	Fermentas GmbH, St. Leon-Rot
Rotiphorese® gel 30	Carl Roth GmbH + Co. KG, Karlsruhe
S.O.C. medium	Invitrogen GmbH, Karlsruhe
Sodium acetate buffer solution	Sigma-Aldrich Chemie GmbH, Munich
Sodium chloride (NaCl)	Merck KGaA, Darmstadt
Sodium hydroxide solution (NaOH)	Merck KGaA, Darmstadt
SuperScript II	Thermo Fisher Scientific, Inc., Waltham, MA, USA
Tamoxifen	Sigma-Aldrich Chemie GmbH, Munich
Tamoxifen chow CreActive TAM400	LASvendi, Soest
TaqMan® reverse transcription reagents	Applied Biosystems, Inc., Carlsbad, CA, USA
TE buffer, pH 8.0	AppliChem GmbH, Darmstadt
TEMED	Carl Roth GmbH + Co. KG, Karlsruhe
Tissue-Tek® O.C.T.™ compound	Sakura Finetek Europe B.V, Alphen aan den Rijn, Netherlands
Tris hydrochloride	J.T.Baker® Chemicals, Phillipsburg, NJ, USA
Tris Pufferan®	Carl Roth GmbH + Co. KG, Karlsruhe
Triton® X-100	Merck KGaA, Darmstadt
Tween® 20	Carl Roth GmbH + Co. KG, Karlsruhe

4.4 Antibodies

Table 4. Antibodies.

Antibody	Source
Akt (C67E7), #4691	Cell Signaling Technology, Inc., Danvers, MA, USA
AlexaFluor® 680 goat anti-mouse IgG, A21058	Invitrogen GmbH, Karlsruhe
AlexaFluor® 750 goat anti-mouse IgG, A21037	Invitrogen GmbH, Karlsruhe
Anti-mouse IgG (H+L) (DyLight® 680 Conjugate), #5470	Cell Signaling Technology, Inc., Danvers, MA, USA
Anti-mouse IgG (H+L) (DyLight® 800 Conjugate), #5257	Cell Signaling Technology, Inc., Danvers, MA, USA
Anti-rabbit IgG (H+L) (DyLight® 680 Conjugate), #5366	Cell Signaling Technology, Inc., Danvers, MA, USA
Anti-rabbit IgG (H+L) (DyLight® 800 Conjugate), #5151	Cell Signaling Technology, Inc., Danvers, MA, USA
Cyclin D1, sc-246 (HD11)	Santa Cruz Biotechnology, Inc., Dallas, TX, USA
Hsp90, sc-13119 (H1704)	Santa Cruz Biotechnology, Inc., Dallas, TX, USA
MEK1, #9146	Cell Signaling Technology, Inc., Danvers, MA, USA
MEK1/2, #4694	Cell Signaling Technology, Inc., Danvers, MA, USA
MEK2, #9147	Cell Signaling Technology, Inc., Danvers, MA, USA
p27, sc-528 (C19)	Santa Cruz Biotechnology, Inc., Dallas, Texas, USA
p44/42 MAPK (Erk1/2) (L34F12), #4696	Cell Signaling Technology, Inc., Danvers, MA, USA
Pdk1, #3062	Cell Signaling Technology, Inc., Danvers, MA, USA
Phospho-Akt (Ser473), #9271	Cell Signaling Technology, Inc., Danvers, MA, USA
Phospho-Akt (Thr308), #2965	Cell Signaling Technology, Inc., Danvers, MA, USA
Phospho-p44/42 MAPK (Erk1/2) (Thr202/Tyr204) (D13.14.4E) XP™, #4370	Cell Signaling Technology, Inc., Danvers, MA, USA
Phospho-Rb (Ser807/811) (D20B12) #8516	Cell Signaling Technology, Inc., Danvers, MA, USA
Phospho-RSK2 (Ser227), #3556	Cell Signaling Technology, Inc., Danvers, MA, USA
Rb, sc-74562 (C2)	Santa Cruz Biotechnology, Inc., Dallas, TX, USA
RSK2, #9340	Cell Signaling Technology, Inc., Danvers, MA, USA
Skp2, sc-7164 (H435)	Santa Cruz Biotechnology, Inc., Dallas, TX, USA
α-tubulin, T6199	Sigma-Aldrich Chemie GmbH, Munich
β-actin, A5316	Sigma-Aldrich Chemie GmbH, Munich

4.5 Molecular biology

All buffers were prepared with bidistilled H_2O.

Table 5. Buffers and solutions for molecular biology.

Buffer	Component
IP buffer, pH 7.9	50 mM HEPES 150 mM NaCl 1 mM EDTA 0.5% Nonidet P40 10% Glycerol Phosphatase inhibitor (add prior to use) Protease inhibitor (add prior to use)
Stacking gel buffer	0.5 M Tris, adjusted to pH 6.8 with HCl
Separating gel buffer	1.5 M Tris, adjusted to pH 8.8 with HCl
Running buffer	25 mM Tris 192 mM Glycine 0.1% SDS
Transfer buffer, pH 8.3	25 mM Tris 192 mM Glycine 20% Methanol
5x Protein loading buffer (Laemmli), pH 6.8	10% SDS 50% Glycerol 228 mM Tris hydrochloride 0.75 mM Bromphenol blue 5% 2-Mercaptoethanol
6x Loading buffer orange G	60% Glycerol 60 mM EDTA 0.24% Orange G
10x Gitschier’s buffer	670 mM Tris, pH 8.8 166 mM (NH4)2SO4 67 mM MgCl2
Soriano lysis buffer	0.5% Triton® X-100 1% 2-Mercaptoethanol 1x Gitschier’s buffer 400 µg/mL Proteinase K (add prior to use)
SucRot solution (for PCR)	1.5 mg/mL Cresol red 100 mM Tris, pH 9.0 30% Saccharose
50x Tris acetate EDTA (TAE) buffer, pH 8.5	2 M Tris 50 mM EDTA 5.71% Acetic acid

Table 6. Kits for molecular biology.

Kit	Source
Ambion® WT expression kit	Applied Biosystems, Inc., Carlsbad, CA, USA
EndoFree® plasmid maxi kit	Qiagen GmbH, Hilden
GeneChip® WT terminal labeling kit	Affymetrix, Inc., Santa Clara, CA, USA
QIAamp DNA micro kit	Qiagen GmbH, Hilden
QIAamp DNA mini kit	Qiagen GmbH, Hilden
QIAfilter plasmid midi kit	Qiagen GmbH, Hilden
QIAprep® spin miniprep kit	Qiagen GmbH, Hilden
QIAshredder	Qiagen GmbH, Hilden
QuantiFast SYBR green PCR kit	Qiagen GmbH, Hilden
Qubit® dsDNA BR assay kit	Invitrogen GmbH, Karlsruhe
RNeasy mini kit	Qiagen GmbH, Hilden
TruSeq® Stranded mRNA sample preparation kit	Illumina, San Diego, CA, USA

Table 7. Bacterial strains.

Bacterial strain	Source
One Shot® Stbl3™ chemically competent E. coli	Invitrogen GmbH, Karlsruhe

Table 8. Plasmids.

Plasmid	Source
pWZL-Neo-Myr-Flag-DEST (#15300)	Addgene, Cambridge, MA, USA
pwZL-Neo-Myr-Flag-RPS6KA3 (#20627)	Addgene, Cambridge, MA, USA

4.5.1 Primers

Oligonucleotides were synthesized by Eurofins MWG GmbH (Ebersberg) and diluted in H_2O to a concentration of 10 µM.

Table 9. Primers used for genotyping.

PCR name	Primer name	Sequence (5´ → 3´)
Pdx1-Flp	Pdx1-Flp forward	AGAGAGAAAATTGAAACAAGTGCAGGT
	Pdx1-Flp reverse	CGTTGTAAGGGATGATGGTGAACT
	Gabra forward (Ctrl)	AACACACACTGGAGGACTGGCTAGG
	Gabra reverse (Ctrl)	CAATGGTAGGCTCACTCTGGGAGATGATA
FSF-Kras^{G12D}	FSF-Kras common forward	CACCAGCTTCGGCTTCCTATT
	FSF-Kras WT reverse	AGCTAATGGCTCTCAAAGGAATGTA
	FSF-Kras mut reverse	GCGAAGAGTTTGTCCTCAACC

FSF-Kras^{G12D} recombination	FSF-Kras del forward	AGAATACCGCAAGGGTAGGTGTTG
	FSF-Kras del reverse	TGTAGCAGCTAATGGCTCTCAAA
CreERT2	CreERT2 forward (*R26CAG-CreERT2* line)	GAATGTGCCTGGCTAGAGATC
	CreERT2 reverse (*R26CAG-CreERT2* line)	GCAGATTCATCATGCGGA
	CreERT2 recombined reverse	CGATCCCTGAACATGTCCATC
R26-CAG	R26 common forward	AAAGTCGCTCTGAGTTGTTAT
	R26 WT reverse	GGAGCGGGAGAAATGGATATG
	R26CAG-CreERT2 mut reverse	TCAATGGGCGGGGGTCGTT
Frt-stop-*Frt (FSF)*	FSF forward	TGAATAGTTAATTGGAGCGGCCGCAATA
	FSF reverse	CAGGGTGTTATAAGCAATCCC
FSF recombination	FSF-Cre stop del forward	GTTCGGCTTCTGGCGTGT
	FSF-Cre stop del reverse	CGATCCCTGAACATGTCCATC
Pdk1^{lox}	Pdk1 floxed forward	ATCCCAAGTTACTGAGTTGTGTTGGAAG
	Pdk1 floxed reverse	TGTGGACAAACAGCAATGAACATACACGC
Pdk1^{lox} recombination	Pdk1 recombined forward	CTATGCTGTGTTACTTCTTGGAGCACAG
	Pdk1 non-recombined forward	CCCTCTAGCAAATGTTCTGTCTGGAATGTCT
	Pdk1 floxed reverse	TGTGGACAAACAGCAATGAACATACACGC
Pdk1^{lox} recombination (microdissection)	Pdk1 recombined forward micro	CTATGCTGTGTTACTTCTTGGTGC
	Pdk1 non-recombined forward micro	TCCCTCTAGCAAATGTTCTGTCT
	Pdk1 common reverse micro	GGACAAACAGCAATGAACATACAC
Trp53^{frt}	p53 frt forward	CAAGAGAACTGTGCCTAAGAG
	p53 frt reverse	CTTTCTAACAGCAAAGGCAAGC
LSL-Trp53^{R172H}	Trp53^{R172H} forward	AGCCTTAGACATAACACACGAACT
	Trp53^{R172H} mut forward	GCCACCATGGCTTGAGTAA
	Trp53^{R172H} reverse	CTTGGAGACATAGCCACACTG
Ptf1a^{Cre}	Ptf1a-Cre-GT-LP-URP	CCTCGAAGGCGTCGTTGATGGACTGCA
	Ptf1a-Cre-GT-wt-UP	CCACGGATCACTCACAAAGCGT
	Ptf1a-Cre-GT-mut-UP-neu	GCCACCAGCCAGCTATCAA

LSL-Kras^{G12D}	LSL-Kras common forward	CACCAGCTTCGGCTTCCTATT
	LSL-Kras WT reverse	AGCTAATGGCTCTCAAAGGAATGTA
	LSL-Kras mut reverse	CCATGGCTTGAGTAAGTCTGC
R26-PIK3CA^{H1047R}	R26-PIK3CA^{H1047R} common forward	AAAGTCGCTCTGAGTTGTTAT
	R26-PIK3CA^{H1047R} mut reverse	GCGAAGAGTTTGTCCTCAACC
	R26-PIK3CA^{H1047R} WT reverse	GGAGCGGGAGAAATGGATATG
PIK3CA^{H1047R}	PIK3CA^{H1047R} forward	TGAATAGTTAATTGGAGCGGCCGCAATA
	PIK3CA^{H1047R} reverse	AAATAGCCGCAGGTCACAAAGTCTCCG
Mek1^{lox}	MEK1A4	GACGTGGTGAACAGGAAAGGGATTGGG
	MEK1B2	TGGAGCTGGAGTCACGGGTGGTTGTAA
	MEK1B3	GCGAACTGGGAGCTGGCAACGGTGGAG
Mek2$^{\Delta}$	MEK2 forward	TAACAGAAGGGGAAGGAGAGAGTGG
	MEK2 reverse	CACCCTGGCTGTTCCTTACACCT
	MEK2 mut reverse	TCGTGGTATCGTTATGCGCC
Renilla	Renilla forward	CTCATATCGCCTCCTGGATCACT
	Renilla reverse	GAAGCTCTTGATGTACTTACCCATTTC
Td-Tomato	Td-Tomato forward	CAAGGGAGAGGAGGTCATCAAAG
	Td-Tomato reverse	GCTTGGTGTCCACGTAGTAGTAGC
EGFP	EGFP forward	TGCCCGAAGGCTACGTCCAG
	EGFP reverse	CCATGTGATCGCGCTTCTCGT

#

Table 10. Primers for quantitative real time PCR.

Gene	Primer name	Sequence (5´ → 3´)	Origin
Pdk1	Pdk1 forward	ACGCCCTGAAGACTTCAAGTTTG	Mus musculus
	Pdk1 reverse	GCCAGTTCTCGGGCCAGA	
Cyclophilin	Cyclophilin forward	ATGGTCAACCCCACCGTGT	Mus musculus
	Cyclophilin reverse	TTCTGCTGTCTTTGGAACTTTGTC	
Rsk2	Rsk2 forward	AGCCAAGCTATGCAGACAGT	Homo sapiens
	Rsk2 reverse	TGCAAACAGAGTAGGAGCCAA	
RNA-Seq library	RNA-Seq forward	ATGATACGGCGACCACCGAG	Adapter
	RNA-Seq reverse	CAAGCAGAAGACGGCATACGAG	
Fbp2	Fbp2 forward	TCTTCATGTACCCAGCCAACC	Mus musculus
	Fbp2 reverse	TTGCCATACCTCCTGCTTGC	

Ldha	Ldha forward	CTGCTTCTCCTCGCCAGTC	Mus musculus
	Ldha reverse	TGAGGGTTGCCATCTTGGAC	
Pfkl	Pfkl forward	GACCGGCATGGAAAGCCTA	Mus musculus
	Pfkl reverse	ACATGACCCAGCACAGTCAC	

4.6 Cell culture

Table 11. Cell lines.

Cell line	Source
Gryphon™ Eco retroviral packaging cell line	Allele Biotechnology, San Diego, CA, USA

Table 12. Cell culture media and their components.

Medium	Components
Cancer cell medium	DMEM 10% FCS (Biochrom AG) 1% Penicillin/Streptomycin
Gryphon™ Eco medium	DMEM 10% FCS (Biochrom AG) 1% Penicillin/Streptomycin 1% L-Glutamine
Freezing medium	70% DMEM 20% FCS 10% DMSO

Table 13. Reagents and kits for cell culture.

Reagent / Kit	Source
4-hydroxytamoxifen (≥70% Z isomer)	Sigma-Aldrich Chemie GmbH, Munich
Cell proliferation ELISA, BrdU (colorimetric)	Roche Deutschland Holding GmbH, Grenzach-Wyhlen
Collagenase type 2	Worthington Biochemical Corporation, Lakewood, NJ, USA
Cre protein	Prof. Angelika Schnieke
Dulbecco's modified eagle medium (DMEM) with L-glutamine	Invitrogen GmbH, Karlsruhe
Dulbecco's phosphate buffered saline (PBS)	Invitrogen GmbH, Karlsruhe
Fetal calf serum (FCS)	Biochrom AG, Berlin
Fungizone® antimycotic	Invitrogen GmbH, Karlsruhe
G418, Geneticin®	Invitrogen GmbH, Karlsruhe
Giemsa solution	Sigma-Aldrich Chemie GmbH, Munich
L-Glutamine 200 mM	Invitrogen GmbH, Karlsruhe
MTT reagent	Sigma-Aldrich Chemie GmbH, Munich
Penicillin (10000 units/mL) / Streptomycin (10000 µg/mL) solution	Invitrogen GmbH, Karlsruhe

Puromycin dihydrochloride	Sigma-Aldrich Chemie GmbH, Munich
Effectene® transfection reagent	Qiagen GmbH, Hilden
Trypsin, 0.05% with 0.53 mM EDTA 4Na	Invitrogen GmbH, Karlsruhe
Venor® *GeM* mycoplasma detection kit	Minerva Biolabs GmbH, Berlin

4.7 Histology

Table 14. Reagents and kits for histological analysis.

Reagent / Kit	**Source**
Acetic acid (glacial)	Merck KGaA, Darmstadt
Alcian blue 8GX	Sigma-Aldrich Chemie GmbH, Munich
Aluminium sulfate	Honeywell Specialty Chemicals Seelze GmbH, Seelze
Antigen unmasking solution, citric acid based	Vector Laboratories, Inc., Burlingame, CA, USA
Avidin/biotin blocking kit	Vector Laboratories, Inc., Burlingame, CA, USA
Certistain® Nuclear fast red	Merck KGaA, Darmstadt
DAB peroxidase substrate kit, 3,3'-diaminobenzidine	Vector Laboratories, Inc., Burlingame, CA, USA
Donkey serum D9663	Sigma-Aldrich Chemie GmbH, Munich
Eosine	Waldeck GmbH & Co KG, Münster
Goat serum G9023	Sigma-Aldrich Chemie GmbH, Munich
Hematoxylin	Merck KGaA, Darmstadt
Hydrogen peroxide 30%	Merck KGaA, Darmstadt
Pertex mounting medium	Medite GmbH, Burgdorf
Rabbit serum R9133	Sigma-Aldrich Chemie GmbH, Munich
Roti® Histofix 4%	Carl Roth GmbH + Co. KG, Karlsruhe
Roti® Histol	Carl Roth GmbH + Co. KG, Karlsruhe
Sucrose (saccharose)	Merck KGaA, Darmstadt
Vectashield® mounting medium with DAPI	Vector Laboratories, Inc., Burlingame, CA, USA
Vectastain® elite ABC kit	Vector Laboratories, Inc., Burlingame, CA, USA

Table 15. Buffers for histological analysis.

Buffer	**Component**
Alcian blue, pH 2.5	1% Alcian blue 3% Acetic acid
Nuclear fast red	0.1% Nuclear fast red 2.5% Aluminium sulphate

Table 16. Secondary antibodies for histological analysis.

Antibody	Source
Biotinylated anti-goat IgG (H+L)	Vector Laboratories, Inc., Burlingame, CA, USA
Biotinylated anti-mouse IgG (H+L)	Vector Laboratories, Inc., Burlingame, CA, USA
Biotinylated anti-rabbit IgG (H+L)	Vector Laboratories, Inc., Burlingame, CA, USA
Biotinylated anti-rat IgG (H+L)	Vector Laboratories, Inc., Burlingame, CA, USA

4.8 Software

Table 17. Software.

Software	Source
AxioVision 4.8	Carl Zeiss AG, Oberkochen
Excel	Microsoft Corporation, Redmont, WA, USA
GraphPad Prism 5	La Jolla, CA, USA
Inveon research workstation	Siemens AG, Munich
Odyssey® v1.2	Li-Cor Biosciences, Lincoln, NE, USA
OsiriX 6.5	Open-source software (Rosset et al., 2004)
Quantity One	Bio-Rad Laboratories GmbH, Munich
SimplePCI software	Hamamatsu Photonics K.K., Herrsching
StepOne™ v2.3	Applied Biosystems, Inc., Carlsbad, CA, USA

5 Methods

5.1 Mouse experiments

All animal studies were conducted in compliance with the European guidelines for the care and use of laboratory animals and were approved by the local authorities. Mice were on a mixed C57BL6/J;129/S6 background.

5.1.1 Mouse strains

Conditional Cre/*loxP* and Flp/*frt* mouse models were used in this study. Mice carrying genes which are flanked by *loxP*/*frt* sites or silenced by an *LSL*/*FSF* cassette can be interbred with a mouse strain expressing Cre or Flp recombinase under the control of a tissue-specific promoter to allow conditional inactivation of genes or deletion of the *LSL* or *FSF* cassette to activate expression of genes. Combining the Flp/*frt* recombination system for tumor initiation and the Cre/*loxP* system for secondary genetic manipulation enables sequential inactivation of Ras effectors in PanIN lesions and PDAC cells *in vitro* and *in vivo.*

***Ptf1a*$^{Cre/+}$** (Nakhai et al., 2007). This knock-in mouse strain was kindly provided by Dr. Hassan Nakhai (Klinikum rechts der Isar, Technical University Munich). The Ptf1a is a subunit of the pancreas transcription factor and plays a fundamental role in endocrine and ecxocrine pancreas development in mice. Cre recombinase is expressed under the control of the *Ptf1a* promoter and is therefore specifically expressed in pancreatic precursor cells.

***LSL-Kras*$^{G12D/+}$** (Hingorani et al., 2003; Jackson et al., 2001). This knock-in mouse strain was kindly provided by Prof. Tyler Jacks (Massachusetts Institute of Technology, Cambridge, MA, USA). *LSL-Kras*$^{G12D/+}$ mice carry a point mutation in codon 12, which corresponds to the mutation frequently found in human PDAC leading to an amino acid substitution of glycine by aspartate. After Cre-mediated deletion of the *LSL* cassette, the GTPase activity of Kras is impaired resulting in constitutive Kras signaling.

***LSL-PIK3CA*$^{H1047R/+}$** (Eser et al., 2013). This knock-in mouse strain was generated in the laboratory of Prof. Dieter Saur. A latent oncogenic *PIK3CA*^{H1047R} allele silenced by an *LSL* cassette was constructed as a knock-in at the *Rosa26* locus. *LSL-PIK3CA*$^{H1047R/+}$ mice harbor a mutation in codon 1047 leading to a substitution of histidine by arginine. After deletion of the *LSL* cassette by a Cre recombinase, the expression of p110α^{H1047R} results in a constitutive activation of the PI3K signaling pathway.

LSL-Trp53$^{R172H/+}$ (Hingorani et al., 2005; Olive et al., 2004). This knock-in mouse strain was kindly provided by Prof. Tyler Jacks (Massachusetts Institute of Technology, Cambridge, MA, USA). *LSL-Trp53^{R172H}* mice carry a missense mutation in codon 172 of endogenous *Trp53*, which corresponds to the human R175H mutation often found in patients with the Li-Fraumeni syndrome and in spontaneous human tumors. After excision of the *LSL* cassette, dominant-negative oncogenic Trp53 is expressed (de Vries et al., 2002; Liu et al., 2000).

Pdk1$^{lox/+}$ (Lawlor et al., 2002). In this mouse strain, exon 3 and exon 4 of the *Pdk1* locus are flanked by *loxP* sites, permitting conditional deletion of *Pdk1*.

Mek1$^{lox/+}$ (Catalanotti et al., 2009). This mouse strain was kindly provided by Prof. Manuela Baccarini (Max F. Perutz Laboratories, Vienna, Austria). Exon 2 of the *Mek1* locus is flanked by *loxP* sites and can be deleted by Cre expression resulting in conditional deletion of *Mek1*.

Mek2$^{\Delta/+}$ (Skarnes et al., 2011). In this "knock-out first" mouse strain an *frt*-flanked *lacZ-neomycin* cassette is inserted into the first intron of the *Mek2* locus and exon 2 is flanked by *loxP* sites. Without Cre and Flp expression, this strain harbors a general *Mek2*-KO. After Flp-expression followed by Cre-expression a conditional *Mek2*-KO is created.

Pdx1-Flp (Schönhuber et al., 2014). This transgenic mouse strain was generated in the laboratory of Prof. Dieter Saur. The codon-optimized Flp-o recombinase is expressed under the control of the *Pdx1* promotor, which is active in pancreatic progenitor cells and in adult pancreatic acini, ducts and islets.

FSF-Kras$^{G12D/+}$ (Schönhuber et al., 2014). This knock-in mouse strain was generated in the laboratory of Prof. Dieter Saur. Expression of the *FSF* silenced oncogenic *Kras^{G12D}* allele from its endogenous locus can be activated by Flp expression.

FSF-R26$^{CAG\text{-}CreERT2/+}$ (Schönhuber et al., 2014). This mouse strain was generated in the laboratory of Prof. Dieter Saur. To manipulate Flp-recombined cells sequentially with the Cre recombination system, a latent tamoxifen-inducible *CreER^{T2}* allele silenced by an *FSF* cassette under the control of the strong *CAG* promoter was constructed as a knock-in at the *Rosa26* locus.

Trp53$^{frt/+}$ (Lee et al., 2012). This mouse strain was kindly provided by Dr. David Kirsch (Duke University School of Medicine, Durham, NC, USA). Exons 2 to 6 of the *Trp53* gene are flanked by *frt* sites and p53 can be inactivated by Flp expression.

***R26*$^{dual/+}$** (unpublished). This mouse strain was generated in the laboratory of Prof. Dieter Saur. Firefly luciferase (fLuc) and EGFP expression are induced by Flp recombinase whereas Cre recombines the *fLuc-EGFP* cassette and thereby activates renilla luciferase (rLuc) and td-Tomato expression.

5.1.2 Genotyping

Around 2–3 weeks after birth, a 1 mm long tail biopsy was taken from the previously anesthetized mouse with a sterile scalpel. The wound was disinfected with a silver nitrate applicator. Each mouse got explicit earmarks representing a number code. DNA was extracted from the tails as described in 5.4.1.

5.1.3 Tamoxifen treatment of mice

To analyze the effect of *Pdk1* deletion on tumor progression, mice were fed with tamoxifen-containing chow (400 mg tamoxifen citrate per kilogram chow) for 4 weeks to activate CreER^{T2} at the age of 3 months. Tumor mice were injected with 4 mg of tamoxifen dissolved in peanut oil supplemented with 10% ethanol twice per week to study the impact of *Pdk1* deletion on already established tumors.

5.1.4 Orthotopic implantation

After anesthesia of NOD Scid Il2 receptor gamma$^{-/-}$ (*NOD.Cg-Prkdc*^{scid}*Il2rg*^{tm1Wjl}/SzJ) mice with MMF (5 mg/kg midazolam, 500 µg/kg medetomidine, 50 µg/kg fentanyl) via intraperitoneal injection, a small abdominal incision was made. The spleen was exposed by a gentle pull and 2500 cells solved in 25 µL DMEM were carefully injected into the pancreas using a microliter syringe with a 27-gauge needle. After the operation, MMF anesthesia was antagonized by applying AFN (750 µg/kg atipamezole, 500 µg/kg flumazenil, 1.2 mg/kg naloxone) via subcutaneous injection. Mice were monitored postoperatively. When a tumor was palpable, one cohort of mice was treated with 4 mg tamoxifen intraperitoneally (i.p.) twice a week whereas the control cohort remained untreated. All mice were sacrificed at the same day (around 3–4 weeks after implantation).

5.1.5 Subcutaneous implantation

2500 syngenic tumor cells in DMEM were subcutaneously injected into the right and left flank of C57BL6/J wild type (WT) mice using a 1 mL syringe with a 27 gauge needle. Mice were sacrificed around 1 month post implantation.

5.1.6 Magnetic resonance imaging (MRI) of tumor mice

Mice were screened for tumors on a regular basis by magnetic resonance imaging (MRI) using a Discovery 901 7 Tesla MRI system with a 205/120 HD gradient coil and a flexible receive array coil following a protocol adapted to the abdomen (for endogenous tumor mice) or the flanks (for subcutaneously implanted mice). Animals with average tumor diameters around 5 mm were enrolled in the treatment study. Longitudinal T2-weighted (T2w), fatsaturated turbo spin-echo imaging (slice thickness = 0.7 mm, in-plane resolution = 128x128 mm^2, TR/TE = 5000 ms/43 ms, NEX = 6, total scan duration 10 min) and a T1-weighted sequence (slice thickness = 0.7mm, TR/TE = 30 ms/1.872 ms, NEX = 16) were performed for tumor detection and volumetric analysis in cooperation with Michael Michalik (AG Schwaiger). Tumor volumes were quantified using the OsiriX software package.

5.1.7 Positron emission tomography (PET) of tumor mice

Glucose metabolism in subcutaneously implanted and endogenous tumor mice was analyzed by fluorine-18-2-fluoro-2-deoxy-D-glucose-positron emission tomography (F18-FDG-PET). PET scans were performed by the PET core facility using a MicroPET 120 system after injection of F18-FDG of approximately 11.1 x 10^6 Bq (300 µCi) via the tail vein and a waiting time of around 45 min. Data analysis was performed with the Inveon Research Workstation Software and OsiriX version 6.5 by Benedikt Feuerecker (AG Schwaiger). Based on the PET, computed tomography (CT) and MRI images, fusion images were generated. Regions of interest (ROI) were drawn on selected F18-FDG images and the maximal standardized uptake value (SUV_{max}) was obtained. Moreover, the SUV_{max} of a representative muscle of the posterior limbs was determined and a tumor-to-muscle ratio (T/M ratio) was calculated.

5.1.8 *In vivo* bioluminescence imaging (BLI)

Bioluminescence imaging (BLI) is based on an enzymatic reaction and permits quantification of gene expression. In a redox reaction requiring ATP, O_2 and Mg^{2+} the firefly (*Photinus pyralis*) luciferase catalyses the oxidation of its substrate D-luciferin to oxyluciferin which leads to emission of light. Coelenterazine is converted to coelenteramide by renilla (*Renilla reniformis*) luciferase. In this study *R26*$^{dual/+}$ mice were used to monitor Flp and Cre expression *in vivo* by measuring firefly and renilla luciferase signal intensities. Mice were first anesthetized with MMF as described in 5.1.4 and the fur was shaved at the position of expected signal emission. Afterwards, to detect firefly luciferase expression, 4.5 mg D-luciferin were injected intraperitoneally and imaging was conducted after 5 min using a cooled back-thinned, charge-coupled device camera equipped with an image intensifier

(OrcaII ER). In the first step a grayscale bright field photo was taken at gain 600 for 0.2–0.4 s, then BLI was performed at gain 900, starting with low exposure times of 10 s up to 10 min maximum, depending on the signal intensity. In order to compare different measurements, the exposure times were strictly kept constant for each mouse within an experiment. After the imaging, MMF anesthesia was antagonized by AFN injection as described in 5.1.4. For detection of renilla luciferase expression, around 250 µg coelenterazine were injected in the tail vein and the subsequent procedure was the same like for D-luciferin imaging. For analysis of BLI data, a pseudocolor image of the original bioluminescence photo was generated and subsequently projected on the bright field grayscale image using SimplePCI software.

5.1.9 Mouse dissection

Prior to dissection the mouse was euthanatized with isoflurane, fixed and disinfected with 70% ethanol. The abdomen was cut open and samples were taken as sterile as possible. Pancreatic tissue samples for following RNA and protein isolation were homogenized in 1 mL RLT buffer supplemented with 10 µL 2-mercaptoethanol or 600 µL IP buffer containing phosphatase and proteinase inhibitors using SilentCrusher M, respectively. A small piece of tissue was removed for subsequent DNA isolation. All samples were snap-frozen and stored at -80 °C until use. The size and the weight of the pancreas tissue were determined. Pancreas, spleen, liver, lung, heart, stomach, intestine and kidneys were fixed overnight in 4% Roti® Histofix to be processed to histological analysis.

5.2 Histological analysis

5.2.1 Paraffin sections

Tissue samples for histological analysis were fixed in 4% Roti® Histofix for 24 h, dehydrated using the tissue processor ASP300, embedded in paraffin and stored at room temperature (RT) until further use. For following stainings, series of 2.5–3 µm thick serial sections were cut using the microtome Microm HM355S.

5.2.2 Hematoxylin and eosin (H&E) staining of tissue sections

Paraffin-embedded sections were dewaxed by incubation in Roti® Histol (2 x 5 min), rehydrated in a decreasing ethanol series (2 x 99%, 2 x 96% and 2 x 80%) and washed with distilled water. Afterwards sections were placed into hematoxylin for 5 s and subsequently blueing was performed by bathing slides in tap water for around 5 min. Slides were then stained in eosin for 20 s, washed again in distilled water and applied to an ascending ethanol

series (2 x 80%, 2 x 96% and 2 x 99%) and incubated in Roti® Histol (2 x 5 min) before they were covered with Pertex mounting medium.

5.2.3 Alcian blue (AB) staining

Paraffin-embedded sections were dewaxed and rehydrated as described in 5.2.2. Then alcian blue staining was performed by incubating the slides in aqueous alcian blue solution for 5 min. After washing them in water, sections were counterstained with nuclear fast red solution for 5 min, rehydrated and mounted as described in 5.2.2.

5.2.4 Immunohistochemistry (IHC)

Paraffin-embedded tissue sections were dewaxed and rehydrated as described in 5.2.2. Antigen retrieval was performed by boiling sections in a microwave at 360 W for 10 min in citric acid-based antigen unmasking solution. After cooling down for at least 20 min at RT in the citrate buffer, the sections were rinsed with water and incubated in 3% H_2O_2 in the dark for 15 min to inhibit endogenous peroxidase activity. Next they were washed with water and three times with PBS before blocking for 1 h at RT with 3–5% serum in PBS. The sections were washed again three times with PBS and incubated with the first antibody diluted in 3–5 % serum in PBS at dilution ranges from 1:50 to 1:500 overnight at 4 °C. The avidin/biotin blocking kit was generally applied. The next day, they were washed three times with PBS before incubation with the biotinylated secondary antibody, which was diluted in 3–5 % serum in PBS 1:500, for 1 h at RT. Slides were washed again with PBS. Detection was performed using the Vectastain® elite ABC kit and the DAB peroxidase substrate kit according to manufacturer's protocol. Finally, the slides were counterstained with hematoxylin, dehydrated and mounted as described in 5.2.2.

5.2.5 Analysis of stainings

For documentation of the staining results from H&E staining and IHC as well as for counting Ki67-positive cells, slides were photographed using the microscope Axio Imager.A1 with AxioCam HRc and software AxioVision 4.8. Representative images are shown in the results part. Scale bars generally indicate 50 µm. Quantification and grading of mouse ADM and PanIN lesions was performed on three sections per mouse and three mice per 9 month-time point according to the established nomenclature for the grading of PanIN lesions in mice (Hruban et al., 2006).

5.2.6 Laser capture microdissection

Normal acini and PanIN lesions from 8 µm thick, dewaxed, H&E-stained, formalin-fixed paraffin tissue sections were microdissected using a PALM laser-capture microdissection system. DNA was isolated from the microdissected cells using the QIAamp DNA Micro Kit.

5.3 Cell Culture

Primary murine pancreatic cancer cells were established from tumor mice and were maintained in cancer cell medium (DMEM supplemented with 10% FCS and 1% penicillin/streptomycin) at 37 °C, 5% CO_2 and 100% humidity.

5.3.1 Generation and culture of primary mouse PDAC cell lines

For isolation of primary murine pancreatic cancer cells, all conditions were kept as sterile as possible. During mouse dissection a piece of the tumor was cut out and transferred to sterile PBS. Under a biological safety cabinet, it was cut into small pieces with a scalpel and incubated in 5 mL cancer cell medium supplemented with 200 U/mL collagenase type 2 at 37 °C for 24–48 h. Afterwards the cell suspension was centrifuged for 5 min at 1200 rpm, supernatant was aspirated and the pellet was resolved in 5 mL cancer cell medium for further culturing.

For passaging of cells the medium was aspirated, cells were washed with PBS and detached from the culture dish by incubation with trypsin/EDTA at 37 °C for an appropriate time period. Trypsinization was stopped by addition of medium. Thereafter, the cell suspension was seeded in new vessels depending on the experimental conditions. Cell number was determined by a Neubauer hemacytometer.

For cryopreservation, trypsinized cells were taken up in medium and centrifuged at 1200 rpm for 5 min. The pellet was dissolved in ice-cold freezing medium, transferred to CryoPure tubes, frozen at -80 °C for 24 h and subsequently stored in liquid nitrogen until further use.

Treatment of cells with 4-hydroxytamoxifen (4-OHT)

To activate $CreER^{T2}$ in cell culture experiments, pancreatic cancer cells were treated with vehicle (ethanol) or 600 nM 4-hydroxytamoxifen (4-OHT) for 8 days to delete *loxP*-flanked sequences. Subsequently, cells were seeded for a variety of assays (as described in chapters 5.3.2 to 5.3.6).

Transduction of cells with recombinant Cre protein

First, cells were seeded at a density of 7.5 x 10^4 cells per well of a 12-well plate. One day later the medium was removed, the cells were washed with PBS twice and incubated with 500 µL of 5 µM recombinant Cre protein solved in DMEM containing 0.5% FCS (sterile

filtered). After 2–24 h the cells were washed twice with PBS and DMEM supplemented with 10% FCS was added.

#

5.3.2 MTT assay

The MTT assay is used to measure the viability of cells by determining the activity of cytosolic and mitochondrial dehydrogenases. Yellow 3-(4,5-dimethyl-2-thiazolyl)-2,5-diphenyl-tetrazolium bromide (MTT) is taken up by the cells and converted into water-insoluble dark blue formazan by NADH-dependent reductases.

1000 cells/well were seeded in 96-well plates as triplicates after pretreatment with 4-OHT or vehicle (ethanol). 10 µL of MTT reagent were added to 100 µL of medium (final concentration of MTT dye: 0.5 mg/mL) and incubated for 4 h at 37 °C. After removing the medium, the water-insoluble formazan crystals were solubilized by adding 200 µL of ethanol/DMSO mix (1:1, v/v) and the 96-well plate was shaken for 10 min at RT. The optical density of the samples at a wavelength of 600 nm was determined by the plate spectrophotometer Anthos 2001. The MTT assay was performed on five consecutive days to quantify the cell proliferation.

#

5.3.3 BrdU assay

1000 cells/well were seeded on a 96-well plate and cell proliferation was assessed 72 h later using a colorimetric BrdU-enzyme-linked immunosorbent assay (ELISA) according to manufacturer's instructions.

5.3.4 Clonogenic assay

2000 cells/well were seeded on a 6-well plate. When control cells (cells treated with ethanol) showed evenly spread visible colonies (about 1–2 weeks after seeding), cell culture medium was aspirated and cells were fixed by cold 99% methanol while shaking for 30 min at RT. After methanol was removed, colonies were stained with Giemsa solution (diluted 1:20 in distilled water) on an orbital shaker overnight. The next day, Giemsa solution was removed, cells were washed with distilled water and plates were air dried.

5.3.5 F18-FDG uptake assay

For quantification of uptake of F18-FDG into tumor cells, 1 x 10^5 cells were seeded into 24-well plates as quadruples for each condition. On the following day, the cell culture medium was removed, cells were washed twice with glucose-free medium and were incubated in glucose-free cell culture medium that was supplemented with F18-FDG at a radioactivity of 0.185 MBq/mL. After 60, 90 and 120 min plates were put on ice, washed

twice with ice cold PBS and cells were detached with 1 M NaOH and harvested for glucose uptake measurements using a gamma counter. Tumor cell uptake was referred to the F18-FDG standard and cell uptake was displayed as percent of the standard (uptake in %). F18-FDG uptake assays were performed in cooperation with Benedikt Feuerecker (AG Schwaiger).

5.3.6 Glucose and lactate measurements

2000 cells/well were seeded into 96-well plates as triplicates for each condition. The next day glucose and lactate were measured in the supernatant by using the YSI2950 biochemistry analyzer. Based on these values, the glucose and lactate turnover of the cells was calculated.

5.3.7 Retrovirus production: Transfection of Gryphon™ Eco cells

Gryphon™ Eco Packaging cell lines were created by placing constructs capable of producing gag, pol and envelope into HEK293T cells. Transfection of Gryphon™ Eco cells was performed by using the Effectene® transfection reagent. On the first day, Gryphon™ Eco cells were seeded at a density of 1–5 x 10^6 cells in 10 mL medium in a 10-cm dish. Around 24 h later, the cells should be ~60–70% confluent and were transfected with expression plasmids. First 3 µg of plasmid DNA was filled up with EC buffer to 300 µL, condensed by addition of 48 µL of enhancer and vortexed for 1s. After incubation at RT for 2–5 min, 30 µL of Effectene® reagent were mixed with the DNA by vortexing for 10 s. 10 min later the formed Effectene®-DNA complexes were mixed with medium and added dropwise to the cells. At 2 days post-transfection, media containing retrovirus were harvested and replaced with 10 mL new media, 24 h later viral harvesting was repeated. The viral supernatant was transferred to a storage tube by filtration with a 0.45 µm filter to remove any packaging cells that were collected during harvesting.

5.3.8 Retroviral transduction

One day before transduction, target cells were seeded at density of 1 x 10^5/mL per well in a 12-well plate. For retroviral transduction, the old medium was removed and 1 mL of filtrated virus supernatant and 8 µg/mL polybrene were added per well. 2 days later, transduced cells were selected by usage of appropriate antibiotics.

5.4 Molecular biology

5.4.1 Isolation of genomic DNA

Genomic DNA for subsequent genotyping and recombination PCR analysis was isolated by adding 50-200 µL of Soriano lysis buffer to a small piece of tissue or a cell pellet. Lysis was performed in a thermocycler at 55 °C for 90 min. Proteinase K was heat inactivated for 15 min at 95 °C. After vortexing the sample, the DNA-containing supernatant was separated from the debris by centrifugation at 14000 rpm and 4 °C for 10 min, transferred into a new tube and stored at 4 °C for short term or at -20 °C for a longer time period.

5.4.2 Polymerase chain reaction

Polymerase chain reaction (PCR). For standard genotyping or recombination PCR (Mullis et al., 1986) a PCR pre-mix containing buffer, polymerase and dNTPs was used (Table 18). The standard PCR reaction setup and conditions are shown in Table 19. Primer amounts were optimized depending on the PCR product. If necessary, DMSO was added to improve PCR outcome. PCR products were stored at 4 °C until further analysis by gel electrophoresis.

Table 18. Composition of pre-mix for PCR.

Solution	Volume for one reaction
distilled water	4.375 µL
10x buffer S	2.5 µL
30% sucrose	2.5 µL
SucRot	2.5 µL
PeqTaq	0.125 µL
dNTPs (10 µM each)	0.5 µL

Table 19. Reaction mix and conditions for standard PCR.

Reaction Mix		Conditions		
12.5 µL	PCR pre-mix	95 °C	3 min	
0.25–2 µL	forward primer (10 µM)	95 °C	45 s	40x
0.25–2 µL	reverse primer (10 µM)	55 °C–72 °C	60 s	
1.5 µL	DNA	72 °C	90 s	
ad 25 µL	distilled water	25 °C	hold	

Genotyping and recombination PCR. To determine the genotype of a mouse, tail DNA, which was isolated as described in 5.4.1, was used. For each allele, specific primers were designed (Table 9). Annealing temperatures and PCR products are indicated in Table 20. To

check whether recombination of sequences flanked by *loxP* or *frt* sites took place, a piece of tissue or a cell pellet was lysed as described in Table 20.

Table 20. Annealing temperatures and PCR products of genotyping and recombination PCRs.
mut = mutated allele; WT = wild type allele; rec = mutated allele without translational stop element after recombination

PCR name	Annealing temperature	PCR products (bp)
Pdx1-Flp	55 °C	620 (mut) / 300 (internal control)
FSF-Kras^{G12D}	55 °C	350 (mut) / 270 (WT)
FSF-Kras^{G12D} recombination	60 °C	196 (rec)
FSF	60 °C	600 (mut)
CreER^{T2}	55 °C	190 (mut)
R26-CAG	62 °C	450 (mut) / 650 (WT)
FSF recombination	60 °C	490 (rec)
Pdk1^{lox}	63 °C	280 (mut) / 200 (WT)
Pdk1^{lox} recombination	63 °C	250 (rec) / 380 (mut) / 350 (WT)
Pdk1^{lox} recombination (microdissection)	touchdown	230 (rec) / 390 (mut)
Mek1^{lox}	72 °C	600 (rec) / 520 (mut) / 470 (WT)
Mek2$^{\Delta}$	62 °C	190 (mut) / 310 (WT)
Trp53^{frt}	57 °C	292 (mut) / 258 (WT)
Ptf1a^{Cre}	60 °C	400 (mut) / 600 (WT)
LSL-Kras^{G12D}	55 °C	170 (mut) / 270 (WT)
R26-PIK3CA^{H1047R}	62 °C	400 (mut) / 600 (WT)
PIK3CA^{H1047R}	64 °C	630 (mut)
LSL-Trp53^{R172H}	60 °C	270 (mut) / 570 (WT)
Renilla	61 °C	600 bp (mut)
Td-Tomato	60 °C	580 bp (mut)
EGFP	64 °C	380 bp (mut)

Touchdown PCR for microdissected PanINs. Genomic DNA from microdissected PanIN lesions was used for a touchdown PCR (Table 21 and Table 22) to check *Pdk1* recombination of single PanINs.

Table 21. Reaction mix for touchdown PCR.

Reaction Mix	
5 µL	10x buffer
1 µL	dNTPs (10 mM each)
1 µL	Pdk1 Recombined forward micro (10 µM)
0.4 µL	Pdk1 Non-Recombined forward micro (10 µM)
0.6 µL	Pdk1 common reverse micro (10 µM)
4 µL	DNA
37.75 µL	distilled water
0.25 µL	Hot Star Taq polymerase

Table 22. Touchdown PCR program for amplification of DNA from microdissected PanIN lesions.

Temperature	**Time**	**Cycles**
95 °C	15 s	1
95 °C	30 s	1
72 °C	30 s	1
72 °C	30 s	1
95 °C	30 s	1
70 °C	30 s	1
71 °C	30 s	1
95 °C	30 s	2
68 °C	30 s	
71 °C	45 s	
95 °C	30 s	2
66 °C	30 s	
71 °C	1 min	
95 °C	30 s	3
65 °C	30 s	
71 °C	1 min	
95 °C	30 s	3
64 °C	30 s	
71 °C	1 min	
95 °C	30 s	47
63 °C	30 s	
71 °C	1 min	
70 °C	2 min	1
25 °C	hold	

5.4.3 Separation of DNA by agarose gel electrophoresis

Nucleic acids were separated by electrophoresis in 1% agarose gels. Agarose was dissolved in 1x TAE buffer by boiling in a microwave. Ethidium bromide which intercalates into DNA was added to the gel prior to gelling. DNA samples were pipetted into the gel pockets and separated at 120 V. For documentation nucleic acids were visualized by excitation with UV light.

5.4.4 Whole exome sequencing of Pdk1-resistant clones

Genomic DNA of cultured cells was isolated by using the QIAamp® DNA Mini kit. DNA concentrations were determined by using the Qubit® dsDNA BR Assay Kit on a Qubit® 2.0 fluorometer. Samples were adjusted to a concentration of 50 ng/µL and a total amount of 3 µg DNA was submitted for 100 bp paired-end whole exome sequencing on the Illumina HiSeq2000 platform at the German Cancer Research Center (DKFZ) Sequencing Core Facility. Bioinformatical preparation was performed by Thomas Engleiter (AG Rad). Raw read sequences were filtered using TrimmOmatic (Bolger et al., 2014). Nucleotides with a Phred quality score Q < 20 at the 3' or 5' end were clipped. Subsequently, reads were mapped to the GRCm38.p3 reference genome (http://www.ensembl.org/index.html) with Burrows-Wheeler transform (BWA) v0.7.12 (Li and Durbin, 2009) using default settings. Duplicates were marked with Picardtools v1.129 (http://picard.sourceforge.net.) for downstream analysis. Realignment and base recalibration were performed with GATK v3.3 (McKenna et al., 2010), followed by variant calling with Mutect v1.1.7 (Cibulskis et al., 2013) using default settings. Mutations were considered as potentially relevant when mutation frequency (f_mut) ≥ 0.05 and read depth at variant site (count_mut) ≥ 8. Copy number changes were detected with CopywriteR (Kuilman et al., 2015). An amplification was indicated by a $\log_2$-ratio > 0.2.

5.4.5 Plasmid DNA isolation from glycerol stocks

An ice splinter from the frozen bacterial glycerol stock was placed into a sterile culture tube containing 0.5 mL LB medium without antibiotics and shaken at 37 °C and 200 rpm in the incubator for 30 min to develop ampicillin resistance. Then 25–50 µL of this bacteria suspension were streaked onto prewarmed LB agar plates containing 100 µg/mL ampicillin and incubated for 15–20 h at 37 °C. Plasmid DNA was amplified by inoculation of 5 mL LB medium with ampicillin (LB-amp) with a single bacterial colony from the agar plates.

After shaking in the incubator at 200 rpm and 37 °C over night, DNA of the saturated culture (OD about 1.1) was prepared with the QIAprep® spin miniprep kit. To obtain higher DNA amounts, 50 mL of LB-amp were inoculated to perform a preparation with the QIAfilter™

plasmid midi kit or 250 mL LB-amp for the use of the EndoFree® plasmid maxi kit, respectively. After that, DNA concentration was assessed by the spectrophotometer NanoDrop 1000. Glycerol stocks were obtained by mixing glycerol and freshly shaken bacterial culture 1:1 and stored at -80 °C.

5.4.6 RNA isolation and cDNA synthesis

RNA isolation from cells. For extraction of RNA, cells were cultured in plates with 10 cm diameter until they reached around 80% confluency. Medium was aspirated and 600 µL of RLT buffer supplemented with 6 µL 2-mercaptoethanol were added to the plate, the lysate was collected with a scraper and stored at -80 °C until further use. RNA isolation was carried out with QIAshredder columns and the RNeasy mini kit according to the manufacturer´s protocol. DNA was digested using the RNase-free DNase set. RNA concentration was determined with the spectrophotometer NanoDrop 1000 and samples were stored at -80 °C or directly used for cDNA synthesis.

cDNA synthesis was performed using the TaqMan® reverse transcription reagents following the manufacturer´s instructions. Generally, 2 µg of RNA were used for generation of cDNA, which was stored at -20 °C.

5.4.7 Quantitative real time PCR

Primer design. To obtain suitable primers for quantitative real time PCR (qRT-PCR), DNA sequences were acquired at www.ncbi.nlm.nih.gov/nucleotide and primers were generated using Primer-Blast at the NCBI homepage (www.ncbi.nlm.nih.gov/tools/primer-blast). The length of the amplicons was 50–150 bp and the binding sites of forward and reverse primer were always separated by an intron to avoid unintentional amplification of genomic DNA.

qRT-PCR was performed with the StepOnePlus™ real time PCR system. As fluorescent DNA binding dye, QuantiFast® SYBR® green PCR master mix was used in a 25 µL mixture. 300 nM both forward and reverse primer (listed in Table 10) were added. mRNA expression was analyzed on 5 µL of 1:5 in TE buffer diluted cDNA in either duplicate or triplicate. The ubiquitously expressed housekeeping gene cyclophilin (CypA) was used as a reference gene. A melt curve was always done after the run to check for unwanted primer dimerization. Data analysis was performed with StepOne™ software and Excel according to the $2^{-\Delta\Delta Ct}$ method or by including a standard curve into the run.

$2^{-\Delta\Delta Ct}$ method. If primer efficiency was between 1.8 and 2.2 (Mukhopadhyay et al., 2008), the $2^{-\Delta\Delta Ct}$ method (Pfaffl, 2001) was used for relative mRNA expression analysis. Calculation was performed as follows:

ΔCt= Ct [gene of interest] – Ct [control gene]

$\Delta\Delta$Ct= ΔCt [treated sample] – ΔCt [reference sample]

$2^{-\Delta\Delta Ct}$ was used for data analysis and presentation of results.

Standard curve method. If exact quantification of the absolute amounts of mRNA was required or the primer efficiency was not sufficient, a standard curve with samples containing known copy numbers was included into the run. Therefore, plasmid DNA from the myristoylated kinase library was applied. The number of molecules per µL was calculated according to the following formula:

$$\frac{molecules}{\mu L} = plasmid\,concentration\left(\frac{g}{\mu L}\right) x \frac{6.022x10^{23}\,\frac{molecules}{mol}}{bp\,plasmid\,x\,660\,\frac{g}{mol}}$$

Serial dilutions in TE buffer were prepared from the plasmid DNA. 5 µL of five standards for each gene of interest were included into the run, the used dilutions were determined by specific mRNA expression level.

5.4.8 RNA sequencing

To compare gene signatures and underlying signaling pathways, whole genome expression analysis of murine pancreatic tumor cells treated with EtOH and 4-OHT was performed. mRNA was extracted as described in 5.4.6. Quality was checked by separating around 500 ng of RNA on a 1% agarose gel at 80 V. In case of intact samples, two intensive bands were observed representing the 28S and 18S ribosomal RNA (rRNA). The 28S rRNA band should be approximately 1.5–2.5 times as intense as the 18S rRNA band. 2 µg of each sample without any degradation or salt contamination were taken for further processing for Illumina sequencing with the TruSeq® Stranded mRNA Sample Preparation Kit with Agencourt AMPure XP Beads and SuperScript II as reverse transcriptase. After first- and second-strand synthesis of cDNA followed by adaptor ligation, DNA fragments with adaptors ligated on both sides were enriched by PCR. The integrity of the cDNA was analyzed on an agarose gel and the quantity was determined by qRT-PCR with primers specific for the barcodes added during the preparation procedure and by using the Qubit® dsDNA BR Assay Kit on a Qubit® 2.0 fluorometer. Highquality samples with product sizes between 200–500 bp were pooled in equimolar concentrations and submitted for 50 bp single read sequencing on the Illumina HiSeq2500 platform at the DKFZ Core Facility. Bioinformatical and statistical analysis of RNA

sequencing data was performed by Maxim Barenboim (AG Rad). Reads were aligned to the mouse genome with TopHat (Trapnell et al., 2009). Counts for each gene were obtained from mapped reads with HTSeq and served as input for the R/BioConductor package DeSeq (version2). DeSeq considers biological variability between independent replicates applying negative binomial distribution. False discovery rate (FDR) was controlled with the Benjamini-Hochberg method so that p values were adjusted for multiple testing accordingly (Benjamini and Hochberg, 1995). For differential expression analysis, fold-changes of counts between treated and control cells were calculated. Analysis of gene set enrichments was performed by the Molecular Signatures Database version 5.1 (Liberzon et al., 2011) on the webpage of the Broad Institute (Cambridge, MA, USA). Genes with $\log_2$-fold changes of < -0.6 and > 0.6 were used as the input for this analysis.

5.5 Protein biochemistry

5.5.1 Protein extraction

Cells were cultured until they reached about 70–80% confluency. Then medium was aspirated, cells were washed with PBS twice and an appropriate volume (e.g. 150 µL for a 10-cm dish) of cold IP lysis buffer supplemented with protease and phosphatase inhibitors was added to the plate. Cells were harvested using a cell scraper and snap frozen in liquid nitrogen. The lysate was stored at -80 °C. For subsequent determination of protein concentration, it was centrifuged at 4 °C and 13200 rpm for 20 min and the supernatant was transferred into a new reaction tube.

5.5.2 Protein concentration estimation

The protein concentrations of cell lysates were determined by using the Bradford assay (Bradford, 1976). 300 µL of Bradford reagent diluted 1:5 in water were placed into a well of a 96-well plate. 1 µL of the sample of interest was added. After 10 min of incubation, absorbance was measured at 600 nm with the microplate reader Anthos 2001 and protein concentration was estimated using a defined BSA dilution series as reference. Each sample was measured in triplicates. By adding protein loading buffer (Laemmli, 1970) and IP buffer, protein concentration of all samples was adjusted to one level. Protein samples were subsequently denatured at 95 °C for 5 min and stored at -20 °C.

5.5.3 SDS polyacrylamide gel electrophoresis (SDS-PAGE)

SDS-PAGE (Laemmli, 1970) using 10% or 12% separating gels depending on the size of the protein of interest was performed to separate the proteins concerning their molecular weight. At first the reagents for the separating gel were mixed, as shown in Table 23. After pouring into a gel caster, the gel was covered with a layer of 2-propanol and allowed to polymerize. After the stacking gel mixture was prepared, poured and polymerized, 80–120 µg of the protein samples were loaded on the SDS polyacrylamide gel. For concentration of the proteins in the stacking gel, electrophoresis was carried out at 80 V for about 45 min. Then proteins were separated at 120 V.

5.5.4 Immunoblot

After separation with SDS-PAGE the proteins were blotted onto a PVDF membrane which was activated previously by incubation in 100% methanol for 30 s and then equilibrated in transfer buffer (Towbin et al., 1979). The proteins were electro-blotted in a tank blot system onto the activated membrane at 100 V and 4 °C for 2 h or at 30 V and 4 °C for 16 h. After protein transfer the membranes were blocked by incubation in 5% BSA in PBS or 5% milk at RT for 30–60 min to prevent unspecific binding of the antibody. Subsequently, the membranes were transferred into a specific primary antibody solution diluted in 5% BSA and incubated at 4 °C over night. After three washing steps with PBS-Tween for each 15 min the membranes were incubated with the secondary antibody diluted in 5% BSA in PBS or 5% milk for 1 h at RT in the dark. Membranes were again washed three times with PBS-Tween for each 15 min and scanned at 700 nm or 800 nm wavelength using Odyssey® infrared imaging system.

Table 23. Recipe for preparation of three SDS polyacrylamide gels.

Compounds	10% separating gel	12% separating gel	Stacking gel
H_2O	6150 µL	5100 µL	4500 µL
Separating gel buffer	3900 µL	3900 µL	-
Stacking gel buffer	-	-	1950 µL
Rotiphorese® gel 30	4950 µL	6000 µL	1125 µL
10% SDS	150 µL	150 µL	75 µL
10% APS	75 µL	75 µL	37.5 µL
TEMED	22.5 µL	22.5 µL	15 µL

5.6 Statistical analysis

Graphical depiction, data correlation and statistical analysis were performed with GraphPad Prism 5. Unless otherwise indicated, all data were obtained from at least three independent experiments and expressed as mean values ± standard deviation (SD) or standard error of mean (SEM). Generally, cell culture-based assays were performed in triplicate, only radioactive glucose uptake assays in quadruplicate. To calculate statistical differences between certain data sets, normality and variance were analyzed and a two-tailed Student's t test was employed. Statistical comparisons between MTT curves were made with a two-way analysis of variance (ANOVA) test. For survival analysis, Kaplan-Meier estimator was used. Log rank test was done for statistical analysis of survival curves. $p < 0.05$ was considered to be statistically significant. If more than one statistical test was performed on a single data set, a Bonferroni-correction was applied to account for the increased possibility of false-positive results. For RNA sequencing analysis, enrichment of gene sets was analyzed using the Molecular Signature Database (Broad Institute, Cambridge, MA, USA). Statistical significance was determined using a nominal p value. Since the significance of the results can be influenced by multiple testing, the FDR was used to estimate the probability that a false-positive result was obtained (Benjamini and Hochberg, 1995). Adjusted p values based on the Fisher´s exact test were provided by the software. Findings with $p < 0.05$ and FDR $q < 0.05$ were considered as statistically significant.

6 Results

6.1 Kras^{G12D}-driven PDAC progression depends on intact Pdk1 expression

Recently, it has been shown that inactivation of *Pdk1* blocks PanIN formation and PDAC initiation in a *Ptf1a*$^{Cre/+}$*;LSL-Kras*$^{G12D/+}$ mouse model (Eser et al., 2013). To investigate the role of Pdk1 as a potential therapeutic target in PDAC, *Pdx1-Flp;FSF-Kras*$^{G12D/+}$*;FSF-R26*$^{CAG\text{-}CreERT2/+}$ mice were crossed with mice harboring either homozygously or heterozygously floxed *Pdk1* (Figure 1A). Hereafter, the resulting mouse models *Pdx1-Flp;FSF-Kras*$^{G12D/+}$*;FSF-R26*$^{CAG\text{-}CreERT2/+}$;*Pdk1*$^{lox/lox}$ and *Pdx1-Flp;FSF-Kras*$^{G12D/+}$*;FSF-R26*$^{CAG\text{-}CreERT2/+}$;*Pdk1*$^{lox/+}$ are abbreviated *Pdk1*$^{lox/lox}$ and *Pdk1*$^{lox/+}$ or referred to as *Pdk1*-KO and control, respectively. This system allowed us to induce Cre expression in the pancreas by application of tamoxifen (TAM) at various disease stages. To study the effect of *Pdk1*-KO during PDAC progression, TAM was administered after formation of PanIN lesions at the age of 3 months. *Pdk1*$^{lox/+}$ animals were used as controls, because it was demonstrated that the deletion of one *Pdk1* allele does not change PanIN or PDAC formation during Kras^{G12D}-driven carcinogenesis (Eser et al., 2013). Moreover, *Pdk1*$^{lox/+}$ controls have the advantage over Pdk1 wild type (WT) controls that it can be excluded that the observed effects on PDAC progression are due to TAM itself. *Pdk1*$^{lox/lox}$ and *Pdk1*$^{lox/+}$ mice were treated with TAM food for 1 month and sacrificed at the age of 9 months. Pancreata of TAM-treated *Pdk1*$^{lox/+}$ controls showed macroscopic signs of tumor development and increased relative pancreas weight. On the contrary, *Pdk1*-KO mice presented with macroscopically normal pancreata and a relative pancreas weight similar to WT mice (Figure 1B). Histological analysis revealed that PanIN lesions of grade 1A, 1B, 2 and 3 were significantly reduced in *Pdk1*-KO mice compared to control mice (Figure 1C,D). The remaining lesions stained positive for Pdk1 (Figure 1C), suggesting incomplete recombination of the *Pdk1* locus. This hypothesis was confirmed by laser capture microdissection of single PanIN lesions and subsequent *Pdk1* recombination PCR. All lesions displayed the floxed *Pdk1* band (Figure 1E). These data show that *Pdk1* deletion blocks Kras^{G12D}-driven PDAC progression.

6.2 An inducible *Pdk1*-KO system *in vitro*

To assess the impact of Pdk1 on PDAC maintenance, pancreatic cancer cell lines from *Pdk1*$^{lox/lox}$ mice without tamoxifen treatment were generated. These cell lines were treated with 4-hydroxytamoxifen (4-OHT) to activate CreER^{T2} expression and thereby delete *Pdk1*. The recombination efficiency of 4-OHT was compared to recombinant Cre protein.

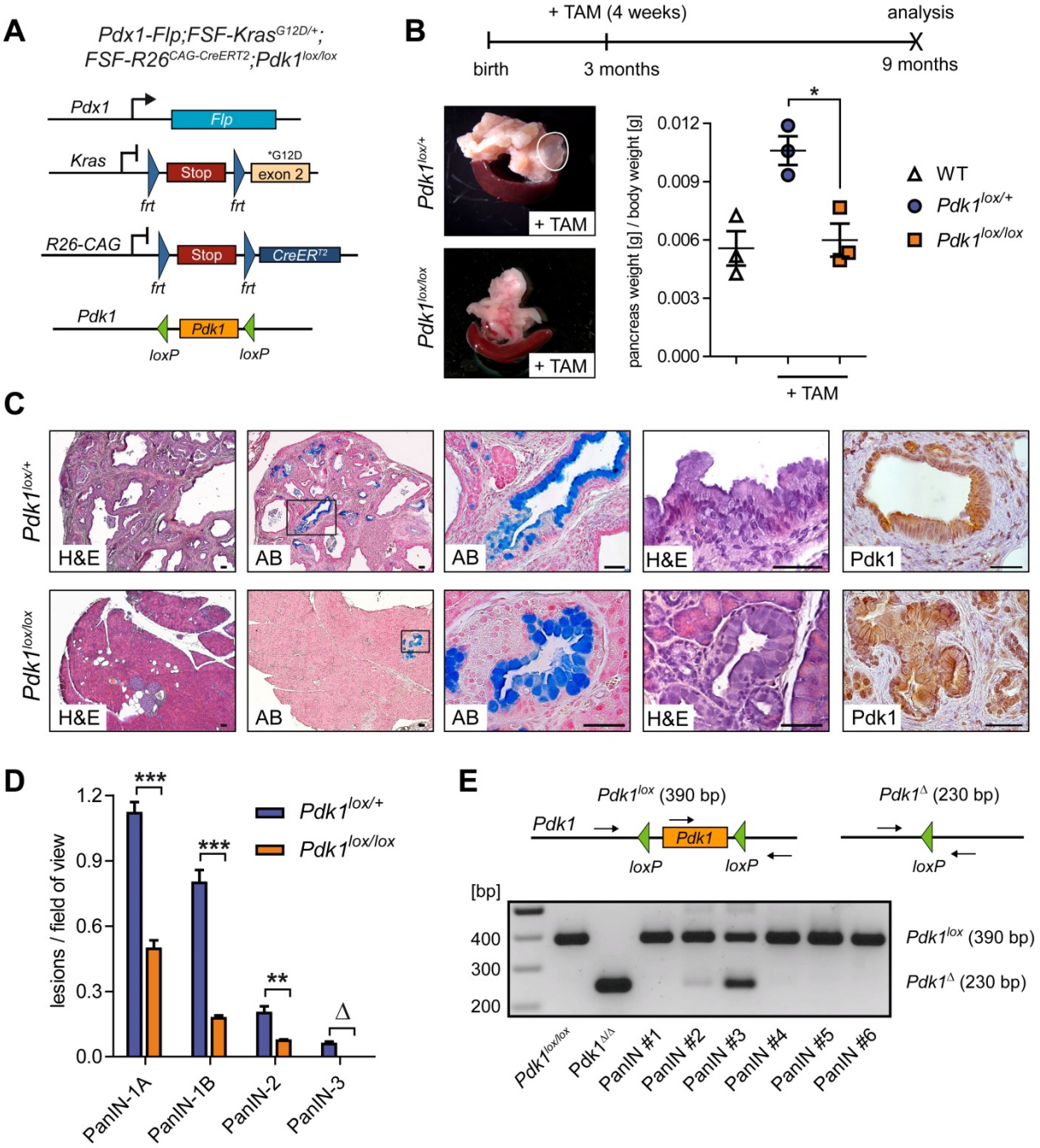

Figure 1. Role of Pdk1 in PDAC progression.
(A) Genetic strategy to delete Pdk1 in established PanIN lesions by time-specific TAM-mediated CreER^{T2} activation. *Pdx1-Flp*-activated expression of Kras^{G12D} induces PanIN lesions and CreER^{T2} is activated in the Flp lineage by TAM administration to delete Pdk1.
(B) Top, schematic of TAM treatment protocol. Bottom, representative macroscopic view (left) and weight (right) of pancreata from TAM-treated *Pdk1$^{lox/lox}$* and age- and sex-matched TAM-treated *Pdk1$^{lox/+}$* controls. Visible signs of tumorigenesis are outlined in white. WT, wild type. Data represent mean ± SEM; n = 3 female mice per genotype; *p = 0.0148, Student's t test.
(C) Representative pancreatic sections of TAM-treated *Pdk1$^{lox/+}$* control (top) and *Pdk1$^{lox/lox}$* (bottom) mice stained with H&E or alcian blue (AB) to visualize mucinous PanIN lesions and immunohistochemical Pdk1 staining. Scale bars indicate 50 µm.

(legend continued on next page)

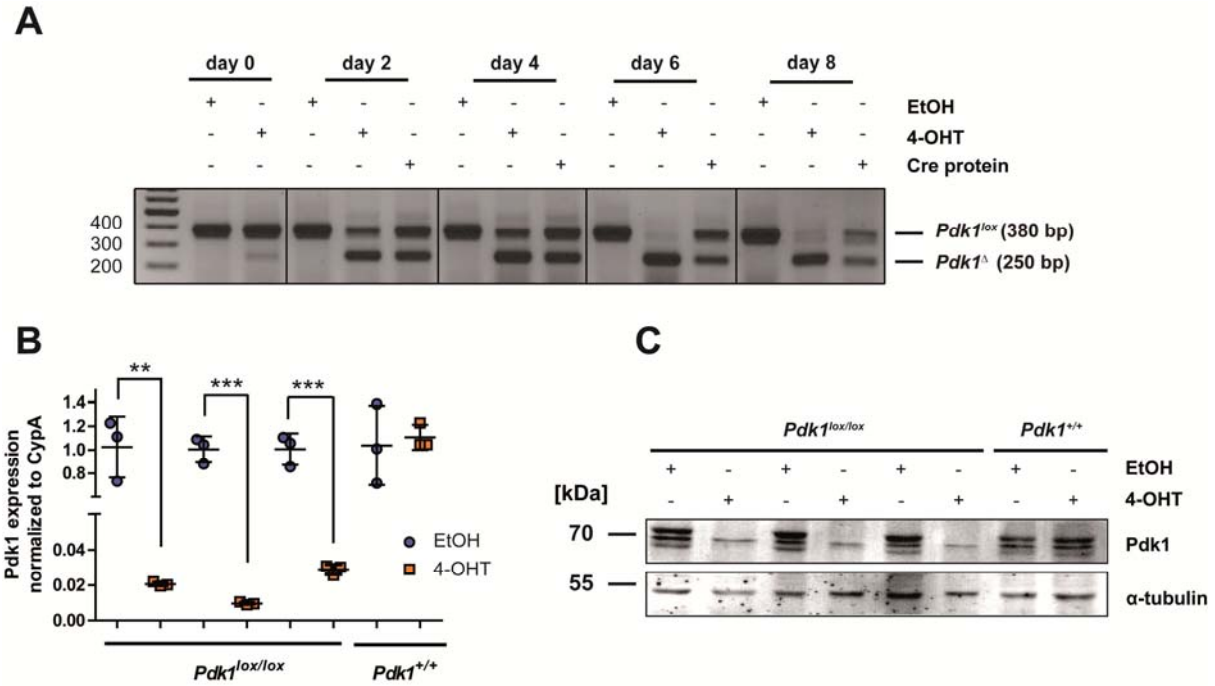

Figure 2. Establishment of an inducible *Pdk1*-KO system *in vitro*.
(A) PDAC cells isolated from *Pdk1*$^{lox/lox}$ mice, which had not been treated with TAM, were incubated with ethanol (EtOH) as control or with 600 nM 4-hydroxytamoxifen (4-OHT) to delete Pdk1. Recombination PCR was performed after 2 d, 4 d, 6 d and 8 d of treatment and recombination efficiency was compared to Cre protein treatment.
(B) qRT-PCR analysis of Pdk1 mRNA expression in *Pdk1*$^{lox/lox}$ and *Pdk1*$^{+/+}$ cells after 8 d of 4-OHT treatment. Data are shown as fold change versus EtOH-treated controls. ***p < 0.001, **p < 0.01, Student's t test. The experiment was performed by Constanze Mattes.
(C) Immunoblot analysis of Pdk1 expression in *Pdk1*$^{lox/lox}$ and *Pdk1*$^{+/+}$ cells after 8 d of 4-OHT treatment. α-tubulin served as loading control. The experiment was performed by Constanze Mattes.

Cells were treated with 600 nM 4-OHT or 5 µM Cre protein, respectively, and DNA was harvested at days 0, 2, 4, 6 and 8. As depicted in Figure 2A, an incubation with 4-OHT for 6 d led to a complete recombination of *loxP* sequences surrounding exons 3 and 4 of *Pdk1*. Treatment with Cre protein was less efficient yielding only partial *Pdk1* recombination. It was decided to pretreat PDAC cells with 600 nM of 4-OHT for 8 d for subsequent functional experiments. For this time point, the *Pdk1* deletion was confirmed on RNA and protein level by quantitative real time PCR (qRT-PCR) and western blot, respectively (Figure 2B,C). As expected, treatment with 600 nM of 4-OHT did not impair Pdk1 expression in *Pdk1*$^{+/+}$ cells. To conclude, the inducible *Pdk1*-KO system is functional and suitable to study the effect of *Pdk1*-KO on PDAC cells *in vitro*.

(D) Absolute quantification of PanIN lesions in 9-month-old sex-matched TAM-treated mice with genotypes as indicated (mean ± SEM; n = 3 female mice per genotype; 3 representative slides per mouse; ***p < 0.001, **p < 0.01, Student's t test; Δp = 0.05, Fisher's exact test).
(E) Top, genotyping strategy to detect *Pdk1* alleles. Bottom, PCR analysis of non-recombined *Pdk1*$^{lox/lox}$ DNA from a mouse without Cre expression, recombined pancreatic tissue from a *Ptf1a*$^{Cre/+}$;*LSL-Kras*$^{G12D/+}$;*Pdk1*$^{lox/lox}$ (*Pdk1*$^{Δ/Δ}$) mouse (positive control for recombined allele) and microdissected PanIN lesions from TAM-treated *Pdk1*$^{lox/lox}$ mice (modified from Schönhuber et al., 2014).

6.3 *Pdk1* deletion impairs growth of PDAC cells *in vitro*

The consequences of *Pdk1* inactivation in Kras^{G12D}-driven PDAC cell lines were analyzed by viability assays. In order to accelerate tumorigenesis, *Pdk1$^{lox/lox}$* mice were interbred with the *LSL-Trp53$^{R172H/+}$* mouse line (Olive et al., 2004). After deletion of the *LSL* cassette by Cre recombinase, oncogenic Trp53^{R172H} is expressed, which corresponds to the *TP53^{R175H}* mutation commonly found in human cancers. Three *Pdk1$^{lox/lox}$;LSL-Trp53$^{R172H/+}$* cell lines were generated and treated for 8 d with 600 nM 4-OHT to delete Pdk1 or with vehicle (EtOH). Subsequently, behavior of PDAC cells was studied by MTT and clonogenic assays. The growth of all tested pancreatic cancer cell lines was significantly impaired upon *Pdk1* deletion (Figure 3A) and colony formation was strongly reduced (Figure 3F). Moreover, *Pdk1$^{lox/lox}$;Trp53$^{frt/+}$* cells, harboring an *frt*-flanked Trp53 allele (*Trp53$^{frt/+}$*) (Lee et al., 2012), were generated and the experiment was repeated yielding the same result. Treatment with 4-OHT blocked cell viability, growth and colony formation almost completely (Figure 3B,F). Several control experiments were performed to validate that the *Pdk1* deletion is responsible for this effect. First, the same experiment was performed on a cell line without *CreER^{T2}* to exclude tamoxifen cytotoxicity (Figure 3C,F). In addition to *Pdk1* deletion, oncogenic Trp53^{R172H} is activated by 4-OHT administration in *Pdk1$^{lox/lox}$;LSL-Trp53$^{R172H/+}$* cells. However, *Pdk1$^{+/+}$;LSL-Trp53$^{R172H/+}$* cells grew normally after 8 d of 4-OHT treatment and the number of colonies formed in the clonogenic assay remained unchanged (Figure 3D,F). This experiment demonstrated that neither Cre expression itself nor expression of Trp53^{R172H} were responsible for the observed effects in *Pdk1*-KO cells. Consistent with previous data about Pdk1 during PDAC initiation (Eser et al., 2013) and progression (Figure 1), *Pdk1$^{lox/+}$;LSL-Trp53$^{R172H/+}$* cells were not affected by 4-OHT treatment suggesting that heterozygous *Pdk1* deletion has no inhibitory effect on PDAC growth (Figure 3E,F).

To conclude, Pdk1 expression is essential for Kras^{G12D}-driven PDAC maintenance *in vitro*. For better readability, all *Pdk1*-KO cell lines will be abbreviated as *Pdk1$^{lox/lox}$* in the following sections, unless the Trp53 status is important for the results.

6.4 Rsk2 is an important Pdk1 downstream effector in PDAC

Pdk1 activates diverse signaling pathways via distinct functional domains: The PH domain mediates activation of Akt kinases, whereas the PIF-pocket domain is essential for signaling through S6K, RSK, SGK and PKC isoforms (Bayascas et al., 2008). Although investigation of downstream substrates of Pdk1 is of fundamental importance for the development of highly specific targeted therapies, the functional role of these substrates is poorly defined in pancreatic cancer. Akt is activated by phosphorylation of S473 and T308, which is mediated

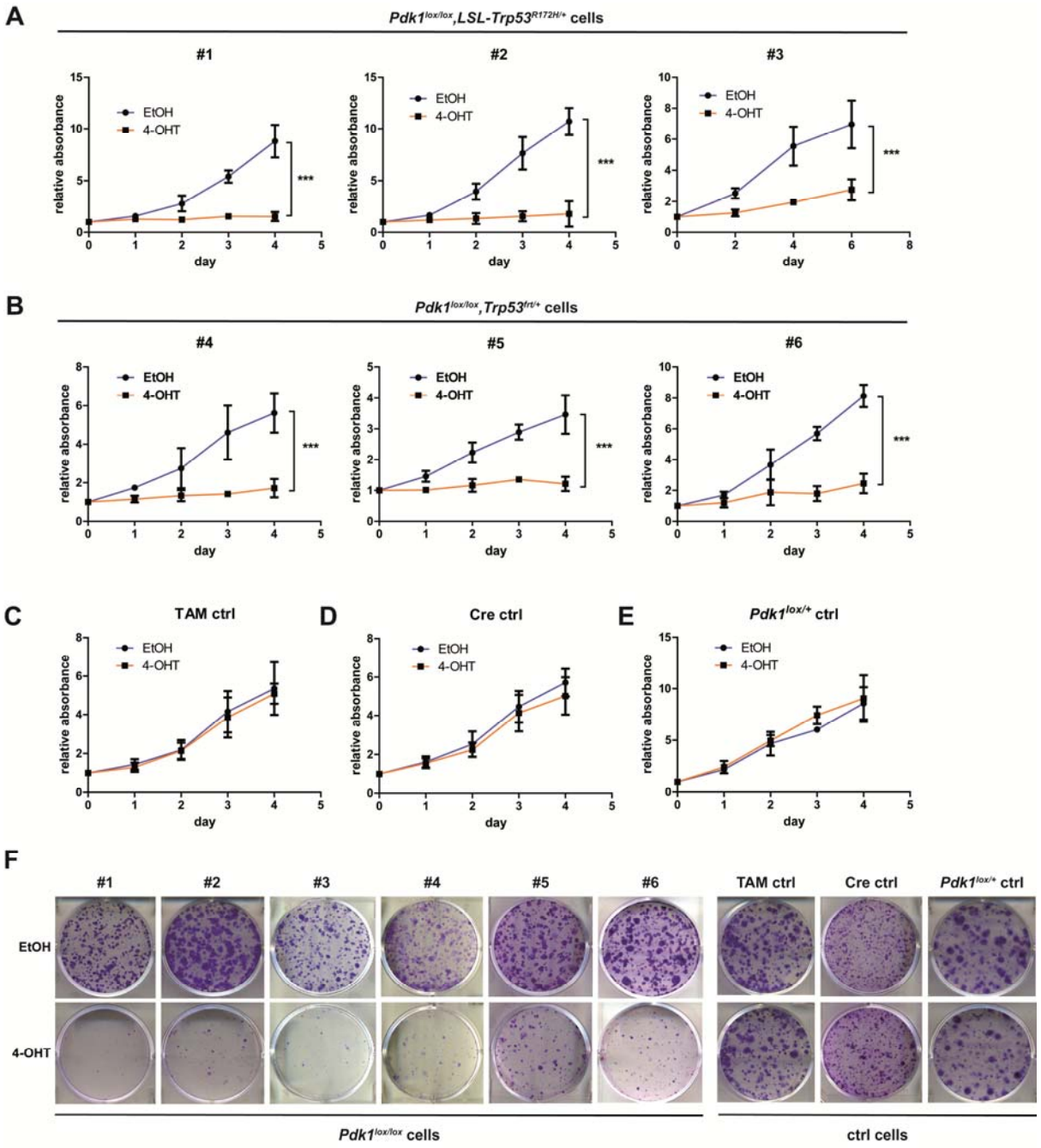

Figure 3. Deletion of *Pdk1* impairs proliferation and colony formation in primary PDAC cell lines *in vitro*.
(A) MTT assays of 4-OHT-treated *Pdk1*$^{lox/lox}$*;LSL-Trp53*$^{R172H/+}$ cell lines compared to EtOH-treated ones. Data are shown as mean ± SD; n = 3 replicates. ***p < 0.001, two-way ANOVA.
(B) MTT assays of 4-OHT-treated *Pdk1*$^{lox/lox}$*;Trp53*$^{frt/+}$ cells compared to EtOH-treated cells. Data are shown as mean ± SD; n = 3 replicates. ***p < 0.001, two-way ANOVA.
(C) MTT assays of 4-OHT-treated *Pdx1-Flp;FSF-Kras*^{G12D} control cells compared to EtOH-treated cells. Data are shown as mean ± SD; n = 3 replicates.
(D) Clonogenic assays of *Pdk1*$^{lox/lox}$ cells and control cells treated with EtOH (upper row) and 4-OHT (lower row). A representative image of n = 3 experiments is shown.

by mTOR and Pdk1, respectively (Alessi et al., 1997; Stephens et al., 1998). Rsk2 is phosphorylated at T577 of the C-terminal kinase domain (CTKD), T365 and S369 by Erk

(Cho et al., 2009; Smith et al., 1999), leading to Rsk2 autophosphorylation by CTKD at S386. Thus, Pdk1 is recruited and can phosphorylate S227 in the N-terminal kinase domain (Jensen et al., 1999) resulting in fully activated Rsk2. Immunoblot analysis of *Pdk1*-depleted cells demonstrated dephosphorylation of Akt at T308 and Rsk2 at S227 upon *Pdk1* elimination (Figure 4A). Thereby, both serine/threonine kinases were inactivated. In order to analyze the functional importance of Rsk2, *Pdk1*$^{lox/lox}$ cells were transduced with an empty vector (EV) or an expression vector of human myristoylated RSK2 (RSK2-myr) (Boehm et al., 2007) and treated with 4-OHT or vehicle for 8 d before analysis by MTT and clonogenic assays. The RSK2-myr expression vector was functional, as verified by qRT-PCR (Figure 4B). As expected, *Pdk1* deletion resulted in a cytostatic effect in 4-OHT-treated EV cells.

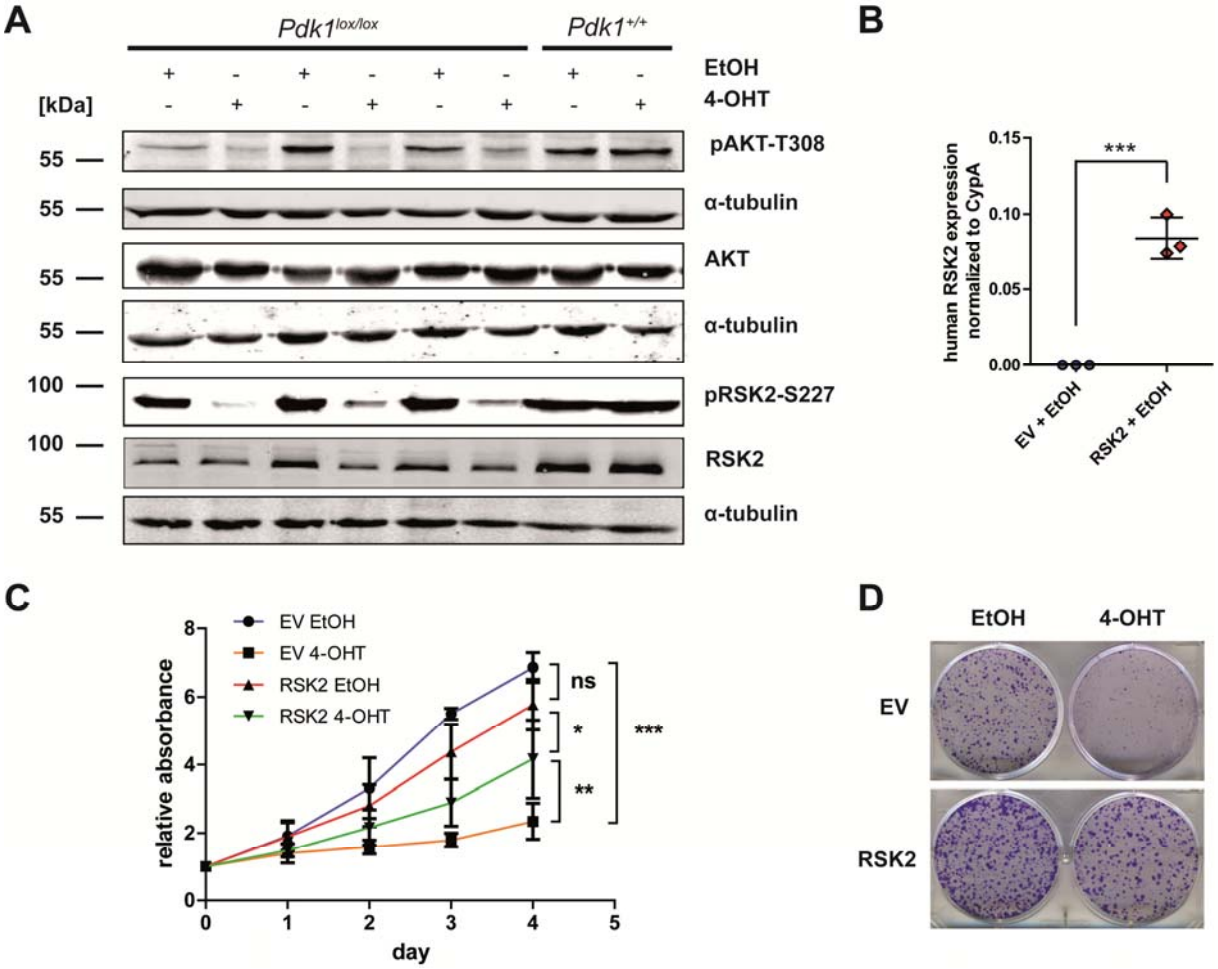

Figure 4. *Pdk1*-KO phenotype is partially mediated by RSK2 signaling.
(A) Immunoblot analysis of Pdk1 downstream signaling in 4-OHT-treated *Pdk1*$^{lox/lox}$ cell lines compared to EtOH-treated controls. α-tubulin served as loading control.
(B) qRT-PCR of human RSK2 expression in cells transduced with empty vector (EV) compared to RSK2-myr (RSK2) expression vector. ***p < 0.001, Student's t test.
(C) MTT assay of EtOH- and 4-OHT-treated *Pdk1*$^{lox/lox}$ cells transduced with EV or RSK2 expression plasmid. Data are shown as mean ± SD; n = 3 replicates. ***p < 0.001, **p < 0.01, *p < 0.05, ns p > 0.05, stepwise two-way ANOVA with Bonferroni correction.
(D) Clonogenic assay of EtOH- and 4-OHT-treated EV and RSK2 cells. A representative picture is shown, n = 3 replicates.

Expression of a myristoylated form of RSK2, which activates RSK2, did not impair the growth compared to EV when cells were cultured with EtOH. In the presence of 4-OHT, RSK2-myr cells significantly grew more and formed more colonies than EV cells. However, RSK2-myr cells treated with 4-OHT did not grow as fast as RSK2-myr cells treated with EtOH (Figure 4C,D). To summarize, this experiment demonstrates that Rsk2 is able to rescue the *Pdk1*-KO phenotype partially, suggesting that Rsk2 is an important Pdk1 effector molecule in PDAC.

6.5 *Pdk1* deletion has slight effects on cell cycle regulators

Since deletion of *Pdk1* resulted in such a strong reduction of cell viability and colony formation, the cell cycle of *Pdk1*-KO and control cells was analyzed in more detail. It was shown that Pdk1 regulates the cell cycle in mouse embryonic fibroblasts by controlling cyclin D1 and p27 expression (Nakamura et al., 2008). However, no alterations of cyclin D1 and p27 were observed after treatment of *Pdk1*$^{lox/lox}$ PDAC cells with EtOH or 4-OHT for 8 d. Phosphorylation of the retinoblastoma protein (RB) at S807/11 was not changed upon *Pdk1*

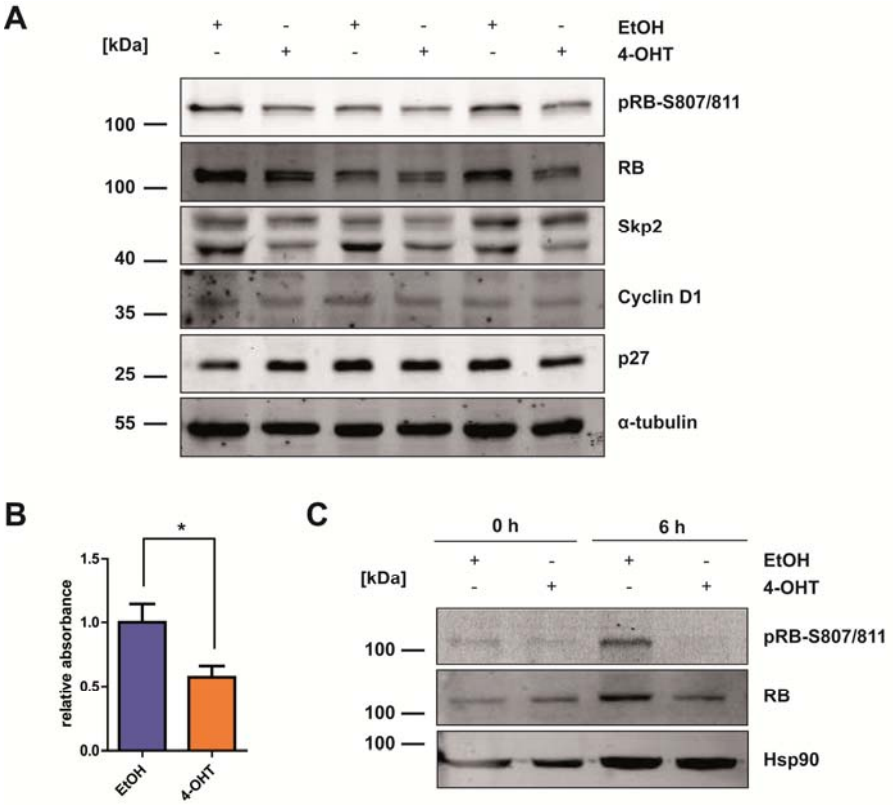

Figure 5. Effects of *Pdk1* deletion on the cell cycle.
(A) Immunoblot analysis for cell cycle genes of *Pdk1*$^{ox/lox}$ cells treated with EtOH or 4-OHT for 8 d. α-tubulin was used as loading control.
(B) BrdU assay of 4-OHT-treated *Pdk1*$^{lox/lox}$ cell lines compared to controls. Data are shown as mean ± SD; n = 3 replicates. *p < 0.05, Student´s t test.
(C) Immunoblot analysis of EtOH- and 4-OHT-treated cells after starvation of cells by removing FCS for 72 h. Hsp90 served as loading control.

deletion. Quantification using the Odyssey software revealed that the ratio of pRB relative to RB was 0.88, 0.8 and 1.19 for 4-OHT-treated cells when normalized to EtOH controls, respectively. One splice variant of the oncogene S-phase kinase-associated protein 2 (Skp2), which is involved in ubiquitination and degradation of cell cycle regulators like p21 and p27, was downregulated in *Pdk1*-KO cells (Figure 5A). By using a colorimetric BrdU assay, significantly less BrdU was shown to be incorporated in S phase in *Pdk1*-KO cells compared to control cells (Figure 5B). To analyze whether the effects on cell cycle regulators on the protein level could be potentiated, cells were synchronized by serum starvation for 3 d. As demonstrated in Figure 5C, EtOH-treated cells showed RB phosphorylation 6 h after reapplication of serum, whereas 4-OHT-treated cells failed to re-enter the cell cycle.
To summarize, *Pdk1* deletion has some effects on the cell cycle although they are probably not strong enough to explain the *Pdk1*-KO phenotype. However, it is also possible that Pdk1 exerts effects on other cell cycle-regulated genes, which have not been analyzed in this work.

6.6 Glucose metabolism is impaired upon *Pdk1*-KO in PDAC cells

To gain further mechanistic insight into the molecular consequences upon *Pdk1* deletion, global RNA expression changes were analyzed by RNA sequencing experiments. Two *Pdk1*$^{lox/lox}$;*LSL-Trp53*$^{R172H/+}$ cell lines were treated for 8 d with EtOH or 4-OHT and RNA was isolated, prepared and submitted for sequencing. Around 85% of obtained reads were mapped to the mouse genome. For analysis of differentially expressed genes, counts were computed by DeSeq and fold-changes were calculated. 11 genes were significantly up- and 15 were downregulated in *Pdk1*-KO cells, respectively. Deletion of *Pdk1* could not be observed in the RNA sequencing data, since the floxed exons 3 and 4 are very short. *Pdk1* elimination was verified instead by qRT-PCR using exon-specific primers (as shown in Figure 2B). The *Trp53* mRNA level was 26.7-fold increased in 4-OHT-treated compared to EtOH-treated cells. Thus, *Trp53* was the top upregulated gene upon 4-OHT treatment (log_2-fold change TAM/EtOH = 4.74, p = 3.6E-72, adjusted p = 4.6E-68). Since oncogenic Trp53^{R172H} was expressed in *Pdk1*$^{lox/lox}$;*LSL-Trp53*$^{R172H/+}$ cells upon CreER^{T2} activation, this finding validates the RNA sequencing data as a proof of principle. Histone deacetylase 9 (*Hdac9*) represented another significantly upregulated gene in *Pdk1*-KO cells (log_2-fold change TAM/EtOH = 1.40, p = 3.6E-06, adjusted p = 0.0052). This histone-modifying enzyme has recently been described as a potential tumor suppressor in Kras-driven lung cancer (Okudela et al., 2014) and might therefore be relevant to pancreatic carcinogenesis as well. Interestingly, expression of fructose-1,6-bisphophatase isozyme 2 (Fbp2), which is involved

in gluconeogenesis and glycolysis, was strongly reduced upon *Pdk1* ablation (log_2-fold change TAM/EtOH = -1.33, p = 1.1E-05, adjusted p = 0.0127).

To systematically identify signaling pathways which were affected due to *Pdk1* deletion, gene set enrichment analysis was performed. The DePinho group showed that many glycolysis genes are around 25%–50% downregulated in pancreatic tumors after $Kras^{G12D}$ extinction compared to controls (Ying et al., 2012). This observation could be reproduced in an initial microarray experiment on *Pdk1*-KO cells (data not shown). Therefore, the thresholds for genes considered up- or downregulated upon tamoxifen application were defined as log_2 (TAM/EtOH) > 0.6 or log_2 (TAM/EtOH) < -0.6 in this study. Accordingly, 136 genes were included as downregulated and 133 genes as upregulated upon 4-OHT treatment. Enrichment of KEGG and REACTOME gene sets in *Pdk1*-KO or control cells was assessed by using the Molecular Signature Database (Broad Institute). Neither *Pdk1*-KO nor control cells showed an enrichment of cell cycle-related gene sets. *Pdk1*-KO cells displayed an upregulation of axon guidance and cell-cell interaction gene sets. Netrin1 signaling, another gene set enriched upon *Pdk1* deletion, plays a role in axonal guidance as well as in neuronal migration and morphogenesis (Table 24).

Table 24. Potentially relevant gene signatures upregulated upon *Pdk1* deletion.

KEGG gene set	**Gene overlap**	**p value**	**FDR q value**
AXON_GUIDANCE	7/129	4.47E-8	8.32E-6
ABC_TRANSPORTERS	3/44	1.97E-4	1.84E-2
P53_SIGNALING_PATHWAY	3/69	7.45E-4	4.08E-2
REACTOME gene set	**Gene overlap**	**p value**	**FDR q value**
AXON_GUIDANCE	7/251	3.97E-6	2.67E-3
SEMAPHORIN_INTERACTIONS	4/68	2.87E-5	6.44E-3
DEVELOPMENTAL_BIOLOGY	7/396	7.36E-5	1.24E-2
NETRIN1_SIGNALING	3/41	1.6E-4	2.15E-2

Table 25. Potentially relevant gene signatures upregulated in control cells.

KEGG gene set	**Gene overlap**	**p value**	**FDR q value**
TERPENOID_BACKBONE_BIOSYNTHESIS	5/15	4.2E-10	3.97E-8
GLYCOLYSIS_GLUCONEOGENESIS	7/62	4.27E-10	3.97E-8
STEROID_BIOSYNTHESIS	5/17	8.62E-10	4.75E-8
METABOLISM_OF_XENOBIOTICS_BY_ CYTOCHROME_P450	7/70	1.02E-9	4.75E-8
DRUG_METABOLISM_CYTOCHROME_P450	6/72	5.08E-8	1.89E-6
PHENYLALANINE_METABOLISM	3/18	1.59E-5	4.94E-4
RETINOL_METABOLISM	4/64	3.01E-5	8.01E-4

KEGG gene set	**Gene overlap**	**p value**	**FDR q value**
PEROXISOME	4/78	6.57E-5	1.53E-3
FRUCTOSE_AND_MANNOSE_METABOLISM	3/34	1.13E-4	2.34E-3
TYROSINE_METABOLISM	3/42	2.14E-4	3.97E-3
ARACHIDONIC_ACID_METABOLISM	3/58	5.56E-4	9.4E-3
GLYOXYLATE_AND_DICARBOXYLATE_ METABOLISM	2/16	8.73E-4	1.35E-2
ASCORBATE_AND_ALDARATE_METABOLISM	2/25	2.15E-3	3.07E-2
GALACTOSE_METABOLISM	2/26	2.32E-3	3.08E-2
PENTOSE_PHOSPHATE_PATHWAY	2/27	2.5E-3	3.1E-2
PENTOSE_AND_GLUCURONATE_ INTERCONVERSIONS	2/28	2.69E-3	3.13E-2
HISTIDINE_METABOLISM	2/29	2.88E-3	3.16E-2
GLYCINE_SERINE_AND_THREONINE_ METABOLISM	2/31	3.29E-3	3.4E-2
PROPANOATE_METABOLISM	2/33	3.72E-3	3.65E-2
PYRUVATE_METABOLISM	2/40	5.43E-3	4.81E-2
REACTOME gene set	**Gene overlap**	**p value**	**FDR q value**
CHOLESTEROL_BIOSYNTHESIS	10/24	3.16E-20	2.13E-17
METABOLISM_OF_LIPIDS_AND_LIPOPROTEINS	15/478	5.2E-12	1.75E-9
BIOLOGICAL_OXIDATIONS	7/139	1.24E-7	2.79E-5
O_LINKED_GLYCOSYLATION_OF_MUCINS	4/59	2.18E-5	3.68E-3
TERMINATION_OF_O_GLYCAN_BIOSYNTHESIS	3/24	3.9E-5	4.13E-3
GLUCOSE_METABOLISM	4/69	4.06E-5	4.13E-3
PHASE_II_CONJUGATION	4/70	4.29E-5	4.13E-3
SLC_MEDIATED_TRANSMEMBRANE_TRANSPORT	6/241	5.69E-5	4.8E-3
GLYCOLYSIS	3/29	6.98E-5	5.23E-3
GLUCONEOGENESIS	3/34	1.13E-4	7.63E-3
TRANSMEMBRANE_TRANSPORT_OF_SMALL_ MOLECULES	7/413	1.52E-4	9.3E-3
POST_TRANSLATIONAL_PROTEIN_MODIFICATION	5/188	1.78E-4	9.98E-3
METABOLISM_OF_CARBOHYDRATES	5/247	6.2E-4	3.21E-2
PHASE1_FUNCTIONALIZATION_OF_COMPOUNDS	3/70	9.63E-4	4.64E-2

Interestingly, *Pdk1* ablation resulted in a statistically significant downregulation of numerous metabolic gene sets like glucose metabolism, biosynthesis of cholesterol and steroids, amino acid metabolism and glycosylation (Table 25). This finding suggests that Pdk1 is essential for

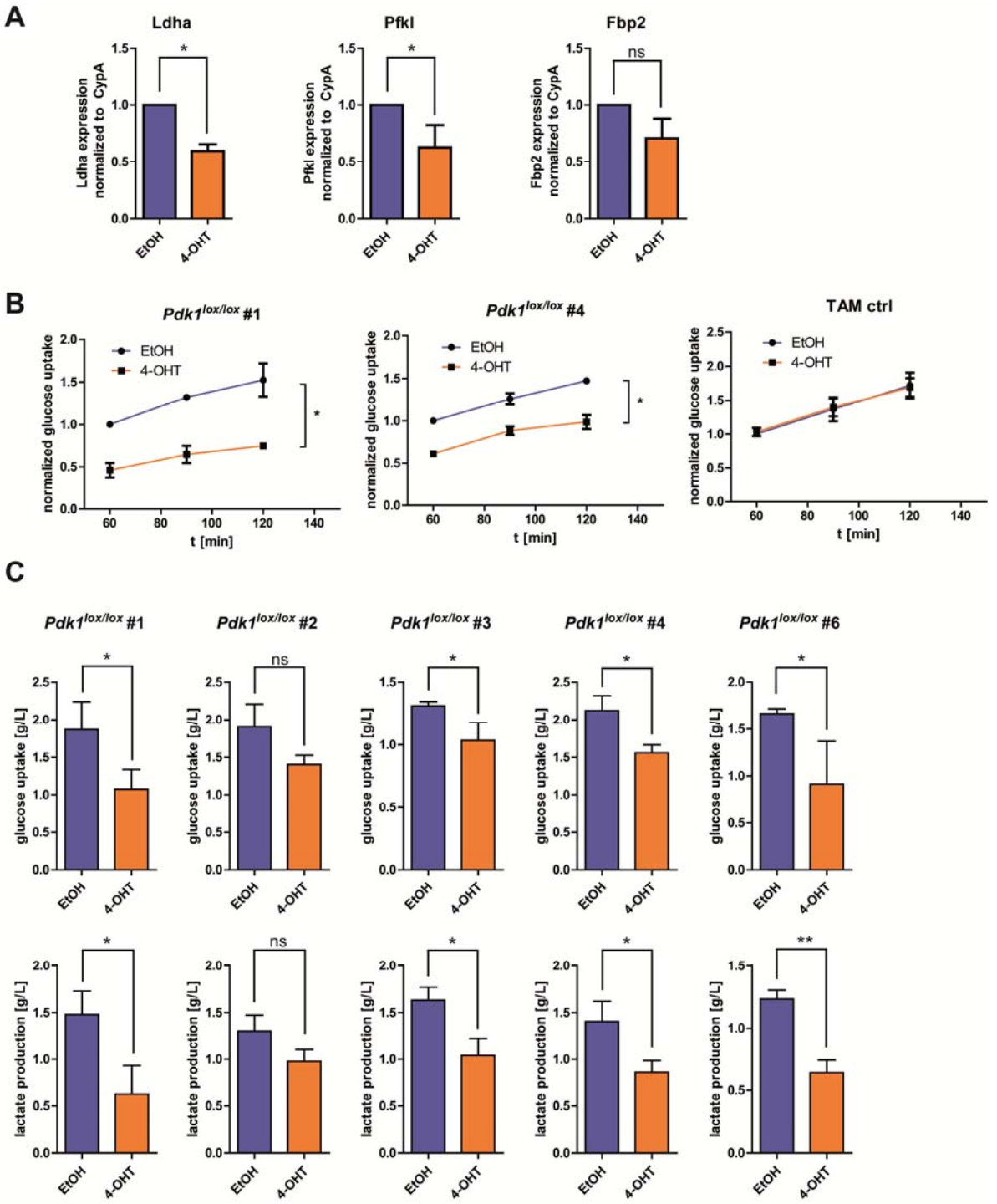

Figure 6. Pdk1 controls tumor metabolism by stimulation of glucose uptake.
(A) qRT-PCR of genes involved in glucose metabolism after treatment of three *Pdk1*$^{lox/lox}$*;Trp53*$^{frt/+}$ cell lines with EtOH and 4-OHT for 8 d. *p < 0.05, paired Student´s t test.
(B) Two *Pdk1*$^{lox/lox}$ cell lines and a control were treated with EtOH and 4-OHT for 8 d. F18-FDG uptake was measured at indicated time points. Data are shown as mean ± SD; n = 3 replicates. *p < 0.05, two-way ANOVA.
(C) Medium of six *Pdk1*$^{lox/lox}$ cell lines treated with EtOH and 4-OHT was analyzed by the YSI 2950 biochemistry analyzer to determine the effect of Pdk1 ablation on relative changes of glucose uptake and lactate production. Data are shown as mean ± SD; n = 3 replicates. *p < 0.05, **p < 0.01, Student´s t test.

metabolic reprogramming of cancer cells and plays a pivotal role in controlling tumor cell metabolism. To exclude any effects of $Trp53^{R172H}$, these results were verified by qRT-PCR for genes involved in glucose metabolism by using 4-OHT- and EtOH-treated *Pdk1*$^{lox/lox}$*;Trp53*$^{frt/+}$ cells. Thereby, it was proven that *Pdk1* deletion results in a significant downregulation of lactate dehydrogenase A (Ldha), the enzyme responsible for converting pyruvate to lactate. Moreover, expression of the liver isoform of the rate-limiting glycolytic enzyme phosphofructokinase (Pfkl), mediating the conversion of fructose-6-phosphate to fructose-1,6-bisphosphate, was reduced in *Pdk1*-KO cells. Fbp2, which catalyzes the opposite reaction, was shown to be downregulated to 40% in *Pdk1*$^{lox/lox}$;*LSL-Trp53*$^{R172H/+}$ cells by the RNA sequencing data. However, qRT-PCR revealed only a tendency of Fbp2 being reduced to 70% upon *Pdk1* deletion in *Pdk1*$^{lox/lox}$*;Trp53*$^{frt/+}$ cells (Figure 6A).

To functionally validate the effect of Pdk1 on glucose metabolism, *Pdk1*$^{lox/lox}$ cells were treated for 8 d with EtOH or 4-OHT and a glucose uptake assay was performed using radioactively labelled glucose (F18-FDG). Upon *Pdk1* ablation, cells showed a strong reduction in glucose uptake. No change of glucose uptake instead was observed in control cells excluding effects of 4-OHT on glucose metabolism (Figure 6B). These results were confirmed by an enzymatic assay measuring glucose and lactate in the cell culture supernatant. As depicted in Figure 6C, *Pdk1* deletion led to significantly decreased glucose uptake and lactate production in 4 out of 5 different cell lines, demonstrating that Pdk1 enhances the glycolytic flux in PDAC.

To summarize, transcriptomic and metabolic analyses indicate that Pdk1 serves an important role in controlling tumor metabolism, which can be explained at least partially through stimulation of glucose uptake.

6.7 Generation of Pdk1-independent clones

To analyze resistance mechanisms towards *Pdk1* ablation, *Pdk1*$^{lox/lox}$ cell lines were treated with 4-OHT for 8 d and seeded in the same setting like for a clonogenic assay. For each cell line, growing colonies were picked and recultured until DNA could be isolated and cells could be frozen for further analysis. By this approach, 13–26 clones were generated for each cell line, respectively. As demonstrated in Figure 7A, *Pdk1* recombination of growing colonies was verified by PCR. In five of six cell lines, around 30% of colonies were Pdk1-independent clones whereas one cell line did not yield any recombined clones. The remaining colonies arose due to incomplete recombination, since recombination efficiency was not 100% (Figure 7B). Seven of the clones resistant to *Pdk1* inactivation were submitted to an MTT assay. These clones presented with a significantly increased growth compared to the parental

A

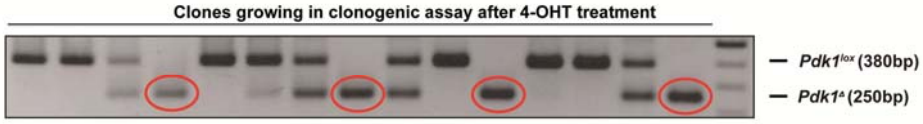

B

Cell line	recombined	not completely recombined
Pdk1$^{lox/lox}$ #1	6 (23.1%)	20 (76.9%)
Pdk1$^{lox/lox}$ #2	6 (33.3%)	12 (66.7%)
Pdk1$^{lox/lox}$ #3	6 (24.0%)	19 (76.0%)
Pdk1$^{lox/lox}$ #4	0 (0%)	21 (100%)
Pdk1$^{lox/lox}$ #5	4 (30.8%)	9 (69.2%)
Pdk1$^{lox/lox}$ #6	5 (22.7%)	17 (77.3%)

C

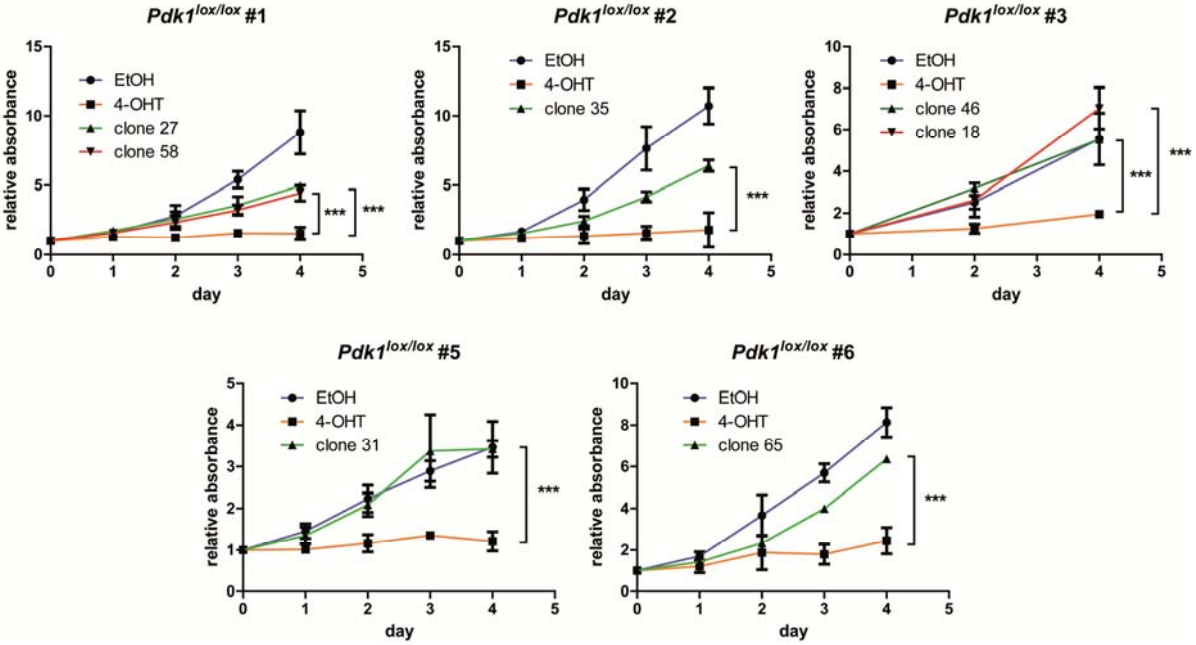

Figure 7. Generation of Pdk1-independent clones.
Pdk1$^{lox/lox}$ cell lines were treated with 4-OHT for 8 d and seeded for a clonogenic assay. Growing clones were picked and recultured.
(A) Recombination of the *Pdk1* locus was assessed by PCR. Pdk1-independent clones are highlighted by red circles.
(B) Frequency of fully recombined clones derived from five *Pdk1*$^{lox/lox}$ cell lines.
(C) MTT assays of Pdk1-independent clones in comparison to the EtOH- and 4-OHT-treated parental *Pdk1*$^{lox/lox}$ cell line. Data are shown as mean ± SD; n = 3 replicates. ***p < 0.001, two-way ANOVA.

Pdk1$^{lox/lox}$ cell line treated with 4-OHT. Growth of parental cells and clones was indistinguishable in slower growing cell lines. However, in case of faster growing cells, the clones proliferated less than the parental EtOH-treated cell line (Figure 7C). To summarize, a subpopulation of PDAC cells survived *Pdk1* inactivation and gave rise to resistant clones, although the majority of cells showed a marked response towards *Pdk1* deletion.

To gain further insights into resistance mechanisms towards *Pdk1* inactivation, whole exome sequencing of six resistant clones was performed. EtOH-treated cells and tails served as controls. First of all, the Kras status of cell lines and clones was analyzed using the whole exome sequencing and copy number variation (CNV) data of the *Kras* locus (Table 26). In

the sequencing data of the tail DNA, around half of the reads presented a cytosine (C) leading to the amino acid G at codon 12 and the other half a thymine (T) leading to amino acid D at position 12. This means that in the tail DNA one *Kras*^{G12D} and one *Kras WT* allele were present as expected. The EtOH-treated parental cell lines displayed heterogeneous Kras allelic ratios. Two of them were heterozygous for mutant *Kras*, two of them heterozygous with an increased fraction of mutant *Kras* and one of them homozygous for mutant *Kras*. Moreover, a $\log_2$ value > 0.2 for the *Kras* locus in the CNV analysis indicated the presence of more than two chromosomes. By combining sequencing and CNV data, increased frequencies of mutant *Kras* concomitantly with a $\log_2$ value > 0.2 were explained as amplification of *Kras*^{G12D}. However, these conclusions have to be validated by fluorescence *in situ* hybridisation (FISH).

Table 26. Kras status in Pdk1-independent clones. Data of parental cells are depicted in gray.

Description	**Whole exome sequencing**	**Zygosity status for *Kras*^{G12D}**	**Copy number variation (CNV)**
Pdk1$^{lox/lox}$ #1 E8	50% C (WT), 50% T (mut)	heterozygous	
Pdk1$^{lox/lox}$ #1 clone 27	21% C (WT), 79% T (mut)	heterozygous	*Kras* amplification, $\log_2$ value = 0.2965
Pdk1$^{lox/lox}$ #1 clone 58	100% T (mut)	homozygous	
Pdk1$^{lox/lox}$ #2 E8	21% C (WT), 79% T (mut)	heterozygous	*Kras* amplification, $\log_2$ value = 0.26
Pdk1$^{lox/lox}$ #2 clone 35	18% C (WT), 82% T (mut)	heterozygous	*Kras* amplification, $\log_2$ value = 0.5625
Pdk1$^{lox/lox}$ #3 E8	100% T (mut)	homozygous	
Pdk1$^{lox/lox}$ #3 clone 18	50% C (WT), 50% T (mut)	heterozygous	
Pdk1$^{lox/lox}$ #5 E8	30% C (WT), 70% T (mut)	heterozygous	*Kras* amplification, $\log_2$ value = 0.3795
Pdk1$^{lox/lox}$ #5 clone 31	30% C (WT), 70% T (mut)	heterozygous	*Kras* amplification, $\log_2$ value = 0.2404
Pdk1$^{lox/lox}$ #6 E8	53% C (WT), 47% T (mut)	heterozygous	
Pdk1$^{lox/lox}$ #6 clone 65	49% C (WT), 51% T (mut)	heterozygous	

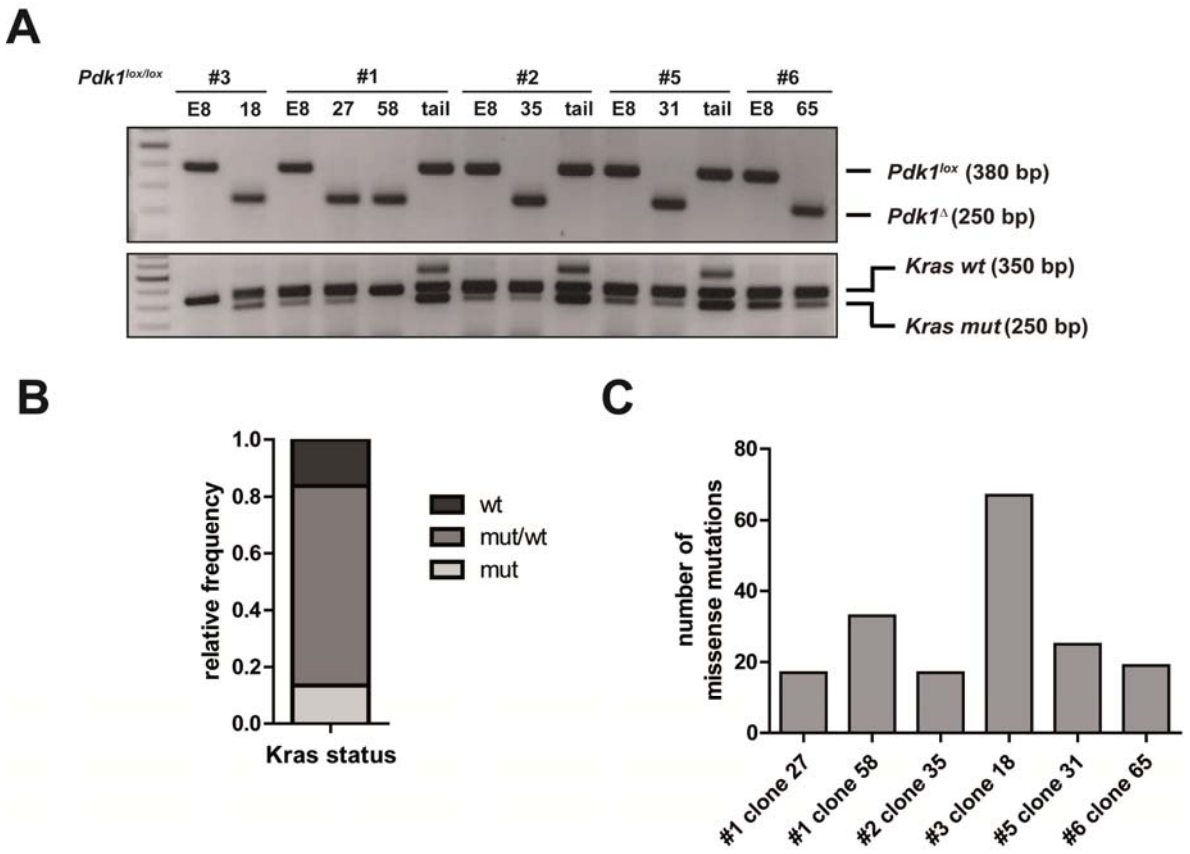

Figure 8. Characterization of mutational status of Pdk1-independent clones.
Six Pdk1-independent clones were analyzed in detail by whole exome sequencing.
(A) *FSF-Kras* and *Pdk1* recombination PCR for Pdk1-independent clones, *Pdk1*$^{lox/lox}$ cell lines and tails sent for whole exome sequencing. Pdk1-independent clones are named with a number, EtOH-treated parental cell lines are indicated by E8.
(B) Frequency of *Kras WT*, *mut/WT* and *mut* in all generated Pdk1-independent clones.
(C) Number of mutations exclusively detected in the Pdk1-independent clones by whole exome sequencing.

As shown in Table 26, for three clones there was no change in the Kras status compared to the parental cell line. The cell line *Pdk1*$^{lox/lox}$ #1 was heterozygous for *Kras*^{G12D} whereas the two analyzed clones harbored *Kras*^{G12D} amplification and a copy-number neutral loss of heterozygosity (LOH) for the *Kras WT* allele, respectively. On the contrary, the *Kras WT* allele was absent in cell line *Pdk1*$^{lox/lox}$ #3, but occurred in the Pdk1-independent clone. The Pdk1 recombination and the *Kras*^{G12D} status of these examples were confirmed by PCR (Figure 8A). PCR analysis of 37 Pdk1-independent clones revealed that 70.3% of the clones were characterized by heterozygous *Kras*^{G12D} and 16.2% showed only the mutated band. Surprisingly, 13.5% of the Pdk1-independent clones displayed exclusively the WT band (Figure 8B). *Pdk1* deletion was confirmed by PCR in these clones (data not shown) eliminating the possibility that the clones were derived from a fibroblast. The Kras status in the Pdk1-independent clones is diverse suggesting that the allelic Kras ratio is not a major factor for cells to acquire resistance towards inhibition of the PI3K-Pdk1 signaling axis.

Missense mutations detected in the whole exome sequencing data with a mutation frequency (f_mut) ≥ 0.05 and read depth at variant site (mut_count) ≥ 8 were taken for further analysis of potential resistance-mediating mutations. By comparing Pdk1-independent clones with parental cell lines and tails, on the average 25 mutations were exclusively detected in the resistant clones (Figure 8C). The clone harboring 70 mutations was characterized by equal growth compared to the parental cell line. Apart from this observation, no correlation between Kras status or number of mutations with the growth rate of clones was found.

The mutational profile of the different clones was heterogeneous and no recurrent mutations were observed. For the top hits like ubiquitin protein ligase E3 component N-recognin 1 (*Ubr1*), tenascin C (*Tnc*), poly (ADP-ribose)-polymerase 2 (*Parp2*) and ceramide synthase 4 (*Cers4*) the clones displayed a frequency of around 70% of mutated reads for these genes (Table 27). However, there were clones in which the highest mutation frequency was at 30%, suggesting that extra-genetic factors (e.g. epigenetics) may influence acquisition of resistance towards *Pdk1* inhibition. When all mutations occurring in the six clones were analyzed by using the Molecular Signature Database (Broad Institute), gene clusters connected with epithelial mesenchymal transition (EMT) (*Tnc, Fbn1, Tgfbr3, Wipf1, Vim, Calu*), JAK-STAT signaling (*Pim1, Dntt, A2m, Map3k8*), G2/M checkpoint (*Ccnf, Numa1, Stag1, Tacc3, Cul4a*), mTORC1 signaling (*Ccnf, Slc37a4, Psat1, Sla*) and O-glycan biosynthesis (*St6galnac2, Muc2, Muc6*) were found.

Table 27. Potentially relevant genes mutated in clones resistant towards Pdk1 inhibition.
Variants in whole exome data were considered as mutations when read depth at variant site (count_mut) ≥ 8 and mutation frequency (f_mut) ≥ 0.05. Only potentially relevant mutations are shown here.

#1 clone 27				
Gene	**Amino acid change**	**Count_mut (f_mut) clone**	**Count_mut (f_mut) cell line**	**Gene name**
Ubr1	p.Pro161Leu	8 (0.727273)	0 (0)	ubiquitin protein ligase E3 component N-recognin 1
Chmp4b	p.Tyr111His	18 (0.72)	0 (0)	charged multivesicular body protein 4B
Pcdhb19	p.His461Asp	116 (0.462151)	0 (0)	protocadherin beta 19
Gnai3	p.Phe196Val	28 (0.424242)	18 (0.22)	guanine nucleotide binding protein (G protein), alpha inhibiting activity polypeptide 3
Dnah11	p.Glu804Val	59 (1.00)	30 (0.31)	dynein, axonemal, heavy chain 11
Jag2	p.Glu348Gly	98 (1.00)	48 (0.34)	jagged 2
Gpx2	p.Lys104Thr	20 (1.00)	13 (0.39)	glutathione peroxidase 2 (gastrointestinal)

#1 clone 58				
Gene	**Amino acid change**	**Count_mut (f_mut) clone**	**Count_mut (f_mut) cell line**	**Gene name**
Tnc	p.Ile1625Met, p.Ile1716Met	11 (0.733333)	0 (0)	tenascin C
Numa1	p.Ala1093Gly	9 (0.692308)	0 (0)	nuclear mitotic apparatus protein 1
Slc6a13	p.Gly100Ala, p.Gly111Ala	14 (0.56)	0 (0)	solute carrier family 6 (neurotransmitter transporter), member 13
Pcdhgc4	p.Thr533Ala	21 (0.512195)	0 (0)	protocadherin gamma subfamily C, 4
Arhgef5	p.Ser1095Arg, p.Ser363Arg	10 (0.131579)	0 (0)	Rho guanine nucleotide exchange factor (GEF) 5
Gnai3	p.Phe196Val	27 (0.54)	18 (0.22)	guanine nucleotide binding protein (G protein), alpha inhibiting activity polypeptide 3
Nckap5l	p.Lys809Met	30 (1.00)	13 (0.36)	NCK-associated protein 5-like

#2 clone 35				
Gene	**Amino acid change**	**Count_mut (f_mut) clone**	**Count_mut (f_mut) cell line**	**Gene name**
Slc6a18	p.Phe405Ser	12 (0.26087)	0 (0)	solute carrier family 6 (neutral amino acid transporter), member 18
Erbb4	p.Ser1225Cys, p.Ser1209Cys	8 (0.228571)	0 (0)	Erb-B2 receptor tyrosine kinase 4
Pik3r4	p.Arg126His	27 (0.296703)	5 (0.068493)	phosphoinositide-3-kinase, regulatory subunit 4

#3 clone 18				
Gene	**Amino acid change**	**Count_mut (f_mut) clone**	**Count_mut (f_mut) cell line**	**Gene name**
Parp2	p.Lys159Thr	15 (0.714286)	0 (0)	poly (ADP-ribose) polymerase 2
Slc10a3	p.Lys4Arg	33 (0.52381)	0 (0)	solute carrier family 10, member 3
Pomgnt1	p.Lys488Arg, p.Lys499Arg, p.Lys521Arg	38 (0.487179)	0 (0)	protein O-linked mannose N-acetylglucosaminyltransferase 1 (beta 1,2-)
Rangap1	p.Gly50Ser	30 (0.337079)	0 (0)	Ran GTPase activating protein 1
Cers1	p.Ser145Cys	13 (0.317073)	0 (0)	ceramide synthase 1
Abcc6	p.Gln953His	11 (0.282051)	0 (0)	ATP-binding cassette, sub-family C (CFTR/MRP), member 6
Notch1	p.Pro2228Ala	15 (0.254237)	0 (0)	notch1
Tgfbr3	p.Pro500Ser	25 (0.186567)	0 (0)	transforming growth factor, beta receptor III

#3 clone 18				
Gene	**Amino acid change**	**Count_mut (f_mut) clone**	**Count_mut (f_mut) cell line**	**Gene name**
Prkacb	p.Asp172His, p.Asp173His, p.Asp185His, p.Asp232His	16 (0.170213)	0 (0)	protein kinase, CAMP-dependent, catalytic, beta

#5 clone 31				
Gene	**Amino acid change**	**Count_mut (f_mut) clone**	**Count_mut (f_mut) cell line**	**Gene name**
Actrt2	p.Arg77Gln	15 (0.306122)	0 (0)	actin-related protein T2
Phldb2	p.Ser867Arg, p.Ser912Arg	15 (0.283019)	0 (0)	pleckstrin homology-like domain, family B, member 2
Pcdh15	p.Ile935Val, p.Ile335Val, p.Ile541Val, p.Ile859Val, p.Ile893Val, p.Ile908Val, p.Ile930Val, p.Ile937Val, p.Ile942Val	40 (0.277778)	0 (0)	protocadherin-related 15
Csmd1	p.Ser2515Cys	22 (0.222222)	0 (0)	CUB and sushi multiple domains 1
Lrp1b	p.Lys1528Arg, p.Lys1383Arg	18 (0.193548)	0 (0)	low density lipoprotein receptor-related protein 1B
Arhgap11a	p.His637Arg	24 (0.12973)	0 (0)	Rho GTPase activating protein 11A
Irs2	p.His1156Asp	17 (0.113333)	0 (0)	insulin receptor substrate 2

#6 clone 65				
Gene	**Amino acid change**	**Count_mut (f_mut) clone**	**Count_mut (f_mut) cell line**	**Gene name**
Cers4	p.Thr337Arg	8 (0.727273)	0 (0)	ceramide synthase 4
Slc8a3	p.Glu717Val, p.Glu87Val, p.Glu716Val, p.Glu710Val	8 (0.333333)	0 (0)	solute carrier family 8 (sodium / calcium exchanger), member 3
Srms	p.Trp216Arg	8 (0.216216)	0 (0)	src-related kinase lacking C-terminal regulatory tyrosine and N-terminal myristoylation sites
Ccnf	p.Asn99Tyr	11 (0.192982)	0 (0)	cyclin F
Slc37a4	p.Ser341Thr	11 (0.126437)	0 (0)	solute carrier family 37 (glucose-6-phosphate transporter), member 4

Recently, a pancreas-specific transposition system was generated by interbreeding *Pdx1-Cre;LSL-Kras*$^{G12D/+}$ with *ATP1-S2* mice, harboring mutagenic *ATP1* transposons, and *LSL-R26*^{PB} mice, containing the *piggyBac* transposase as a knock-in at the *Rosa26* locus, preceded by an *LSL* cassette. Thereby, expression of *piggyBac* transposase and subsequent *ATP1* transposon mobilization were induced in the pancreas resulting in significantly accelerated tumor formation compared to *Pdx1-Cre;LSL-Kras*$^{G12D/+}$ mice. This model allowed the identification of genes relevant to pancreatic carcinogenesis in an unbiased manner and their functional validation (Rad et al., 2015). As presented in Table 28, a small subset of genes, which were mutated in Pdk1-independent clones, was also found in the *piggyBac* transposon screen indicating a functional relevance. Two inactivating transposon insertions in *Ubr1* were detected with high and intermediate coverage, most other overlapping genes with low coverage.

To conclude, the mutational landscape of the Pdk1-resistant clones was very heterogeneous and around 25 mutations were exclusively found in each clone.

Table 28. Genes mutated in Pdk1-resistant clones, which were found in a *Pdx1-Cre;LSL-Kras*$^{G12D/+}$ transposon screen.

Gene	Insertions in transposon screen	Coverage
Ubr1	2x, inactivating	high and intermediate
Numa1	2x, inactivating	low
Pcdh15	5x, probably inactivating	low
Csmd1	1x, probably inactivating	low
Lrp1b	4x, inactivating	low
Erbb4	3x, inactivating	low
Tpx2	1x, inactivating	low
Gnai3	3x, probably inactivating	low and intermediate

6.8 Pdk1 controls size and lymph node metastasis of orthotopic pancreatic tumors

To validate the impact of *Pdk1* deletion on tumor maintenance *in vivo*, *Pdk1*$^{lox/lox}$*;Trp53*$^{frt/+}$ cells were implanted orthotopically into the pancreata of NSG mice. After a tumor was palpable, one cohort of mice was treated with 4 mg TAM i.p. twice per week, whereas a control cohort remained untreated. All mice were sacrificed at the same day and tumor volume, tumor weight, volume of ascites and number of enlarged lymph nodes were compared (Figure 9A). Treatment efficiency was validated by PCR for recombination of the *Pdk1* locus (Figure 9B). As shown by macroscopic analysis and measurements of tumor parameters (Figure 9C,D), tamoxifen-treated tumors displayed a significantly reduced weight

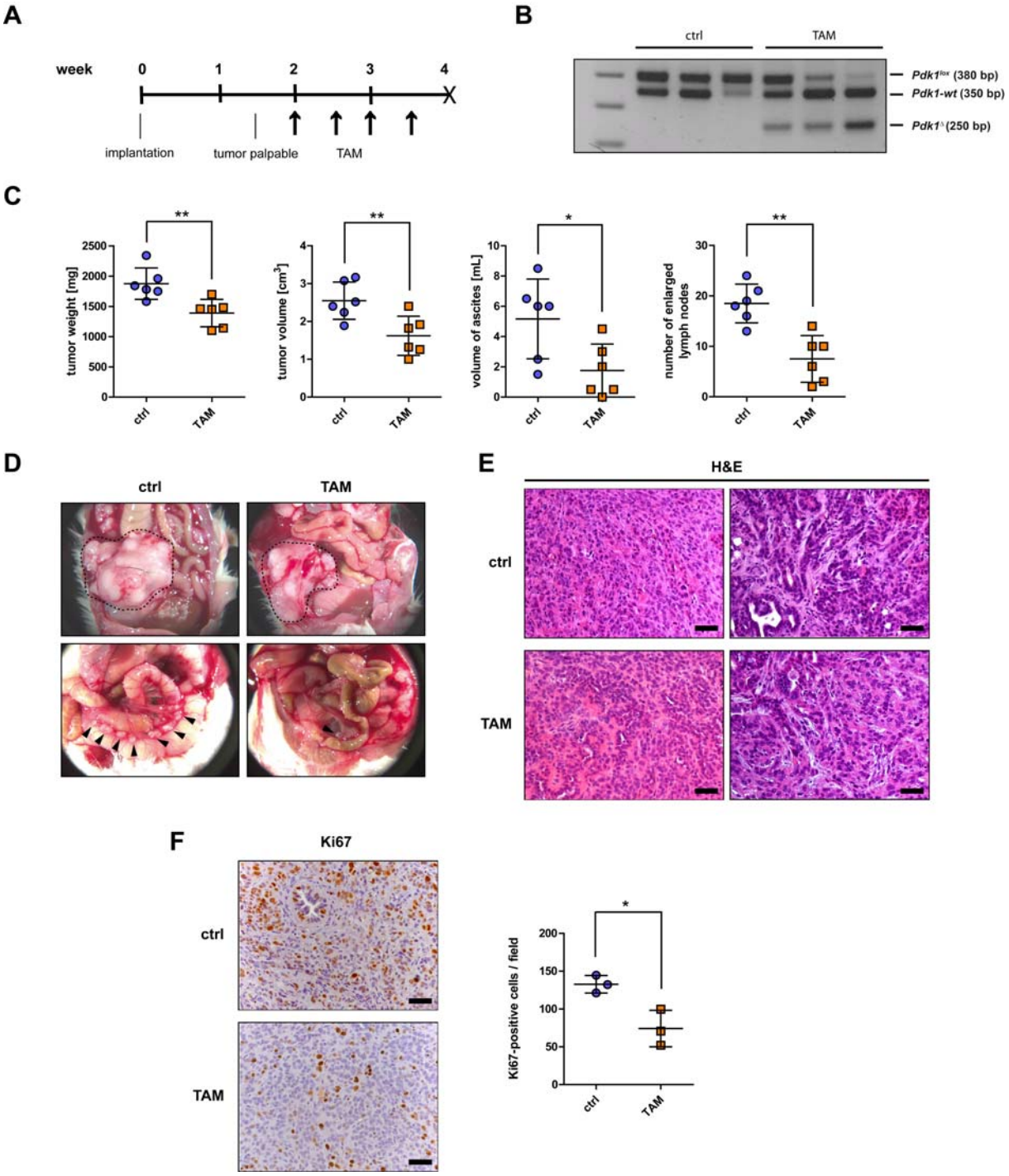

Figure 9. Impact of *Pdk1* deletion on maintenance of Kras^{G12D}-driven tumors.
(A) Experimental strategy to delete Pdk1 in tumors from orthotopically implanted *Pdk1*$^{lox/lox}$ cells.
(B) Recombination of the *Pdk1* locus was assessed by PCR analysis.
(C) Tumor parameters (tumor weight, volume, ascites, lymph node metastasis) of TAM-treated mice compared to control mice. Data represent mean ± SD; n = 6 mice per group; **p < 0.01, *p < 0.05, Student´s t test.
(D) Macroscopic pictures of tumors *in situ* (upper row) and enlarged lymph nodes (lower row) of ctrl and TAM-treated mice. Pancreatic tumors are outlined in black dotted circles and lymph nodes are indicated by arrows.
(E) H&E staining of tumors from ctrl and TAM-treated mice. Left: poorly differentiated tumor areas, right: well-differentiated tumor areas. Scale bars indicate 50 µm.
(F) Left: Immunhistochemical Ki67 staining of tumors from ctrl and TAM-treated mice. Scale bars indicate 50 µm. Right: Quantification of Ki67 staining. *p < 0.05. Student´s t test.

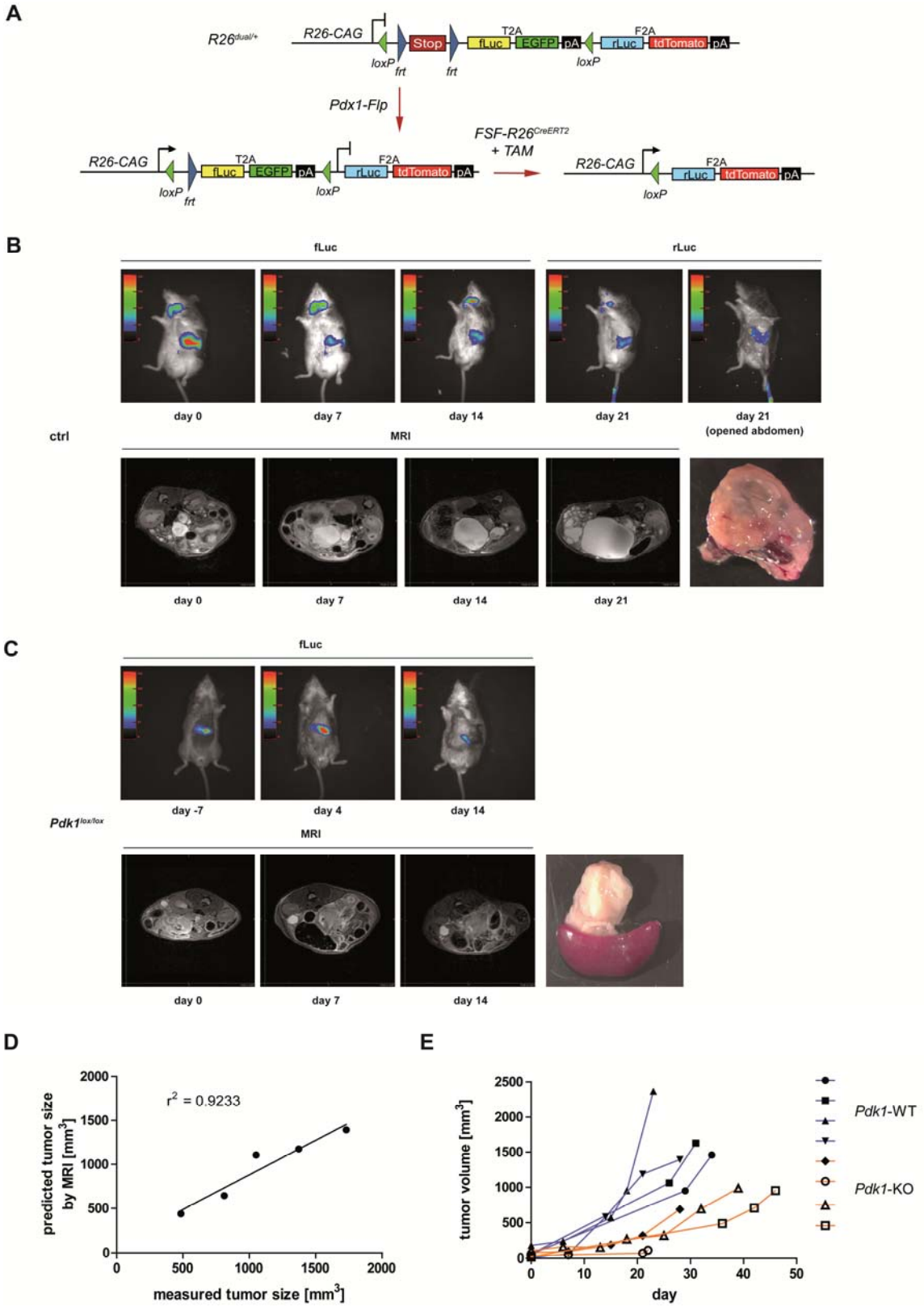

Figure 10. Role of Pdk1 in maintenance of endogenous Kras^{G12D}-driven PDAC.
(A) Scheme of the *R26^{dual}* reporter allele. Flp recombinase induces firefly luciferase (fLuc) and EGFP expression, Cre recombines the *fLuc-EGFP* cassette and activates renilla luciferase (rLuc) and td-Tomato expression.
(B) Top: *In vivo* imaging of fLuc and rLuc expression in the pancreas of a *Pdk1$^{lox/+}$;R26$^{dual/+}$;Trp53$^{frt/+}$* mouse treated with TAM. Bottom: MRI to assess the tumor volume of the same mouse.
Start of TAM treatment is depicted as day 0.

(legend continued on next page)

and were significantly smaller than control tumors. Moreover, *Pdk1*-KO tumors produced significantly less ascites and enlarged lymph nodes (Figure 9C,D). Tumors were histologically indistinguishable both yielding well-differentiated and poorly differentiated tumor areas (Figure 9E). Immunohistochemistry for the proliferation marker Ki67 showed that tamoxifen-treated tumors exhibited significantly less proliferation than control tumors (Figure 9F).

To conclude, *Pdk1* deletion leads to smaller and less proliferative tumors forming less lymph node metastases in the mesentery.

6.9 Role of Pdk1 in endogenous established Kras^{G12D}-driven PDAC

To evaluate whether Pdk1 could serve as potential target for therapy of Kras^{G12D}-driven PDAC, *Pdk1$^{lox/lox}$;Trp53$^{frt/+}$* mice and control mice with established tumors harboring heterozygously floxed *Pdk1* or WT *Pdk1* were treated twice per week with 4 mg TAM i.p. until mice had to be sacrificed. Recently, a *R26^{dual}* reporter allele was generated in our group, which allows visualization of Flp- and Cre-mediated recombination (Figure 10A). This reporter was used in TAM treatment experiments to monitor both recombination events and to check the effect of TAM administration. As shown in Figures 10B and 10C, a *Pdk1$^{lox/+}$;Trp53$^{frt/+}$* and a *Pdk1$^{lox/lox}$;Trp53$^{frt/+}$* mouse were selected for monitoring tumor development by MRI and BLI. After PDAC formation, a strong firefly luciferase signal was detected in the pancreas due to Flp expression. The existence of the tumor was verified by MRI. By TAM application, activated CreER^{T2} recombined the *fLuc-EGFP* cassette and induced rLuc expression. Therefore, the fLuc signal decreased upon TAM treatment (Figure 10B,C), whereas expression of rLuc was detected (Figure 10B). The tumor of the control mouse was growing quite fast within the following weeks, which was assessed by repeated MRI measurements. The presented pancreas displayed a cystic morphology. In contrast, tamoxifen treatment slowed down tumor growth in the *Pdk1$^{lox/lox}$;Trp53$^{frt/+}$* mouse (Figure 10C). To validate MRI as a screening tool for PDAC volume, five mice were sacrificed at the same day when the MRI measurement was performed. As depicted in Figure 10D, the volume measured by MRI correlated well with the size of the tumor determined after dissection of the mouse. For the systematic analysis of PDAC development upon *Pdk1* deletion, four *Pdk1$^{lox/lox}$;Trp53$^{frt/+}$* and four control mice bearing solid tumors were chosen.

(C) Top: *In vivo* imaging of fLuc expression in the pancreas of a *Pdk1$^{lox/lox}$;R26$^{dual/+}$;Trp53$^{frt/+}$* mouse treated with TAM. Bottom: MRI of the same mouse. Start of TAM treatment is depicted as day 0.
(D) Correlation of tumor volume predicted by MRI and the volume measured after sacrificing the mouse. Regression analysis, $r^2 = 0.9233$, n = 5 mice.
(E) The development of the tumor volume was assessed by MRI in control and *Pdk1*-KO mice.

All *Pdk1*-deleted animals displayed a slower tumor progression or even stable disease, whereas control animals showed rapid disease progression (Figure 10E).
To summarize, Pdk1 was shown to be relevant for maintenance of $Kras^{G12D}$-driven PDAC in an endogenous mouse model and could present an attractive target for therapeutic interventions in pancreatic cancer.

6.10 Effect of *Pdk1* deletion on cancer metabolism *in vivo*

To assess the role of *Pdk1* deletion on tumor metabolism *in vivo*, $Pdk1^{lox/lox};Trp53^{frt/+}$ cells were implanted subcutaneously in C57BL6/J WT mice and MRI and PET scans were performed on a regular basis. After tumor detection, animals were divided into a TAM and a control group. As shown in Figure 11A, *Pdk1* deletion was verified by PCR. *Pdk1* ablation resulted in a constant SUV whereas tumors of the control group displayed a time-dependent increase in glucose uptake (Figure 11B). As depicted in Figure 11C, the FDG-PET signal was absent in TAM-treated mice at week 4 in contrast to control mice. Moreover, *Pdk1*-deleted tumors showed a heterogeneous pattern in T2-weighted MRI images with hypointense areas in the center after 4 weeks, indicative of therapy-related cell death (Figure 11C, data not shown). The analysis was more difficult in endogenous $Pdk1^{lox/lox};Trp53^{frt/+}$ and control tumor mice due to high heterogeneity / variability between different individuals (data not shown). Therefore, MRI and PET measurements were perfomed for the same animal at different time points. In this mouse, the SUV_{max} was normalized to the tumor volume and compared for 1 week and 2 weeks after beginning of TAM treatment yielding a strong reduction in glucose metabolism (Figure 11D,E). These initial data indicate that Pdk1 controls glucose metabolism of $Kras^{G12D}$-driven PDAC *in vivo*. However, more TAM-treated $Pdk1^{lox/lox};Trp53^{frt/+}$ mice have to be monitored by MRI and PET at two different time points to confirm this observation.

6.11 *Mek1* deletion neither blocks $Kras^{G12D}$- nor $PIK3CA^{H1047R}$-driven PDAC formation

Recently, it has been demonstrated that deletion of *Mek1* or *Mek2* in a $Kras^{G12V}$-driven NSCLC mouse model had no significant effect on tumor formation due to compensatory activities. However, ablation of both Mek kinases prevented tumor development (Blasco et al., 2011; Karreth et al., 2011). To elucidate the contribution of Mek1 in pancreatic cancer initiation, *Mek1* was inactivated in the pancreatic epithelial cells using floxed *Mek1* mice (Figure 12A). $Ptf1a^{Cre/+};LSL\text{-}Kras^{G12D/+};Mek1^{lox/lox}$ and $Ptf1a^{Cre/+};LSL\text{-}PIK3CA^{H1047R/+};Mek1^{lox/lox}$ mice were compared to $Ptf1a^{Cre/+};LSL\text{-}Kras^{G12D/+}$ and $Ptf1a^{Cre/+};LSL\text{-}PIK3CA^{H1047R/+}$ mice, respectively. Surprisingly, all pancreas-specific *Mek1*-KO mice developed tumors consisting

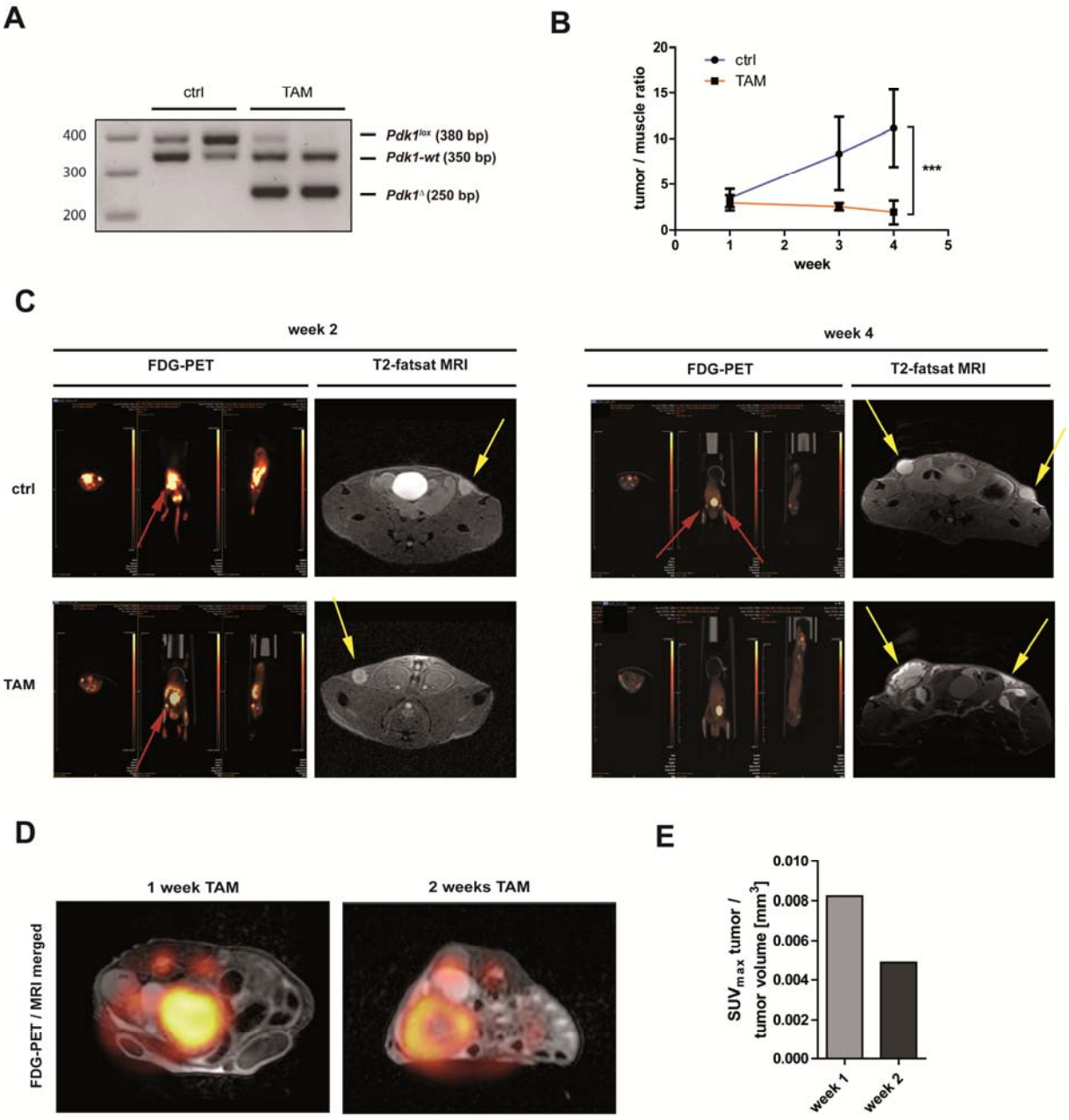

Figure 11. Role of Pdk1 on glucose metabolism of Kras^{G12D}-driven pancreatic cancer *in vivo*.
(A) Recombination of the *Pdk1* locus in TAM-treated subcutaneous tumors was assessed by PCR.
(B) Glucose uptake in TAM-treated and control subcutaneous tumors, derived from *Pdk1$^{lox/lox}$;Trp53$^{frt/+}$* cells, assessed by F18-FDG-PET. Uptake values of the tumors were normalized to uptake values of a representative muscle of the posterior limbs.
(C) Representative FDG-PET and MRI images for control (upper part) and TAM-treated (lower part) tumors at 2 and 4 weeks. Yellow arrows indicate the subcutaneous tumors in the MRI image, red arrows indicate the PET signal.
(D) Merged FDG-PET/MRI picture of an endogenous *Pdk1$^{lox/lox}$;Trp53$^{frt/+}$* tumor bearing mouse 1 week and 2 weeks after beginning of TAM treatment.
(E) Quantification of reduction of glucose uptake upon *Pdk1* deletion, as shown in (D).

of numerous small cysts in both the *Kras^{G12D}* and the *PIK3CA^{H1047R}* model (Figure 12B). On the contrary, *Ptf1a$^{Cre/+}$;LSL-Kras$^{G12D/+}$* mice formed exclusively solid PDAC and cystic tumors were not observed. In *Ptf1a$^{Cre/+}$;LSL-PIK3CA$^{H1047R/+}$* mice, both solid and cystic tumors were found. As depicted in Figure 12C, there was no difference in survival of tumor mice in the

Kras$^{G12D/+}$ model (428 d for *Ptf1a*$^{Cre/+}$;*LSL-Kras*$^{G12D/+}$;*Mek1*$^{lox/lox}$ versus 466 d for *Ptf1a*$^{Cre/+}$;*LSL-Kras*$^{G12D/+}$). *Ptf1a*$^{Cre/+}$-induced ablation of *Mek1* in the PIK3CA^{H1047R}-driven PDAC model did not block, but delayed tumor development. *Ptf1a*$^{Cre/+}$;*LSL-PIK3CA*$^{H1047R/+}$;*Mek1*$^{lox/lox}$ showed an improved median survival of 551 d compared to 397 d for *Ptf1a*$^{Cre/+}$;*LSL-PIK3CA*$^{H1047R/+}$ mice. However, this prolongation was not statistically significant (Figure 12D).

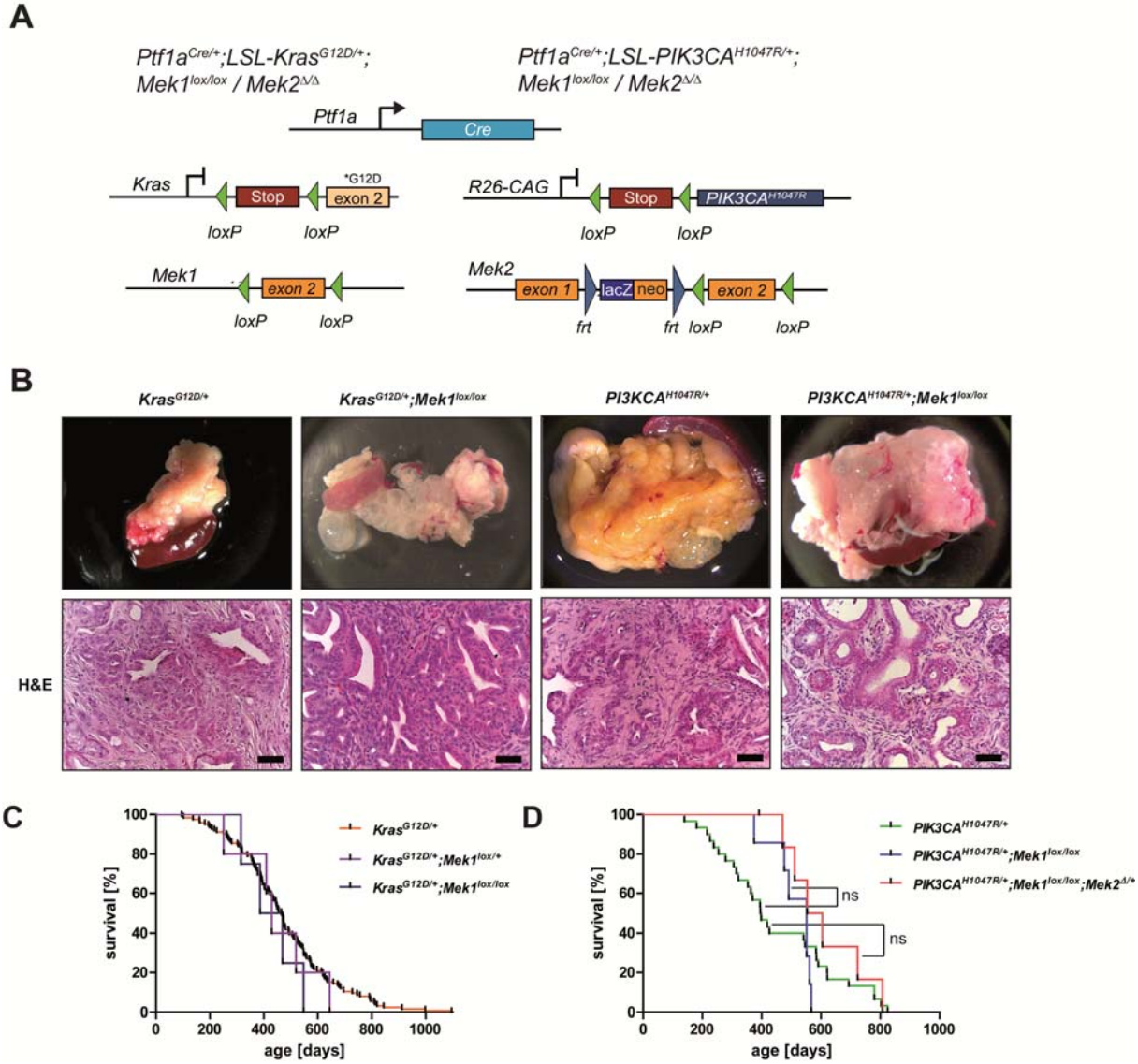

Figure 12. Deletion of epithelial *Mek1* does neither block Kras^{G12D}- nor PIK3CA^{H1047R}-driven pancreatic carcinogenesis.

(A) Genetic strategy used to study the cell-autonomous role of Mek1 and Mek2 in Kras^{G12D}- and PIK3CA^{H1047R}-driven pancreatic cancer formation. Expression of *Ptf1a*$^{Cre/+}$ leads to activation of Kras^{G12D} and PIK3CA^{H1047R} in the pancreas, respectively, and simultaneously conditional deletion of *Mek1*. *Mek2* is eliminated ubiquitously.

(B) Representative macroscopic pictures (upper row) and H&E-stained sections (lower row) of PDAC. Scale bars indicate 50 µm.

(C-D) Kaplan-Meier survival analysis of indicated genotypes. + denotes the WT allele, lox the conditional allele. The number of animals and the median survival time are shown in brackets.

(C) Kras^{G12D} genotypes: *Ptf1a*$^{Cre/+}$;*LSL-Kras*$^{G12D/+}$ (n = 124, 466 d), *Ptf1a*$^{Cre/+}$;*LSL-Kras*$^{G12D/+}$;*Mek1*$^{lox/+}$ (n = 5, 429 d), *Ptf1a*$^{Cre/+}$;*LSL-Kras*$^{G12D/+}$;*Mek1*$^{lox/lox}$ (n = 4, 428 d).

(D) PIK3CA^{H1047R} genotypes: *Ptf1a*$^{Cre/+}$;*LSL-PIK3CA*$^{H1047R/+}$ (n = 30, 397 d), *Ptf1a*$^{Cre/+}$;*LSL-PIK3CA*$^{H1047R/+}$;*Mek1*$^{lox/lox}$ (n = 7, 551 d), *Ptf1a*$^{Cre/+}$;*LSL-PIK3CA*$^{H1047R/+}$;*Mek1*$^{lox/lox}$;*MEK2*$^{Δ/+}$ (n = 6, 579 d). ns, not significant, log-rank test.

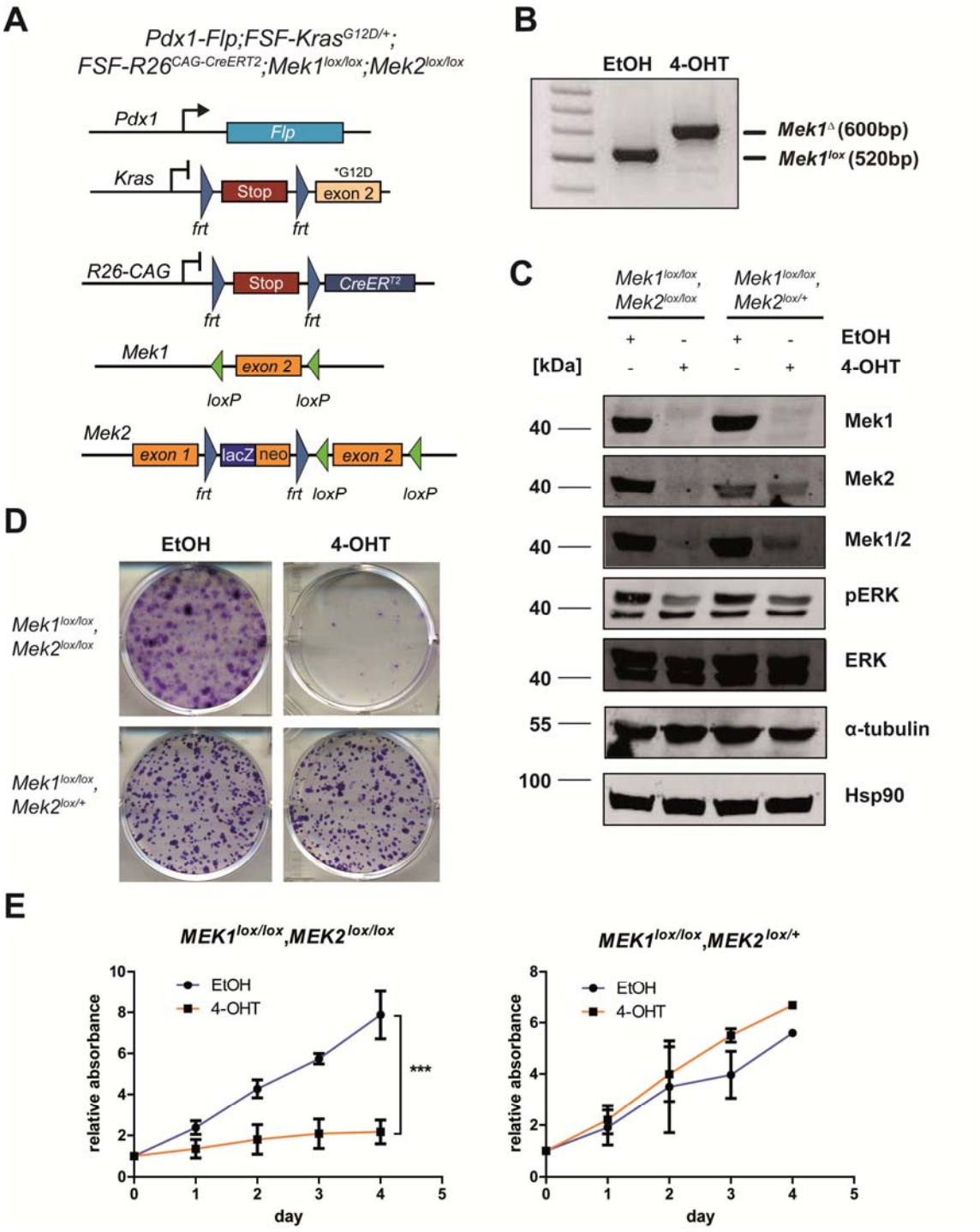

Figure 13. Deletion of epithelial *Mek1* and *Mek2* inhibits growth of Kras^{G12D}-driven PDAC cells *in vitro*.

(A) Genetic strategy used to analyze the cell-autonomous role of Mek1 and Mek2 on tumor maintenance in Kras^{G12D}-driven pancreatic cancer cells. *Pdx1-Flp*-activated expression of Kras^{G12D} induces PDAC. CreER^{T2} is activated in the cell lines by 4-OHT administration to delete *Mek1* and *Mek2*.

(B) PCR analysis of non-recombined *Mek1$^{lox/lox}$* DNA from cells treated with EtOH and recombined DNA from cells treated with 600 nM 4-OHT for 8 d.

(C) Immunoblot analysis of Mek and Erk signaling in protein lysates of PDAC cell lines after 8 d of EtOH and 4-OHT treatment. Hsp90 and α-tubulin were used as loading controls.

(D) Clonogenic assay after pretreatment of cells with EtOH and 4-OHT for 8 d.

(E) MTT viability assay of the same cells shown in (D). Data are depicted as mean ± SD, ***p < 0.001, two-way ANOVA.

Efficient deletion of both *Mek1* alleles was proven by recombination PCR and loss of Mek1 protein expression was verified by immunoblotting and immunohistochemistry of samples from *Ptf1a*$^{Cre/+}$*;LSL-PIK3CA*$^{H1047R/+}$*; Mek1*$^{lox/lox}$ mice (data not shown). Consequently, the possibility that tumors formed due to incomplete *Mek1* deletion was excluded. Next, mice with ubiquitous *Mek2*-KO (*Mek2*$^{\Delta/\Delta}$ mouse line) were interbred with *Ptf1a*$^{Cre/+}$*;LSL-PIK3CA*$^{H1047R/+}$*;Mek1*$^{lox/lox}$ mice in order to analyze whether ablation of both Mek kinases could block pancreatic cancer formation. However, alive *Mek1/Mek2* double KO mice were never obtained so that the effect of complete *Mek* deletion could not be addressed. *Ptf1a*$^{Cre/+}$*;LSL-PIK3CA*$^{H1047R/+}$*;Mek1*$^{lox/lox}$;*MEK2*$^{\Delta/+}$ mice survived 579 d which was a prolongation of 182 d in comparison to *Ptf1a*$^{Cre/+}$*;LSL-PIK3CA*$^{H1047R/+}$ mice, although the effect was not statistically significant ($p = 0.2096$).

To summarize, *Mek1* elimination does neither block Kras^{G12D}- nor PIK3CA^{H1047R}-driven PDAC formation. The morphology of the tumors shifts from solid tumors to cystic tumors consisting of many small cysts suggesting that Mek1 might play a role in differentiation of pancreatic cells. Since generation of *Mek1/Mek2* double KO tumor mice was impossible (probably due to embryonic lethality), it remains unclear whether Mek1 and Mek2 are essential for initiation of Kras^{G12D}- and PIK3CA^{H1047R}-driven PDAC.

6.12 *Mek1/2* deletion blocks growth of PDAC cells *in vitro*

To study the role of Mek1 and Mek2 in Kras^{G12D}-driven PDAC maintenance *in vitro*, a *Pdx1-Flp;FSF-Kras*$^{G12D/+}$*;FSF-R26*$^{CAG-CreERT2/+}$*;Mek1*$^{lox/lox}$*;Mek2*$^{\Delta/\Delta}$ and a *Pdx1-Flp;FSF-Kras*$^{G12D/+}$*;FSF-R26*$^{CAG-CreERT2/+}$*;Mek1*$^{lox/lox}$*;Mek2*$^{\Delta/+}$ pancreatic cancer cell line were generated. Since the *Mek2* allele used in this work is a ´knock-out-first´ conditional allele (Skarnes et al., 2011), the general *Mek2*-KO was converted into a conditional *Mek2*-KO upon *Pdx1-Flp* expression. By 4-OHT treatment, CreER^{T2} was activated resulting in elimination of *Mek1* and *Mek2* (Figure 13A). Cells were cultured for 8 d with EtOH or 4-OHT, followed by viability assays. As shown in Figure 13B, recombination of the *Mek1* locus was verified by PCR. Furthermore, both the *Mek1*- and *Mek2*-KO were verified on protein level by immunoblotting. In both cell lines phosphorylation of Erk1 (p44) was reduced upon tamoxifen treatment (Figure 13C). Depletion of both Mek kinases blocked tumor growth and colony formation, whereas no effect was observed in cells with deleted *Mek1* and heterozygously expressed *Mek2* (Figure 13D,E). These results suggest that both Mek1 and Mek2 have to be inactivated to inhibit PDAC cell proliferation.

7 Discussion and outlook

Oncogenic *KRAS* mutations are the most frequent mutations in human PDAC. Since no therapies targeting directly mutated *KRAS* have been successfully translated into the clinic yet, the role of Kras effectors in pancreatic carcinogenesis was analyzed in GEMMs in this work. The importance of Pdk1 in $Kras^{G12D}$-driven PanIN progression and PDAC maintenance *in vitro* and *in vivo* was established. Thereby, intervention with Pdk1 signaling may present a useful therapeutic approach in PDAC.

Moreover, the role of the Kras downstream effectors Mek1/2 was studied in pancreatic carcinogenesis. Ablation of *Mek1* in $Kras^{G12D}$- and $PIK3CA^{H1047R}$-driven mouse models did not block PDAC formation. The effect of concomitant *Mek1* and *Mek2* deletion could not be studied, since mice with constitutive deletion of *Mek1* in the pancreas and general deletion of *Mek2* are not viable. Initial data indicated that deletion of both Mek kinases using the DRS in autochtonous PDAC impairs tumor cell growth *in vitro*, whereas deletion of *Mek1* and heterozygous deletion of *Mek2* does not.

Role of Pdk1 in PanIN progression, PDAC maintenance and metastasis

Pdk1 was shown to be essential for PanIN progression in a $Kras^{G12D}$-driven PDAC mouse model in this work. When TAM was applied at the age of 3 months to inactivate *Pdk1*, the number of PanINs was strongly reduced at the age of 9 months. Thus, I validated Pdk1 as a promising drug target for PDAC therapy. Only PanINs which were not completely recombined for *Pdk1* were found in the tissue sections. Therefore, molecular and histological changes in PanINs upon *Pdk1* deletion could not be determined. In future experiments, I will investigate the fate of PanINs after *Pdk1* elimination and elucidate the underlying molecular mechanisms using 3-month-old $Pdk1^{lox/lox}$ mice and $Pdk1^{lox/+}$ control animals treated with TAM. Pancreata will be analyzed directly after treatment for morphological signs of PanIN differentiation to normal acinar or ductal cells. The $R26^{dual}$ reporter allele will be used in these experiments to monitor Flp- and Cre-mediated recombination events and to trace the lineage and fate of recombined cells. Transcriptome and phospho-proteome profiling will be performed to study established PI3K/Pdk1-regulated signaling pathways, cross-signaling to other relevant pathways, e.g. MAPK signaling, apoptosis, DNA damage response (DDR), senescence and autophagy in *Pdk1*-deleted PanINs. In this work, I showed that *Pdk1* deletion results in reduced growth of established tumors in endogenous and orthotopic $Kras^{G12D}$-driven PDAC models. Moreover, less lymph node metastasis and less ascites were observed upon *Pdk1* ablation. These findings argue that Pdk1 is not only relevant to PDAC maintenance, but also plays a role in metastasis formation of pancreatic cancer. Similar observations were made in other tumor entities. Pdk1 was shown to be important for initiation

of melanoma and breast cancer, but also to be essential for tumor progression, maintenance and metastasis (Du et al., 2015; Scortegagna et al., 2014). In the *Braf*^{V600E}*;Pten*$^{-/-}$ melanoma mouse model, FOXO3a was identified as key mediator of the *Pdk1*-KO phenotype (Scortegagna et al., 2014). In the future, global transcriptome and phospho-proteome analyses will be performed for *Pdk1*-depleted tumors to identify effector molecules and key mechanisms, as described for the *Pdk1*-deleted PanINs.

The cytostatic *Pdk1*-KO phenotype is partially mediated by metabolic changes

In this thesis, it was shown that *Pdk1* deletion has cytostatic effects on pancreatic cancer cells. Proliferation and colony formation were reduced, but no signs of cell death were observed. This cytostatic but not cytotoxic effect may explain why Pdk1 or PI3K inhibitors can block tumor growth *in vivo* in *Kras* mutant tumors, but rarely cause tumor regression (Eser et al., 2013). Nakamura and colleagues studied the function of Pdk1 in immortalized MEFs and found out that G1/S phase transition was delayed and G2/M phase progression was impaired upon *Pdk1* deletion (Nakamura et al., 2008). They performed their experiments on chemically synchronized cells. After cell cycle synchronization by serum starvation for 3 d, I could confirm reduction of serum-induced cell cycle progression upon *Pdk1* deletion in my work. However, when I used non-starved cells, only small effects on cell cycle regulators were detected on protein level and RNA sequencing data yielded no downregulated cell cycle gene clusters. These observations indicate that the effect of the *Pdk1*-KO on cell cycle regulators is blunted by serum in the cell culture medium. Transcriptomic analyses of starved *Pdk1*-depleted cells will be performed to validate this theory.

In the pancreas, oncogenic Kras promotes glycolysis and the nonoxidative arm of the PPP, providing precursors for DNA and RNA biosynthesis (Ying et al., 2012). Strikingly, RNA sequencing in my work revealed a downregulation of metabolic gene signatures upon *Pdk1* deletion, e.g. glycolysis and gluconeogenesis and the PPP. These observations were verified by qRT-PCR and functional metabolic assays rendering Pdk1 essential for controlling PDAC metabolism. Since Pdk1 ablation reduces glycolysis and PPP, growth arrest of *Pdk1*-deleted cells might be caused by nucleotide deprivation, leading to defective replication, induction of replicative stress and DDR resulting in intra S-phase checkpoint activation. This hypothesis will be validated by flow cytometry-based cell cycle assays and DDR analysis.

Moreover, cholesterol synthesis and metabolism were significantly reduced upon *Pdk1* deletion. The expression of 3-hydroxy-3-methylglutaryl CoA reductase (*Hmgcr*) encoding the rate-limiting enzyme of cholesterol synthesis was reduced to 68% in the RNA sequencing data. Recently, it was shown that interference with cholesterol uptake sensitizes PDAC cells to chemotherapeutics (Guillaumond et al., 2015). Therefore, the regulation of cholesterol metabolism by Pdk1 will be investigated further.

The metabolic response in $Kras^{G12D}$-driven PDAC cells towards *Pdk1* deletion has to be characterized more detailed by measurements of the extracellular acidification rate and the oxygen consumption rate as well as by metabolomic analyzes of glucose, lipid and amino acid metabolites.

For therapeutic purposes, it would be necessary to obtain a cytotoxic response towards a treatment to eradicate the cancer cells. Therefore, the question arises how to convert the cytostatic *Pdk1*-KO effect into a cytotoxic one. Future work will elucidate whether concomitant inactivation of Pdk1 and Raf/Mek/Erk signaling (i.e. Braf and Craf or Mek1/2 inactivation) or combination of *Pdk1* deletion with additional drugs results in cytotoxic effects.

Enhancing DNA damage might present a strategy to transform the cytostatic *Pdk1*-KO phenotype into a cytotoxic one. Histone deacetylase (HDAC) inhibitors do not only induce histone acetylation but also increase reactive oxygen species and DNA damage (Robert and Rassool, 2012). Recently, it was shown that combinatorial Mek and PI3K inhibition of pancreatic cancer induced only mild apoptosis whereas additional inhibition of HDACs resulted in severe cell death and blocked lung metastasis (Ischenko et al., 2015). Therefore, HDAC inhibitors could potentiate the *Pdk1*-KO phenotype.

Downstream effectors of Pdk1

Pdk1 is the master regulator of a plethora of downstream kinases including Akt, Rsk, S6K, SGK and PKC. It remains unclear which effectors are functionally relevant to pancreatic carcinogenesis. Phosphorylation of T308 at Akt and S227 at Rsk2 were strongly reduced upon *Pdk1* deletion in $Kras^{G12D}$-driven PDAC cell lines *in vitro* indicating functional relevance in PDAC. By overexpression of a myristoylated Rsk2 (Boehm et al., 2007), the growth inhibition effect mediated by *Pdk1* depletion could be rescued partially. Phosphorylation of Rsk2 is increased in human skin cancer patients compared to controls and was shown to be functionally relevant for transformation of skin cells *in vitro* (Cho et al., 2012). Activated RSK2 translocates into the nucleus and phosphorylates a plethora of targets including cyclic AMP responsive element binding (CREB), c-fos, IκBα, activating transcription factor 1 (AFT1), ATF4, ERα, NFAT3, Trp53 and histone modifiers H3, H2B and H2AX (Cho et al., 2005; Cho et al., 2007a; Cho et al., 2007b; Liu et al., 2011a; Sassone-Corsi et al., 1999; Xing et al., 1996; Yang et al., 2004). Moreover, concomitant inhibition of Mek1/2 and Rsk2 induced cell cycle arrest in melanoma cells (Lee et al., 2013). Altogether, these data suggest that Rsk2 is involved in cell proliferation which explains the partial rescue effect of Rsk2-myr expression in *Pdk1*-depleted cells. However, the observation that Rsk2-myr does not completely rescue the *Pdk1*-KO phenotype indicates that Rsk2 is not the only downstream effector of Pdk1 in pancreatic carcinogenesis.

In our group it was shown that expression of a myristylated form of Akt1 (Akt1-myr) (Boehm et al., 2007), which activates Akt1, could completely revert the *Pdk1*-KO phenotype, whereas expression of the transcription factor Myc rescued it partially (unpublished). Akt promotes glycolysis in cancer cells and Akt activity is correlated with high rates of glucose metabolism (Elstrom et al., 2004), presenting one of the major kinases accounting for the Warburg effect (Robey and Hay, 2009). Akt exerts its effects on glycolysis in numerous ways. First, Akt increases the expression of glucose transporters and augments their translocation to the plasma membrane. Expression of Akt1 was shown to increase mRNA expression of Glut1 (Barthel et al., 1999). Translocation of Glut1 to the plasma membrane was reduced when Akt activity was inhibited (Wieman et al., 2007). In adipocytes and muscle cells Glut4 is expressed and Akt stimulates glycolytic flux by translocation of Glut4 to the plasma membrane (Kohn et al., 1996). Second, Akt regulates hexokinase and phosphofructokinase expression and activity (Deprez et al., 1997; Miyamoto et al., 2008). Third, Akt activity augments mTORC1 signaling and thus leads to elevated HIF1α levels which in turn increase expression of Glut1 and glycolytic enzymes (Brugarolas et al., 2003). Recently, it was demonstrated that the Skp2 SCF complex regulates Akt ubiquitination and membrane recruitment resulting in enhanced glycolysis and breast cancer progression. Inactivation of Skp2 impairs Akt activation and glucose uptake and significantly delays tumor formation in a breast cancer mouse model (Chan et al., 2012). In my experiments, phosphorylation of Akt at T308 and expression of one Skp2 isoform were reduced upon *Pdk1*-KO in $Kras^{G12D}$-driven PDAC cells. Additionally, cell growth and glucose uptake were significantly diminished. By expression of a myristoylated Akt1 isoform, the growth inhibition phenotype mediated by *Pdk1*-KO could be rescued. Furthermore, the ratio for the glucose uptake in 4-OHT- and EtOH-treated cells was significantly increased from 50% in EV cells to 80% in Akt1-myr overexpressing cells (data not shown). This observation shows that the glucose uptake is functionally relevant to explain the effect of *Pdk1*-KO on proliferation at least partially. It has to be analyzed whether the reduction in Skp2 expression upon *Pdk1* deletion can be restored to normal levels in Akt1-myr overexpressing cells.

The oncogene Myc is highly expressed in around 16% of PDAC cases (Schleger et al., 2002) and amplifications of the *Myc* gene were shown to correlate with reduced survival in PDAC (Witkiewicz et al., 2015). Stability of the Myc protein is regulated by both T58 and S62 phosphorylation. T58 phosphorylation promotes ubiquitination and subsequent degradation of Myc by the E3 ubiquitin ligase Fbw7, whereas S62 phosphorylation interferes with that process resulting in Myc accumulation (Wang et al., 2011). Recently, it was shown that Pdk1 phosphorylates polo-like kinase 1 (Plk1) which in turn binds to and induces Myc phosphorylation at S62 and thus its stabilization in colorectal cancer cell lines. Thereby, oncogenic transformation was promoted, which was at least partially by upregulation of a

cancer stem cell-like gene signature (Tan et al., 2013). However, in our laboratory expression of Plk1 was not sufficient to rescue the *Pdk1*-KO phenotype in PDAC cell lines, suggesting tissue specificity of Pdk1 downstream signaling. Lentiviral Myc expression was instead capable of partially reverting the growth inhibition upon Pdk1 inactivation. Myc phosphorylation in *Pdk1*-depleted cells has to be analyzed in future work. Furthermore, it remains to be tested whether the partial rescue effect of Myc could be augmented using a stabilized Myc mutant.

Myc was also shown to be involved in metabolism. Overexpression of Myc leads to increased transcription of metabolic enzymes like Ldha, Glut1, Hk2 and enzymes for nucleotide synthesis (DeBerardinis et al., 2008; Osthus et al., 2000; Shim et al., 1997). Recently, it was demonstrated that PDAC stem cells rely on mitochondrial oxidative phosphorylation (OXPHOS) (Sancho et al., 2015). By inhibiting the respiratory chain using metformin (Owen et al., 2000), these stem cells can be targeted whereas the glycolytic differentiated cancer cells cannot be targeted. However, PDAC stem cells can acquire resistance during metformin treatment which can be prevented by genetic elimination of *Myc* (Sancho et al., 2015). Initial experiments with inhibitors of the respiratory chain were performed by treating $Pdk1^{lox/lox};Trp53^{frt/+}$ cells with 4-OHT or EtOH and simultaneously with metformin. No synthetic lethality between Pdk1 and OXPHOS inhibition was observed. Pdk1-independent clones will be treated with metformin to analyze their dependency on OXPHOS. Furthermore, it will be elucidated whether resistance towards OXPHOS inhibition in Pdk1-resistant clones could be reversed by Myc inhibition.

Overexpression of additional Pdk1 targets and cross-signaling partners or inactivation by using the clustered regularly interspaced short palindromic repeats (CRISPR)/CRISPR associated protein 9 (Cas9) technology will allow us to functionally validate effectors of Pdk1 by gain and loss of function approaches. These experiments will show whether the *Pdk1*-KO phenotype can be rescued or recapitulated in Pdk1-proficient cells, respectively.

To further analyze Akt-dependent and -independent Pdk1 signaling, genetically engineered *Pdk1* mutant alleles will be crossed into the $Pdx1\text{-}Flp;FSF\text{-}Kras^{G12D};FSF\text{-}R26^{CAG\text{-}CreERT2};Trp53^{frt/+}$ model. The $Pdk1^{K465E}$ line lacks the PH domain, which is essential for Akt activation whereas the $Pdk1^{L155E}$ mutant harbors no PIF pocket domain, which is necessary for Pkc/Rsk/S6k/Sgk activation. Thereby, the impact of Akt as a Pdk1 effector molecule can be studied in PDAC progression and maintenance and compared to the role of the PIF-dependent kinases.

Comparison of genetic ablation and pharmacological inhibition of Pdk1

In this study, Pdk1 was validated as a therapeutic target in PDAC by using an inducible *Pdk1$^{lox/lox}$;Trp53$^{frt/+}$* model to genetically eliminate *Pdk1* in the established tumor. This approach demonstrated that *Pdk1* deletion delays PDAC growth. However, the cytostatic effect in response to the treatment was not observed as clearly as in the cell culture experiments. That is probably due to the fact that it takes 6 days to achieve a full *Pdk1*-KO, as demonstrated in cell culture experiments. In the *Pdk1$^{lox/lox}$;Trp53$^{frt/+}$* system *Pdk1* is specifically ablated in the pancreas whereas an inhibitor would affect the whole organism. This could be more closely mimicked by usage of the inducible *R26$^{CAG\text{-}CreERT2}$* deleter mouse line instead of the *FSF-R26$^{CAG\text{-}CreERT2}$* mouse line (*Pdx1-Flp;FSF-Kras$^{G12D/+}$;R26$^{CAG\text{-}CreERT2/+}$;Pdk1$^{lox/lox}$;Trp53$^{frt/+}$*). Upon TAM treatment, the *R26$^{CAG\text{-}CreERT2}$* line enables elimination of *Pdk1* in all organs whereas *Pdk1* is specifically deleted in the pancreas using the *FSF-R26$^{CAG\text{-}CreERT2}$* line. For a long time, the available PDK1 inhibitors were poorly specific or ineffective *in vivo*. To overcome this problem, the genetic model was used which harbors the advantage of specificity. In 2005, aminopyrimidines were described as compounds selectively inhibiting PDK1 (Feldman et al., 2005). However, BX-795, a member of this class, proved to inhibit also other kinases like TANK-binding kinase 1 (TANK), inhibitory κB kinase ε (IKKε) and ERK8 (Bain et al., 2007). In 2011, a novel and highly specific small molecule PDK1 inhibitor GSK2334470 was reported (Najafov et al., 2011) suppressing Pdk1 activity at an IC_{50} value of 10 nM *in vitro*. Even at concentrations around 1 µM no effects on 110 tested kinases including closely related AGC kinases were observed. Interestingly, S6K and SGK signaling were inhibited more potently than AKT signaling, indicating variability in PDK1 target suppression. First evidence for *in vivo* efficacy of GSK2334470 was reported in a *Braf^{V600E};Pten$^{-/-}$* melanoma mouse model (Scortegagna et al., 2014). Therefore, it would be interesting to treat *Pdx1-Flp;FSF-Kras$^{G12D/+}$;Trp53$^{frt/+}$* mice with GSK2334470 to compare the outcome to the genetic *Pdk1* ablation.

Analysis of metabolism in pancreatic cancer *in vivo* by PET imaging

Multi-detector CT (MDCT) of the abdomen is the mainstay of diagnostic imaging in human patients with suspected PDAC (Scialpi et al., 2014; Vargas et al., 2004; Zamboni et al., 2007). The reported sensitivity and specificity of MDCT for detection of pancreatic cancer are 86%-94% and 76%-91%, respectively (Bipat et al., 2005). FDG-PET, which uses a glucose analog to image tumors, can also be applied during the diagnosis of pancreatic tumors (Asagi et al., 2013; Tomimaru et al., 2010). This imaging technique – alone or in combination with CT – shows similar sensitivities and specificities for the depiction of pancreatic cancer compared to MDCT (Heinrich et al., 2005; Kauhanen et al., 2009; Lemke et al., 2004; Sendler et al., 2000). The inherently low spatial resolution of FDG-PET imaging and false-

positive results caused by normal physiologic FDG uptake present well-known limitations of this method (Rohren et al., 2004; von Schulthess et al., 2006). For this reason, the role of FDG-PET in identification of pancreatic diseases still has to be established. Due to its wide anatomic coverage and its penetration depth, FDG-PET is considered to be more accurate for the detection / identification of metastases and monitoring of tumor recurrence and therapy response than other imaging systems (Bang et al., 2006; Cameron et al., 2011; Kauhanen et al., 2009; Kuwatani et al., 2009; Ruf et al., 2005; Sperti et al., 2010). Although the role of FDG-PET in identification of PDAC is still undefined, this technique presents a powerful tool to analyze tumor metabolism and check treatment response for this disease. Therefore, FDG-PET was applied in this study to monitor changes in glucose metabolism following TAM treatment of tumor mice. An initial subcutaneous implantation experiment demonstrated that *Pdk1*-deleted tumors exhibit a less prominent glucose metabolism suggesting that Pdk1 plays an important role in PDAC metabolism *in vivo*.

Daemen and colleagues divided PDAC cells into a glycolytic, a lipogenic and a slow growing group by metabolite profiling. Variations in drug response towards metabolic inhibitors were highly concordant to the different subtype, although minor differences occurred within the groups (Daemen et al., 2015). These subgroups may account for the heterogeneity observed when FDG-PET imaging was performed on endogenous *Pdk1*$^{lox/lox}$*;Trp53*$^{frt/+}$ and control tumor mice. Due to the high variation within the two groups, no conclusions about the impact of *Pdk1* deletion on glucose metabolism *in vivo* could be drawn. Therefore, it was started to analyze two time points for the same mouse during TAM treatment. The *Pdk1*$^{lox/lox}$*;Trp53*$^{frt/+}$ mouse, shown in Figure 11D, displayed a reduction in the SUV_{max} within 7 d upon *Pdk1* deletion and thus probably belongs to the glycolytic subtype. However, more mice are needed to validate the effect of *Pdk1* elimination on the change of the SUV_{max} value. Moreover, tumor microenvironment (e.g. extracellular matrix (ECM), stellate cells, immune cells, blood vessel density) could contribute to tumor metabolism and to sensitivity and adaptation towards *Pdk1* deletion.

By matrix-assisted laser desorption/ionization (MALDI) imaging mass spectrometry, the distribution of a plethora of metabolites will be investigated on tissue sections of TAM-treated and untreated *Pdk1*$^{lox/lox}$*;Trp53*$^{frt/+}$ tumors. Thereby, changes on the proteome level upon *Pdk1* deletion *in situ* can be analyzed.

Resistance towards Pdk1 inhibition

Most PDAC cells showed a striking growth-inhibitory response upon *Pdk1* inactivation, whereas a small *Pdk1*-deleted subpopulation gave rise to colonies resistant towards Pdk1 inhibition. The first six Pdk1-independent clones have been analyzed by whole exome sequencing presenting a very heterogeneous mutational landscape and no recurrent

mutations. That is not surprising, because NGS studies show that apart from some well-established genes involved in PDAC tumorigenesis most mutations occur rarely, i.e. in less than 5% of cases (Bailey et al., 2016; Biankin et al., 2012; Waddell et al., 2015; Witkiewicz et al., 2015). 30–40 additional Pdk1-resistant clones have to be sequenced to detect these rare recurrent mutations and in order to define mutation patterns and pathways involved in acquisition of resistance towards Pdk1 inhibition. Moreover, chromosomal amplifications and deletions will be analyzed using the CNV data. Around 25 mutations were exclusively found in each Pdk1-independent clone. By clustering all these mutations, tumor-relevant gene sets like mTORC1 signaling, EMT and G2/M checkpoint were found. Further analysis by KO or overexpression experiments has to reveal whether the mutations are activating or inactivating. The Kras status was very heterogeneous in all Pdk1-independent clones. Some clones did not differ from the parental cell lines regarding the allelic Kras ratio, whereas others were characterized by *Kras* amplifications or loss of *WT Kras* compared to the parental cell line. Surprisingly, a small fraction of clones displayed *Pdk1* deletion, but absence of mutated Kras. Whole exome sequencing will reveal whether these clones acquire mutations Kras downstream effectors or Kras-independent signaling pathways. Overall, the data indicate that the Kras status does not present a general determinant in acquisition of resistance towards *Pdk1* inactivation.

Based on the sequencing results, it is difficult to distinguish between *de novo* mutations and already existing rare mutations in the parental cell line, since the detection limit of NGS is ~0.1% (Robasky et al., 2014). Rare subpopulations comprising less than 0.1% of the whole cell population cannot be detected and will therefore be misleadingly interpreted as de novo mutations. To overcome this limitation, a high-complexity DNA barcode library can be applied to track the evolution of pre-existing resistant clones which are too rare to be detected by NGS (Bhang et al., 2015). Enrichment of a shared set of barcodes between different replicates will indicate selection of pre-existing resistant clones.

In the following, some potentially interesting mutations in Pdk1-independent clones are discussed. In one clone, *Tnc* was the top mutated hit. This gene encodes an ECM protein containing multiple EGF-like and fibronectin type-III domains. The mutation in the Pdk1-independent clone occurred at I1625 M in fibronectin type III domain 12. In humans, a similar mutation I1106M is found in fibronectin type III domain 6 (UniProt database). It has to be elucidated whether the *Tnc* mutation is activating or inactivating, because the role of Tnc in PDAC progression is controversial. Unpublished data of our own group show that a general *Tnc*-KO accelerates tumorigenesis in a *Ptf1a*$^{Cre/+}$*;LSL-Kras*$^{G12D/+}$ model, suggesting that Tnc acts as a tumor suppressor in PDAC. In contrast to this observation, Tnc was shown to increase during progression from PanIN1 to PDAC (Esposito et al., 2006; Paron et al., 2011) arguing for an oncogenic role of Tnc. Another clone showed the highest mutation frequency

for *Ubr1*. Deficiency of this gene was shown to be causative for the rare autosomal recessive disease called Johanson-Blizzard syndrome. Apart from malformations and mental retardation, it is characterized by an exocrine dysfunction of the pancreas (Zenker et al., 2005). According to the human protein atlas, Ubr1 is highly expressed in the normal pancreas, whereas PDAC shows medium expression in 40%, low expression in 50% and absence of Ubr1 in 10%. The E3 ubiquitin ligases Ubr1 and Ubr2 are involved in recognition of N-terminal protein residues, followed by destabilization of target proteins. Expression of Ubr1 and Ubr2 was shown to negatively regulate the leucine-mTOR signaling pathway resulting in reduced S6K phosphorylation whereas knockdown leads to an increase in S6K phosphorylation (Kume et al., 2010). Summarizing the existing data on Ubr1, the mutation in the Pdk1-resistant clone is probably inactivating. This hypothesis is in agreement with the observation that mTORC1 signaling was upregulated in the Pdk1-independent clones based on a gene set enrichment analysis. *Parp2* was mutated in around 70% of cells derived from one Pdk1-independent clone. PARP2 is not expressed in normal human pancreatic tissue. In contrast, 56% of human PDAC are characterized by medium expression and 44% by low expression (human protein atlas). PARP1 and PARP2 are important for genome surveillance and DNA repair. Therefore, *Parp1*-KO and *Parp2*-KO mice are characterized by increased genomic instability (Trucco et al., 1998). Both *Parp1* and *Parp2* deficiency result in accelerated tumor formation in *p53*-KO mice indicating that Parp proteins and p53 cooperate in tumor suppression (Nicolas et al., 2010; Tong et al., 2001). For this reason, it is likely that the *Parp2* mutation occurring in the Pdk1-independent clone is inactivating. It is possible that the *Parp2* mutation leads to a higher number of mutations in the clone through increased genomic instability. For the gene encoding for the regulatory subunit 4 of PI3K (Pik3r4), the R126H mutation in the protein kinase domain was enriched in one Pdk1-independent clone. The same mutation is found in uterine carcinosarcoma in humans (Jones et al., 2014).

Two clones displayed top mutated genes with very low frequencies, i.e. 50% and 30% mutation frequency, respectively. This may indicate that in addition to genetic mutations, epigenetic changes are involved in the acquisition of Pdk1-resistance as well. Common epigenetic alterations are DNA methylation and histone modifications. DNA methylation in promoter regions represses gene transcription. Histone modifications including acetylation, methylation, phosphorylation and ubiquitination alter gene expression by affecting the chromatin structure or recruiting histone modifiers. Resistance acquired by epigenetic events like promoter methylation has been demonstrated to be clinically relevant (Gifford et al., 2004; Watanabe et al., 2007). The resistance phenotype could be reversed by application of a demethylating agent in xenografts (Plumb et al., 2000). Recently, the gene encoding for the histone demethylase KDM5A was identified to be overexpressed in a subpopulation of cancer cells, which were resistant towards EGFR inhibition by erlotinib. When drug-tolerant

cells were treated with HDAC inhibitors, they were again sensitized to EGFR inhibition (Sharma et al., 2010). The role of DNA methylation and histone modifications in Pdk1-independent clones has not been analyzed yet. However, HDAC9 was found to be upregulated upon *Pdk1* deletion in the RNA sequencing data. Like other HDACs, HDAC9 deacetylates histones H3 and H4 *in vitro* and *in vivo* (Petrie et al., 2003). Future epigenetic profiling and HDAC inhibition experiments will reveal further aspects of the functional relevance of epigenetics in Pdk1-independent clones.

Relevant hits emerging from the whole exome sequencing data have to be validated by using the lentiviral CRISPR/Cas9-based loss of function system or overexpression in cell culture experiments. It has to be tested for promising genes whether the effect is maintained under conditions resembling the patient´s tumor more closely like in 3D organoids or mouse models. Furthermore, analysis of the transcriptome and phospho-proteome will be performed with Pdk1-independent clones to characterize changes in PI3K/Pdk1 signaling, MAPK pathway activation, cell cycle regulation, DDR, autophagy as well as inhibition of apoptosis and senescence.

Role of Mek signaling in Kras^{G12D}- and PIK3CA^{H1047R}-driven PDAC

Apart from the PI3K/Pdk1 signaling pathway, the Raf/Mek/Erk pathway presents another well-established effector pathway of oncogenic Kras. Therefore, the role of Mek kinases in PDAC formation and maintenance was assessed in this thesis. Deletion of *Mek1* did neither block Kras^{G12D}- nor PIK3CA^{H1047R}-driven PDAC initiation. This finding is consistent with results obtained by deletion of *Mek1* or *Mek2* in a Kras^{G12V}-driven NSCLC mouse model. No effect on carcinogenesis was observed and phosphorylation of Erk remained unchanged, respectively (Blasco et al., 2011). It was shown that Erk mediates phosphorylation of T292 on Mek1 and thus negatively regulates the stability of the Mek1-Mek2-heterodimer. By deletion of *Mek1* this negative feedback loop is abolished resulting in upregulation of Mek2-dependent Erk signaling (Catalanotti et al., 2009). This mechanism might be a potential explanation why ablation of *Mek1* did not block PDAC formation in the used mouse models.

In this work, simultaneous inactivation of *Mek1* and *Mek2* blocked growth of a Kras^{G12D}-driven PDAC cell lines *in vitro*. Consistently, elimination of both Mek kinases in a Kras^{G12V}-driven mouse model blocked NSCLC formation (Blasco et al., 2011). Treatment of PDAC cell lines or mouse models with dual Mek1/2 inhibitors, e.g. AZD6244 and pimasertib, abolished phosphorylation of Erk completely *in vitro* and *in vivo* (Alagesan et al., 2015; Pettazzoni et al., 2015; Vena et al., 2015). Surprisingly, genetic elimination of both Mek kinases in this work did not result in loss of ERK phosphorylation. Only the phosphorylation of p44 was reduced. This effect was seen in both the 4-OHT-treated *Pdx1-Flp;FSF-Kras$^{G12D/+}$;FSF-R26$^{CAG\text{-}CreERT2/+}$;Mek1$^{lox/lox}$;Mek2$^{\Delta/\Delta}$* and the 4-OHT-treated *Pdx1-Flp;FSF-Kras$^{G12D/+}$;FSF-*

R26$^{CAG\text{-}CreERT2/+}$*;Mek1*$^{lox/lox}$*;Mek2*$^{\Delta/+}$ cell line, demonstrating that the p44 phosphorylation did not account for reduced growth. More cell lines have to be generated to validate these observations. Transcriptome and proteome analyses as well as localization of Erk in *Mek*-deleted Kras^{G12D}-driven cell lines and tumors will be used to elucidate the molecular consequences upon *Mek1/2* deletion.

Conclusion

To summarize, this work sheds light onto the role of PI3K/Pdk1 signaling in progression and maintenance of PDAC in Kras^{G12D}-driven mouse models. Pdk1 was shown to be important for PanIN formation, growth of PDAC and tumor metabolism *in vitro* and *in vivo*. However, a subpopulation of cells was able to survive *Pdk1* deletion giving rise to resistant clones. Further experiments will be needed to validate PI3K/Pdk1 as a therapeutic target in PDAC helping to treat this devastating disease and overcome resistance. Deletion of *Mek1* neither blocked PDAC formation in Kras^{G12D}- nor in PIK3CA^{H1047R}-driven mouse models. Concomitant ablation of *Mek1* and *Mek2* inhibited growth of Kras^{G12D}-driven PDAC cell line whereas homozygous deletion of *Mek1* and heterozygous deletion of *Mek2* did not impair cell viability.

Acknowledgements

Hereby, I would like to thank everyone who contributed to the success of this PhD thesis.

First, I thank Prof. Dr. Dieter Saur for giving me the chance to work on this interesting project, for his advice, valuable comments on the project and revision of the thesis.

I owe my gratitude to Prof. Dr. Roland Schmid for giving me the opportunity to work in his department, the II. Medizinische Klinik at Klinikum rechts der Isar.

I also thank PD Dr. Günter Schneider and PD Dr. Philipp Jost for their kindness being members of my PhD committee.

Furthermore I owe my gratitude to…

… Dr. Benedikt Feuerecker for discussion of experiments and analysis of PET imaging data.
… Michael Michalski for doing MRI scans and teaching me how to perform them myself.
… Dr. Maxim Barenboim and Thomas Engleitner for bioinformatical analysis of RNA sequencing and whole exome sequencing data.
… Dr. Mariel Paul for diligent revision of the thesis.
… Magdalena Zukowska for excellent technical support.
… Lucia Liotta, Constanze Mattes, Vanessa Schöllhorn, Anna Schwarz and Christina Zeller who contributed either to the Pdk1 or the Mek project with their work.
… the PET core team for performing PET scans.
… all animal caretakers for caring for the mice.
… all other colleagues for discussion and the nice atmosphere in the lab.

Last but not least, I thank my family and my friends who always supported me.

References

Aguirre, A. J., Bardeesy, N., Sinha, M., Lopez, L., Tuveson, D. A., Horner, J., Redston, M. S., and DePinho, R. A. (2003). Activated Kras and Ink4a/Arf deficiency cooperate to produce metastatic pancreatic ductal adenocarcinoma. Genes Dev *17*, 3112-3126.

Aichler, M., Seiler, C., Tost, M., Siveke, J., Mazur, P. K., Da Silva-Buttkus, P., Bartsch, D. K., Langer, P., Chiblak, S., Durr, A.*, et al.* (2012). Origin of pancreatic ductal adenocarcinoma from atypical flat lesions: a comparative study in transgenic mice and human tissues. J Pathol *226*, 723-734.

Alagesan, B., Contino, G., Guimaraes, A. R., Corcoran, R. B., Deshpande, V., Wojtkiewicz, G. R., Hezel, A. F., Wong, K. K., Loda, M., Weissleder, R.*, et al.* (2015). Combined MEK and PI3K inhibition in a mouse model of pancreatic cancer. Clin Cancer Res *21*, 396-404.

Alessi, D. R., James, S. R., Downes, C. P., Holmes, A. B., Gaffney, P. R., Reese, C. B., and Cohen, P. (1997). Characterization of a 3-phosphoinositide-dependent protein kinase which phosphorylates and activates protein kinase Balpha. Curr Biol *7*, 261-269.

Ardito, C. M., Gruner, B. M., Takeuchi, K. K., Lubeseder-Martellato, C., Teichmann, N., Mazur, P. K., Delgiorno, K. E., Carpenter, E. S., Halbrook, C. J., Hall, J. C.*, et al.* (2012). EGF receptor is required for KRAS-induced pancreatic tumorigenesis. Cancer Cell *22*, 304-317.

Asagi, A., Ohta, K., Nasu, J., Tanada, M., Nadano, S., Nishimura, R., Teramoto, N., Yamamoto, K., Inoue, T., and Iguchi, H. (2013). Utility of contrast-enhanced FDG-PET/CT in the clinical management of pancreatic cancer: impact on diagnosis, staging, evaluation of treatment response, and detection of recurrence. Pancreas *42*, 11-19.

Asano, T., Yao, Y., Zhu, J., Li, D., Abbruzzese, J. L., and Reddy, S. A. (2004). The PI 3-kinase/Akt signaling pathway is activated due to aberrant Pten expression and targets transcription factors NF-kappaB and c-Myc in pancreatic cancer cells. Oncogene *23*, 8571-8580.

Aune, D., Greenwood, D. C., Chan, D. S., Vieira, R., Vieira, A. R., Navarro Rosenblatt, D. A., Cade, J. E., Burley, V. J., and Norat, T. (2012). Body mass index, abdominal fatness and pancreatic cancer risk: a systematic review and non-linear dose-response meta-analysis of prospective studies. Ann Oncol *23*, 843-852.

Bailey, P., Chang, D. K., Nones, K., Johns, A. L., Patch, A. M., Gingras, M. C., Miller, D. K., Christ, A. N., Bruxner, T. J., Quinn, M. C.*, et al.* (2016). Genomic analyses identify molecular subtypes of pancreatic cancer. Nature *531*, 47-52.

Bain, J., Plater, L., Elliott, M., Shpiro, N., Hastie, C. J., McLauchlan, H., Klevernic, I., Arthur, J. S., Alessi, D. R., and Cohen, P. (2007). The selectivity of protein kinase inhibitors: a further update. Biochem J *408*, 297-315.

Bang, S., Chung, H. W., Park, S. W., Chung, J. B., Yun, M., Lee, J. D., and Song, S. Y. (2006). The clinical usefulness of 18-fluorodeoxyglucose positron emission tomography in the differential diagnosis, staging, and response evaluation after concurrent chemoradiotherapy for pancreatic cancer. J Clin Gastroenterol *40*, 923-929.

Bardeesy, N., Aguirre, A. J., Chu, G. C., Cheng, K. H., Lopez, L. V., Hezel, A. F., Feng, B., Brennan, C., Weissleder, R., Mahmood, U.*, et al.* (2006a). Both p16(Ink4a) and the p19(Arf)-p53 pathway constrain progression of pancreatic adenocarcinoma in the mouse. Proc Natl Acad Sci U S A *103*, 5947-5952.

Bardeesy, N., Cheng, K. H., Berger, J. H., Chu, G. C., Pahler, J., Olson, P., Hezel, A. F., Horner, J., Lauwers, G. Y., Hanahan, D., and DePinho, R. A. (2006b). Smad4 is dispensable for normal pancreas development yet critical in progression and tumor biology of pancreas cancer. Genes Dev *20*, 3130-3146.

Barthel, A., Okino, S. T., Liao, J., Nakatani, K., Li, J., Whitlock, J. P., Jr., and Roth, R. A. (1999). Regulation of GLUT1 gene transcription by the serine/threonine kinase Akt1. J Biol Chem *274*, 20281-20286.

Bayascas, J. R., Wullschleger, S., Sakamoto, K., Garcia-Martinez, J. M., Clacher, C., Komander, D., van Aalten, D. M., Boini, K. M., Lang, F., Lipina, C*., et al.* (2008). Mutation of the PDK1 PH domain inhibits protein kinase B/Akt, leading to small size and insulin resistance. Mol Cell Biol *28*, 3258-3272.

Belteki, G., Haigh, J., Kabacs, N., Haigh, K., Sison, K., Costantini, F., Whitsett, J., Quaggin, S. E., and Nagy, A. (2005). Conditional and inducible transgene expression in mice through the combinatorial use of Cre-mediated recombination and tetracycline induction. Nucleic Acids Res *33*, e51.

Ben, Q., Xu, M., Ning, X., Liu, J., Hong, S., Huang, W., Zhang, H., and Li, Z. (2011). Diabetes mellitus and risk of pancreatic cancer: A meta-analysis of cohort studies. Eur J Cancer *47*, 1928-1937.

Bhang, H. E., Ruddy, D. A., Krishnamurthy Radhakrishna, V., Caushi, J. X., Zhao, R., Hims, M. M., Singh, A. P., Kao, I., Rakiec, D., Shaw, P*., et al.* (2015). Studying clonal dynamics in response to cancer therapy using high-complexity barcoding. Nat Med *21*, 440-448.

Biankin, A. V., Waddell, N., Kassahn, K. S., Gingras, M. C., Muthuswamy, L. B., Johns, A. L., Miller, D. K., Wilson, P. J., Patch, A. M., Wu, J*., et al.* (2012). Pancreatic cancer genomes reveal aberrations in axon guidance pathway genes. Nature *491*, 399-405.

Bipat, S., Phoa, S. S., van Delden, O. M., Bossuyt, P. M., Gouma, D. J., Lameris, J. S., and Stoker, J. (2005). Ultrasonography, computed tomography and magnetic resonance imaging for diagnosis and determining resectability of pancreatic adenocarcinoma: a meta-analysis. J Comput Assist Tomogr *29*, 438-445.

Blasco, R. B., Francoz, S., Santamaria, D., Canamero, M., Dubus, P., Charron, J., Baccarini, M., and Barbacid, M. (2011). c-Raf, but not B-Raf, is essential for development of K-Ras oncogene-driven non-small cell lung carcinoma. Cancer Cell *19*, 652-663.

Boehm, J. S., Zhao, J. J., Yao, J., Kim, S. Y., Firestein, R., Dunn, I. F., Sjostrom, S. K., Garraway, L. A., Weremowicz, S., Richardson, A. L*., et al.* (2007). Integrative genomic approaches identify IKBKE as a breast cancer oncogene. Cell *129*, 1065-1079.

Bolger, A. M., Lohse, M., and Usadel, B. (2014). Trimmomatic: a flexible trimmer for Illumina sequence data. Bioinformatics *30*, 2114-2120.

Bosetti, C., Lucenteforte, E., Silverman, D. T., Petersen, G., Bracci, P. M., Ji, B. T., Negri, E., Li, D., Risch, H. A., Olson, S. H*., et al.* (2012). Cigarette smoking and pancreatic cancer: an analysis from the International Pancreatic Cancer Case-Control Consortium (Panc4). Ann Oncol *23*, 1880-1888.

Bourne, H. R., Sanders, D. A., and McCormick, F. (1990). The GTPase superfamily: a conserved switch for diverse cell functions. Nature *348*, 125-132.

Bradford, M. M. (1976). A rapid and sensitive method for the quantitation of microgram quantities of protein utilizing the principle of protein-dye binding. Anal Biochem *72*, 248-254.

Brugarolas, J. B., Vazquez, F., Reddy, A., Sellers, W. R., and Kaelin, W. G., Jr. (2003). TSC2 regulates VEGF through mTOR-dependent and -independent pathways. Cancer Cell *4*, 147-158.

Buhrman, G., Holzapfel, G., Fetics, S., and Mattos, C. (2010). Allosteric modulation of Ras positions Q61 for a direct role in catalysis. Proc Natl Acad Sci U S A *107*, 4931-4936.

Burris, H. A., 3rd, Moore, M. J., Andersen, J., Green, M. R., Rothenberg, M. L., Modiano, M. R., Cripps, M. C., Portenoy, R. K., Storniolo, A. M., Tarassoff, P.*, et al.* (1997). Improvements in survival and clinical benefit with gemcitabine as first-line therapy for patients with advanced pancreas cancer: a randomized trial. J Clin Oncol *15*, 2403-2413.

Cameron, K., Golan, S., Simpson, W., Peti, S., Roayaie, S., Labow, D., and Kostakoglu, L. (2011). Recurrent pancreatic carcinoma and cholangiocarcinoma: 18F-fluorodeoxyglucose positron emission tomography/computed tomography (PET/CT). Abdom Imaging *36*, 463-471.

Cantley, L. C. (2002). The phosphoinositide 3-kinase pathway. Science *296*, 1655-1657.

Catalanotti, F., Reyes, G., Jesenberger, V., Galabova-Kovacs, G., de Matos Simoes, R., Carugo, O., and Baccarini, M. (2009). A Mek1-Mek2 heterodimer determines the strength and duration of the Erk signal. Nat Struct Mol Biol *16*, 294-303.

Chan, C. H., Li, C. F., Yang, W. L., Gao, Y., Lee, S. W., Feng, Z., Huang, H. Y., Tsai, K. K., Flores, L. G., Shao, Y.*, et al.* (2012). The Skp2-SCF E3 ligase regulates Akt ubiquitination, glycolysis, herceptin sensitivity, and tumorigenesis. Cell *149*, 1098-1111.

Cho, Y. Y., He, Z., Zhang, Y., Choi, H. S., Zhu, F., Choi, B. Y., Kang, B. S., Ma, W. Y., Bode, A. M., and Dong, Z. (2005). The p53 protein is a novel substrate of ribosomal S6 kinase 2 and a critical intermediary for ribosomal S6 kinase 2 and histone H3 interaction. Cancer Res *65*, 3596-3603.

Cho, Y. Y., Lee, M. H., Lee, C. J., Yao, K., Lee, H. S., Bode, A. M., and Dong, Z. (2012). RSK2 as a key regulator in human skin cancer. Carcinogenesis *33*, 2529-2537.

Cho, Y. Y., Yao, K., Bode, A. M., Bergen, H. R., 3rd, Madden, B. J., Oh, S. M., Ermakova, S., Kang, B. S., Choi, H. S., Shim, J. H., and Dong, Z. (2007a). RSK2 mediates muscle cell differentiation through regulation of NFAT3. J Biol Chem *282*, 8380-8392.

Cho, Y. Y., Yao, K., Kim, H. G., Kang, B. S., Zheng, D., Bode, A. M., and Dong, Z. (2007b). Ribosomal S6 kinase 2 is a key regulator in tumor promoter induced cell transformation. Cancer Res *67*, 8104-8112.

Cho, Y. Y., Yao, K., Pugliese, A., Malakhova, M. L., Bode, A. M., and Dong, Z. (2009). A regulatory mechanism for RSK2 NH(2)-terminal kinase activity. Cancer Res *69*, 4398-4406.

Cibulskis, K., Lawrence, M. S., Carter, S. L., Sivachenko, A., Jaffe, D., Sougnez, C., Gabriel, S., Meyerson, M., Lander, E. S., and Getz, G. (2013). Sensitive detection of somatic point mutations in impure and heterogeneous cancer samples. Nat Biotechnol *31*, 213-219.

Collins, M. A., Bednar, F., Zhang, Y., Brisset, J. C., Galban, S., Galban, C. J., Rakshit, S., Flannagan, K. S., Adsay, N. V., and Pasca di Magliano, M. (2012a). Oncogenic Kras is required for both the initiation and maintenance of pancreatic cancer in mice. J Clin Invest *122*, 639-653.

Collins, M. A., Brisset, J. C., Zhang, Y., Bednar, F., Pierre, J., Heist, K. A., Galban, C. J., Galban, S., and di Magliano, M. P. (2012b). Metastatic pancreatic cancer is dependent on oncogenic Kras in mice. PLoS One *7*, e49707.

Collisson, E. A., Sadanandam, A., Olson, P., Gibb, W. J., Truitt, M., Gu, S., Cooc, J., Weinkle, J., Kim, G. E., Jakkula, L.*, et al.* (2011). Subtypes of pancreatic ductal adenocarcinoma and their differing responses to therapy. Nat Med *17*, 500-503.

Collisson, E. A., Trejo, C. L., Silva, J. M., Gu, S., Korkola, J. E., Heiser, L. M., Charles, R. P., Rabinovich, B. A., Hann, B., Dankort, D.*, et al.* (2012). A central role for RAF-->MEK-->ERK signaling in the genesis of pancreatic ductal adenocarcinoma. Cancer Discov *2*, 685-693.

Commisso, C., Davidson, S. M., Soydaner-Azeloglu, R. G., Parker, S. J., Kamphorst, J. J., Hackett, S., Grabocka, E., Nofal, M., Drebin, J. A., Thompson, C. B.*, et al.* (2013). Macropinocytosis of protein is an amino acid supply route in Ras-transformed cells. Nature *497*, 633-637.

Conroy, T., Desseigne, F., Ychou, M., Bouche, O., Guimbaud, R., Becouarn, Y., Adenis, A., Raoul, J. L., Gourgou-Bourgade, S., de la Fouchardiere, C.*, et al.* (2011). FOLFIRINOX versus gemcitabine for metastatic pancreatic cancer. N Engl J Med *364*, 1817-1825.

Crews, C. M., and Erikson, R. L. (1993). Extracellular signals and reversible protein phosphorylation: what to Mek of it all. Cell *74*, 215-217.

Currie, R. A., Walker, K. S., Gray, A., Deak, M., Casamayor, A., Downes, C. P., Cohen, P., Alessi, D. R., and Lucocq, J. (1999). Role of phosphatidylinositol 3,4,5-trisphosphate in regulating the activity and localization of 3-phosphoinositide-dependent protein kinase-1. Biochem J *337 (Pt 3)*, 575-583.

D'Adamo, D. R., Novick, S., Kahn, J. M., Leonardi, P., and Pellicer, A. (1997). rsc: a novel oncogene with structural and functional homology with the gene family of exchange factors for Ral. Oncogene *14*, 1295-1305.

Daemen, A., Peterson, D., Sahu, N., McCord, R., Du, X., Liu, B., Kowanetz, K., Hong, R., Moffat, J., Gao, M.*, et al.* (2015). Metabolite profiling stratifies pancreatic ductal adenocarcinomas into subtypes with distinct sensitivities to metabolic inhibitors. Proc Natl Acad Sci U S A *112*, E4410-4417.

de Vries, A., Flores, E. R., Miranda, B., Hsieh, H. M., van Oostrom, C. T., Sage, J., and Jacks, T. (2002). Targeted point mutations of p53 lead to dominant-negative inhibition of wild-type p53 function. Proc Natl Acad Sci U S A *99*, 2948-2953.

DeBerardinis, R. J., Lum, J. J., Hatzivassiliou, G., and Thompson, C. B. (2008). The biology of cancer: metabolic reprogramming fuels cell growth and proliferation. Cell Metab *7*, 11-20.

DeNicola, G. M., Karreth, F. A., Humpton, T. J., Gopinathan, A., Wei, C., Frese, K., Mangal, D., Yu, K. H., Yeo, C. J., Calhoun, E. S.*, et al.* (2011). Oncogene-induced Nrf2 transcription promotes ROS detoxification and tumorigenesis. Nature *475*, 106-109.

Deprez, J., Vertommen, D., Alessi, D. R., Hue, L., and Rider, M. H. (1997). Phosphorylation and activation of heart 6-phosphofructo-2-kinase by protein kinase B and other protein kinases of the insulin signaling cascades. J Biol Chem *272*, 17269-17275.

Domchek, S. M., Auger, K. R., Chatterjee, S., Burke, T. R., Jr., and Shoelson, S. E. (1992). Inhibition of SH2 domain/phosphoprotein association by a nonhydrolyzable phosphonopeptide. Biochemistry *31*, 9865-9870.

Du, J., Yang, M., Chen, S., Li, D., Chang, Z., and Dong, Z. (2015). PDK1 promotes tumor growth and metastasis in a spontaneous breast cancer model. Oncogene.

Duell, E. J., Lucenteforte, E., Olson, S. H., Bracci, P. M., Li, D., Risch, H. A., Silverman, D. T., Ji, B. T., Gallinger, S., Holly, E. A.*, et al.* (2012). Pancreatitis and pancreatic cancer risk: a pooled analysis in the International Pancreatic Cancer Case-Control Consortium (PanC4). Ann Oncol *23*, 2964-2970.

Duronio, V. (2008). The life of a cell: apoptosis regulation by the PI3K/PKB pathway. Biochem J *415*, 333-344.

Elstrom, R. L., Bauer, D. E., Buzzai, M., Karnauskas, R., Harris, M. H., Plas, D. R., Zhuang, H., Cinalli, R. M., Alavi, A., Rudin, C. M., and Thompson, C. B. (2004). Akt stimulates aerobic glycolysis in cancer cells. Cancer Res *64*, 3892-3899.

Engelman, J. A., Janne, P. A., Mermel, C., Pearlberg, J., Mukohara, T., Fleet, C., Cichowski, K., Johnson, B. E., and Cantley, L. C. (2005). ErbB-3 mediates phosphoinositide 3-kinase activity in gefitinib-sensitive non-small cell lung cancer cell lines. Proc Natl Acad Sci U S A *102*, 3788-3793.

Engelman, J. A., Luo, J., and Cantley, L. C. (2006). The evolution of phosphatidylinositol 3-kinases as regulators of growth and metabolism. Nat Rev Genet *7*, 606-619.

Engelman, J. A., Zejnullahu, K., Mitsudomi, T., Song, Y., Hyland, C., Park, J. O., Lindeman, N., Gale, C. M., Zhao, X., Christensen, J.*, et al.* (2007). MET amplification leads to gefitinib resistance in lung cancer by activating ERBB3 signaling. Science *316*, 1039-1043.

Eser, S., Reiff, N., Messer, M., Seidler, B., Gottschalk, K., Dobler, M., Hieber, M., Arbeiter, A., Klein, S., Kong, B.*, et al.* (2013). Selective requirement of PI3K/PDK1 signaling for Kras oncogene-driven pancreatic cell plasticity and cancer. Cancer Cell *23*, 406-420.

Esposito, I., Penzel, R., Chaib-Harrireche, M., Barcena, U., Bergmann, F., Riedl, S., Kayed, H., Giese, N., Kleeff, J., Friess, H., and Schirmacher, P. (2006). Tenascin C and annexin II expression in the process of pancreatic carcinogenesis. J Pathol *208*, 673-685.

Feldman, R. I., Wu, J. M., Polokoff, M. A., Kochanny, M. J., Dinter, H., Zhu, D., Biroc, S. L., Alicke, B., Bryant, J., Yuan, S.*, et al.* (2005). Novel small molecule inhibitors of 3-phosphoinositide-dependent kinase-1. J Biol Chem *280*, 19867-19874.

Field, J., Broek, D., Kataoka, T., and Wigler, M. (1987). Guanine nucleotide activation of, and competition between, RAS proteins from Saccharomyces cerevisiae. Mol Cell Biol *7*, 2128-2133.

Fruman, D. A., and Rommel, C. (2014). PI3K and cancer: lessons, challenges and opportunities. Nat Rev Drug Discov *13*, 140-156.

Fujii, S., Mitsunaga, S., Yamazaki, M., Hasebe, T., Ishii, G., Kojima, M., Kinoshita, T., Ueno, T., Esumi, H., and Ochiai, A. (2008). Autophagy is activated in pancreatic cancer cells and correlates with poor patient outcome. Cancer Sci *99*, 1813-1819.

Gannon, M., Herrera, P. L., and Wright, C. V. (2000). Mosaic Cre-mediated recombination in pancreas using the pdx-1 enhancer/promoter. Genesis *26*, 143-144.

Giardiello, F. M., Brensinger, J. D., Tersmette, A. C., Goodman, S. N., Petersen‡, G. M., Booker, S. V., Cruz–Correa, M., and Offerhaus, J. A. (2000). Very high risk of cancer in familial Peutz–Jeghers syndrome. Gastroenterology *119*, 1447-1453.

Gifford, G., Paul, J., Vasey, P. A., Kaye, S. B., and Brown, R. (2004). The acquisition of hMLH1 methylation in plasma DNA after chemotherapy predicts poor survival for ovarian cancer patients. Clin Cancer Res *10*, 4420-4426.

Gonzalez-Garcia, A., Pritchard, C. A., Paterson, H. F., Mavria, G., Stamp, G., and Marshall, C. J. (2005). RalGDS is required for tumor formation in a model of skin carcinogenesis. Cancer Cell *7*, 219-226.

Guerra, C., Schuhmacher, A. J., Canamero, M., Grippo, P. J., Verdaguer, L., Perez-Gallego, L., Dubus, P., Sandgren, E. P., and Barbacid, M. (2007). Chronic pancreatitis is essential for induction of pancreatic ductal adenocarcinoma by K-Ras oncogenes in adult mice. Cancer Cell *11*, 291-302.

Guillaumond, F., Bidaut, G., Ouaissi, M., Servais, S., Gouirand, V., Olivares, O., Lac, S., Borge, L., Roques, J., Gayet, O.*, et al.* (2015). Cholesterol uptake disruption, in association with chemotherapy, is a promising combined metabolic therapy for pancreatic adenocarcinoma. Proc Natl Acad Sci U S A *112*, 2473-2478.

Harada, T., Chelala, C., Bhakta, V., Chaplin, T., Caulee, K., Baril, P., Young, B. D., and Lemoine, N. R. (2008). Genome-wide DNA copy number analysis in pancreatic cancer using high-density single nucleotide polymorphism arrays. Oncogene *27*, 1951-1960.

Hata, A. N., Niederst, M. J., Archibald, H. L., Gomez-Caraballo, M., Siddiqui, F. M., Mulvey, H. E., Maruvka, Y. E., Ji, F., Bhang, H. E., Krishnamurthy Radhakrishna, V.*, et al.* (2016). Tumor cells can follow distinct evolutionary paths to become resistant to epidermal growth factor receptor inhibition. Nat Med *22*, 262-269.

Heid, I., Lubeseder-Martellato, C., Sipos, B., Mazur, P. K., Lesina, M., Schmid, R. M., and Siveke, J. T. (2011). Early requirement of Rac1 in a mouse model of pancreatic cancer. Gastroenterology *141*, 719-730, 730 e711-717.

Heinrich, S., Goerres, G. W., Schafer, M., Sagmeister, M., Bauerfeind, P., Pestalozzi, B. C., Hany, T. F., von Schulthess, G. K., and Clavien, P. A. (2005). Positron emission tomography/computed tomography influences on the management of resectable pancreatic cancer and its cost-effectiveness. Ann Surg *242*, 235-243.

Hennessy, B. T., Smith, D. L., Ram, P. T., Lu, Y., and Mills, G. B. (2005). Exploiting the PI3K/AKT pathway for cancer drug discovery. Nat Rev Drug Discov *4*, 988-1004.

Hingorani, S. R., Petricoin, E. F., Maitra, A., Rajapakse, V., King, C., Jacobetz, M. A., Ross, S., Conrads, T. P., Veenstra, T. D., Hitt, B. A.*, et al.* (2003). Preinvasive and invasive ductal pancreatic cancer and its early detection in the mouse. Cancer Cell *4*, 437-450.

Hingorani, S. R., Wang, L., Multani, A. S., Combs, C., Deramaudt, T. B., Hruban, R. H., Rustgi, A. K., Chang, S., and Tuveson, D. A. (2005). Trp53R172H and KrasG12D cooperate to promote chromosomal instability and widely metastatic pancreatic ductal adenocarcinoma in mice. Cancer Cell *7*, 469-483.

Hruban, R. H., Adsay, N. V., Albores-Saavedra, J., Anver, M. R., Biankin, A. V., Boivin, G. P., Furth, E. E., Furukawa, T., Klein, A., Klimstra, D. S.*, et al.* (2006). Pathology of genetically engineered mouse models of pancreatic exocrine cancer: consensus report and recommendations. Cancer Res *66*, 95-106.

Hruban, R. H., Goggins, M., Parsons, J., and Kern, S. E. (2000). Progression model for pancreatic cancer. Clin Cancer Res *6*, 2969-2972.

Iqbal, J., Ragone, A., Lubinski, J., Lynch, H. T., Moller, P., Ghadirian, P., Foulkes, W. D., Armel, S., Eisen, A., Neuhausen, S. L.*, et al.* (2012). The incidence of pancreatic cancer in BRCA1 and BRCA2 mutation carriers. Br J Cancer *107*, 2005-2009.

Ischenko, I., Petrenko, O., and Hayman, M. J. (2015). A MEK/PI3K/HDAC inhibitor combination therapy for KRAS mutant pancreatic cancer cells. Oncotarget *6*, 15814-15827.

Jackson, E. L., Willis, N., Mercer, K., Bronson, R. T., Crowley, D., Montoya, R., Jacks, T., and Tuveson, D. A. (2001). Analysis of lung tumor initiation and progression using conditional expression of oncogenic K-ras. Genes Dev *15*, 3243-3248.

Jensen, C. J., Buch, M. B., Krag, T. O., Hemmings, B. A., Gammeltoft, S., and Frodin, M. (1999). 90-kDa ribosomal S6 kinase is phosphorylated and activated by 3-phosphoinositide-dependent protein kinase-1. J Biol Chem *274*, 27168-27176.

Jones, S., Hruban, R. H., Kamiyama, M., Borges, M., Zhang, X., Parsons, D. W., Lin, J. C., Palmisano, E., Brune, K., Jaffee, E. M.*, et al.* (2009). Exomic sequencing identifies PALB2 as a pancreatic cancer susceptibility gene. Science *324*, 217.

Jones, S., Stransky, N., McCord, C. L., Cerami, E., Lagowski, J., Kelly, D., Angiuoli, S. V., Sausen, M., Kann, L., Shukla, M.*, et al.* (2014). Genomic analyses of gynaecologic carcinosarcomas reveal frequent mutations in chromatin remodelling genes. Nat Commun *5*, 5006.

Jones, S., Zhang, X., Parsons, D. W., Lin, J. C., Leary, R. J., Angenendt, P., Mankoo, P., Carter, H., Kamiyama, H., Jimeno, A.*, et al.* (2008). Core signaling pathways in human pancreatic cancers revealed by global genomic analyses. Science *321*, 1801-1806.

Kanda, M., Matthaei, H., Wu, J., Hong, S. M., Yu, J., Borges, M., Hruban, R. H., Maitra, A., Kinzler, K., Vogelstein, B., and Goggins, M. (2012). Presence of somatic mutations in most early-stage pancreatic intraepithelial neoplasia. Gastroenterology *142*, 730-733 e739.

Karreth, F. A., Frese, K. K., DeNicola, G. M., Baccarini, M., and Tuveson, D. A. (2011). C-Raf is required for the initiation of lung cancer by K-Ras(G12D). Cancer Discov *1*, 128-136.

Kastrinos, F., Mukherjee, B., Tayob, N., Wang, F., Sparr, J., Raymond, V. M., Bandipalliam, P., Stoffel, E. M., Gruber, S. B., and Syngal, S. (2009). Risk of pancreatic cancer in families with Lynch syndrome. JAMA *302*, 1790-1795.

Kauhanen, S. P., Komar, G., Seppanen, M. P., Dean, K. I., Minn, H. R., Kajander, S. A., Rinta-Kiikka, I., Alanen, K., Borra, R. J., Puolakkainen, P. A.*, et al.* (2009). A prospective diagnostic accuracy study of 18F-fluorodeoxyglucose positron emission tomography/computed tomography, multidetector row computed tomography, and magnetic resonance imaging in primary diagnosis and staging of pancreatic cancer. Ann Surg *250*, 957-963.

Kawaguchi, Y., Cooper, B., Gannon, M., Ray, M., MacDonald, R. J., and Wright, C. V. (2002). The role of the transcriptional regulator Ptf1a in converting intestinal to pancreatic progenitors. Nat Genet *32*, 128-134.

Kimmelman, A. C., Hezel, A. F., Aguirre, A. J., Zheng, H., Paik, J. H., Ying, H., Chu, G. C., Zhang, J. X., Sahin, E., Yeo, G.*, et al.* (2008). Genomic alterations link Rho family of GTPases to the highly invasive phenotype of pancreas cancer. Proc Natl Acad Sci U S A *105*, 19372-19377.

Kinross, K. M., Montgomery, K. G., Kleinschmidt, M., Waring, P., Ivetac, I., Tikoo, A., Saad, M., Hare, L., Roh, V., Mantamadiotis, T.*, et al.* (2012). An activating Pik3ca mutation coupled with Pten loss is sufficient to initiate ovarian tumorigenesis in mice. J Clin Invest *122*, 553-557.

Kohn, A. D., Summers, S. A., Birnbaum, M. J., and Roth, R. A. (1996). Expression of a constitutively active Akt Ser/Thr kinase in 3T3-L1 adipocytes stimulates glucose uptake and glucose transporter 4 translocation. J Biol Chem *271*, 31372-31378.

Kuilman, T., Velds, A., Kemper, K., Ranzani, M., Bombardelli, L., Hoogstraat, M., Nevedomskaya, E., Xu, G., de Ruiter, J., Lolkema, M. P.*, et al.* (2015). CopywriteR: DNA copy number detection from off-target sequence data. Genome Biol *16*, 49.

Kume, K., Iizumi, Y., Shimada, M., Ito, Y., Kishi, T., Yamaguchi, Y., and Handa, H. (2010). Role of N-end rule ubiquitin ligases UBR1 and UBR2 in regulating the leucine-mTOR signaling pathway. Genes Cells *15*, 339-349.

Kuwatani, M., Kawakami, H., Eto, K., Haba, S., Shiga, T., Tamaki, N., and Asaka, M. (2009). Modalities for evaluating chemotherapeutic efficacy and survival time in patients with advanced pancreatic cancer: comparison between FDG-PET, CT, and serum tumor markers. Intern Med *48*, 867-875.

Laemmli, U. K. (1970). Cleavage of structural proteins during the assembly of the head of bacteriophage T4. Nature *227*, 680-685.

Lawlor, M. A., Mora, A., Ashby, P. R., Williams, M. R., Murray-Tait, V., Malone, L., Prescott, A. R., Lucocq, J. M., and Alessi, D. R. (2002). Essential role of PDK1 in regulating cell size and development in mice. Embo J *21*, 3728-3738.

Lee, C. L., Moding, E. J., Huang, X., Li, Y., Woodlief, L. Z., Rodrigues, R. C., Ma, Y., and Kirsch, D. G. (2012). Generation of primary tumors with Flp recombinase in FRT-flanked p53 mice. Dis Model Mech *5*, 397-402.

Lee, M. H., Huang, Z., Kim, D. J., Kim, S. H., Kim, M. O., Lee, S. Y., Xie, H., Park, S. J., Kim, J. Y., Kundu, J. K.*, et al.* (2013). Direct targeting of MEK1/2 and RSK2 by silybin induces cell-cycle arrest and inhibits melanoma cell growth. Cancer Prev Res (Phila) *6*, 455-465.

Lemke, A. J., Niehues, S. M., Hosten, N., Amthauer, H., Boehmig, M., Stroszczynski, C., Rohlfing, T., Rosewicz, S., and Felix, R. (2004). Retrospective digital image fusion of multidetector CT and 18F-FDG PET: clinical value in pancreatic lesions--a prospective study with 104 patients. J Nucl Med *45*, 1279-1286.

Lerner, E. C., Zhang, T. T., Knowles, D. B., Qian, Y., Hamilton, A. D., and Sebti, S. M. (1997). Inhibition of the prenylation of K-Ras, but not H- or N-Ras, is highly resistant to CAAX peptidomimetics and requires both a farnesyltransferase and a geranylgeranyltransferase I inhibitor in human tumor cell lines. Oncogene *15*, 1283-1288.

Li, H., and Durbin, R. (2009). Fast and accurate short read alignment with Burrows-Wheeler transform. Bioinformatics *25*, 1754-1760.

Liberzon, A., Subramanian, A., Pinchback, R., Thorvaldsdottir, H., Tamayo, P., and Mesirov, J. P. (2011). Molecular signatures database (MSigDB) 3.0. Bioinformatics *27*, 1739-1740.

Lim, K. H., and Counter, C. M. (2005). Reduction in the requirement of oncogenic Ras signaling to activation of PI3K/AKT pathway during tumor maintenance. Cancer Cell *8*, 381-392.

Lim, K. H., O'Hayer, K., Adam, S. J., Kendall, S. D., Campbell, P. M., Der, C. J., and Counter, C. M. (2006). Divergent roles for RalA and RalB in malignant growth of human pancreatic carcinoma cells. Curr Biol *16*, 2385-2394.

Liu, G., McDonnell, T. J., Montes de Oca Luna, R., Kapoor, M., Mims, B., El-Naggar, A. K., and Lozano, G. (2000). High metastatic potential in mice inheriting a targeted p53 missense mutation. Proc Natl Acad Sci U S A *97*, 4174-4179.

Liu, K., Cho, Y. Y., Yao, K., Nadas, J., Kim, D. J., Cho, E. J., Lee, M. H., Pugliese, A., Zhang, J., Bode, A. M.*, et al.* (2011a). Eriodictyol inhibits RSK2-ATF1 signaling and suppresses EGF-induced neoplastic cell transformation. J Biol Chem *286*, 2057-2066.

Liu, P., Cheng, H., Santiago, S., Raeder, M., Zhang, F., Isabella, A., Yang, J., Semaan, D. J., Chen, C., Fox, E. A.*, et al.* (2011b). Oncogenic PIK3CA-driven mammary tumors frequently recur via PI3K pathway-dependent and PI3K pathway-independent mechanisms. Nat Med *17*, 1116-1120.

Luo, J., Manning, B. D., and Cantley, L. C. (2003). Targeting the PI3K-Akt pathway in human cancer: rationale and promise. Cancer Cell *4*, 257-262.

Majumder, P. K., and Sellers, W. R. (2005). Akt-regulated pathways in prostate cancer. Oncogene *24*, 7465-7474.

Marais, R., Light, Y., Mason, C., Paterson, H., Olson, M. F., and Marshall, C. J. (1998). Requirement of Ras-GTP-Raf complexes for activation of Raf-1 by protein kinase C. Science *280*, 109-112.

Marais, R., Light, Y., Paterson, H. F., and Marshall, C. J. (1995). Ras recruits Raf-1 to the plasma membrane for activation by tyrosine phosphorylation. EMBO J *14*, 3136-3145.

McKenna, A., Hanna, M., Banks, E., Sivachenko, A., Cibulskis, K., Kernytsky, A., Garimella, K., Altshuler, D., Gabriel, S., Daly, M., and DePristo, M. A. (2010). The Genome Analysis Toolkit: a MapReduce framework for analyzing next-generation DNA sequencing data. Genome Res *20*, 1297-1303.

Miyamoto, S., Murphy, A. N., and Brown, J. H. (2008). Akt mediates mitochondrial protection in cardiomyocytes through phosphorylation of mitochondrial hexokinase-II. Cell Death Differ *15*, 521-529.

Moodie, S. A., Willumsen, B. M., Weber, M. J., and Wolfman, A. (1993). Complexes of Ras.GTP with Raf-1 and mitogen-activated protein kinase kinase. Science *260*, 1658-1661.

Morris, J. P. t., Wang, S. C., and Hebrok, M. (2010). KRAS, Hedgehog, Wnt and the twisted developmental biology of pancreatic ductal adenocarcinoma. Nat Rev Cancer *10*, 683-695.

Mukhopadhyay, A., Deplancke, B., Walhout, A. J., and Tissenbaum, H. A. (2008). Chromatin immunoprecipitation (ChIP) coupled to detection by quantitative real-time PCR to study transcription factor binding to DNA in Caenorhabditis elegans. Nat Protoc *3*, 698-709.

Mullis, K., Faloona, F., Scharf, S., Saiki, R., Horn, G., and Erlich, H. (1986). Specific enzymatic amplification of DNA in vitro: the polymerase chain reaction. Cold Spring Harb Symp Quant Biol *51 Pt 1*, 263-273.

Najafov, A., Sommer, E. M., Axten, J. M., Deyoung, M. P., and Alessi, D. R. (2011). Characterization of GSK2334470, a novel and highly specific inhibitor of PDK1. Biochem J *433*, 357-369.

Nakamura, K., Sakaue, H., Nishizawa, A., Matsuki, Y., Gomi, H., Watanabe, E., Hiramatsua, R., Tamamori-Adachi, M., Kitajima, S., Noda, T.*, et al.* (2008). PDK1 regulates cell proliferation and cell cycle progression through control of cyclin D1 and p27Kip1 expression. J Biol Chem *283*, 17702-17711.

Nakhai, H., Sel, S., Favor, J., Mendoza-Torres, L., Paulsen, F., Duncker, G. I., and Schmid, R. M. (2007). Ptf1a is essential for the differentiation of GABAergic and glycinergic amacrine cells and horizontal cells in the mouse retina. Development *134*, 1151-1160.

Nicolas, L., Martinez, C., Baro, C., Rodriguez, M., Baroja-Mazo, A., Sole, F., Flores, J. M., Ampurdanes, C., Dantzer, F., Martin-Caballero, J.*, et al.* (2010). Loss of poly(ADP-ribose) polymerase-2 leads to rapid development of spontaneous T-cell lymphomas in p53-deficient mice. Oncogene *29*, 2877-2883.

Offield, M. F., Jetton, T. L., Labosky, P. A., Ray, M., Stein, R. W., Magnuson, M. A., Hogan, B. L., and Wright, C. V. (1996). PDX-1 is required for pancreatic outgrowth and differentiation of the rostral duodenum. Development *122*, 983-995.

Okudela, K., Mitsui, H., Suzuki, T., Woo, T., Tateishi, Y., Umeda, S., Saito, Y., Tajiri, M., Masuda, M., and Ohashi, K. (2014). Expression of HDAC9 in lung cancer--potential role in lung carcinogenesis. Int J Clin Exp Pathol *7*, 213-220.

Olive, K. P., Tuveson, D. A., Ruhe, Z. C., Yin, B., Willis, N. A., Bronson, R. T., Crowley, D., and Jacks, T. (2004). Mutant p53 gain of function in two mouse models of Li-Fraumeni syndrome. Cell *119*, 847-860.

Omer, C. A., and Kohl, N. E. (1997). CA1A2X-competitive inhibitors of farnesyltransferase as anti-cancer agents. Trends Pharmacol Sci *18*, 437-444.

Ong, S. H., Hadari, Y. R., Gotoh, N., Guy, G. R., Schlessinger, J., and Lax, I. (2001). Stimulation of phosphatidylinositol 3-kinase by fibroblast growth factor receptors is mediated by coordinated recruitment of multiple docking proteins. Proc Natl Acad Sci U S A *98*, 6074-6079.

Osthus, R. C., Shim, H., Kim, S., Li, Q., Reddy, R., Mukherjee, M., Xu, Y., Wonsey, D., Lee, L. A., and Dang, C. V. (2000). Deregulation of glucose transporter 1 and glycolytic gene expression by c-Myc. J Biol Chem *275*, 21797-21800.

Owen, M. R., Doran, E., and Halestrap, A. P. (2000). Evidence that metformin exerts its anti-diabetic effects through inhibition of complex 1 of the mitochondrial respiratory chain. Biochem J *348 Pt 3*, 607-614.

Paron, I., Berchtold, S., Voros, J., Shamarla, M., Erkan, M., Hofler, H., and Esposito, I. (2011). Tenascin-C enhances pancreatic cancer cell growth and motility and affects cell adhesion through activation of the integrin pathway. PLoS One *6*, e21684.

Pawson, T. (2004). Specificity in signal transduction: from phosphotyrosine-SH2 domain interactions to complex cellular systems. Cell *116*, 191-203.

Petrie, K., Guidez, F., Howell, L., Healy, L., Waxman, S., Greaves, M., and Zelent, A. (2003). The histone deacetylase 9 gene encodes multiple protein isoforms. J Biol Chem *278*, 16059-16072.

Pettazzoni, P., Viale, A., Shah, P., Carugo, A., Ying, H., Wang, H., Genovese, G., Seth, S., Minelli, R., Green, T.*, et al.* (2015). Genetic events that limit the efficacy of MEK and RTK inhibitor therapies in a mouse model of KRAS-driven pancreatic cancer. Cancer Res *75*, 1091-1101.

Pfaffl, M. W. (2001). A new mathematical model for relative quantification in real-time RT-PCR. Nucleic Acids Res *29*, e45.

Pinho, A. V., Rooman, I., Reichert, M., De Medts, N., Bouwens, L., Rustgi, A. K., and Real, F. X. (2011). Adult pancreatic acinar cells dedifferentiate to an embryonic progenitor phenotype with concomitant activation of a senescence programme that is present in chronic pancreatitis. Gut *60*, 958-966.

Rad, R., Rad, L., Wang, W., Strong, A., Ponstingl, H., Bronner, I. F., Mayho, M., Steiger, K., Weber, J., Hieber, M.*, et al.* (2015). A conditional piggyBac transposition system for genetic screening in mice identifies oncogenic networks in pancreatic cancer. Nat Genet *47*, 47-56.

Rahib, L., Smith, B. D., Aizenberg, R., Rosenzweig, A. B., Fleshman, J. M., and Matrisian, L. M. (2014). Projecting cancer incidence and deaths to 2030: the unexpected burden of thyroid, liver, and pancreas cancers in the United States. Cancer Res *74*, 2913-2921.

Rebours, V., Boutron-Ruault, M. C., Schnee, M., Ferec, C., Maire, F., Hammel, P., Ruszniewski, P., and Levy, P. (2008). Risk of pancreatic adenocarcinoma in patients with hereditary pancreatitis: a national exhaustive series. Am J Gastroenterol *103*, 111-119.

Robasky, K., Lewis, N. E., and Church, G. M. (2014). The role of replicates for error mitigation in next-generation sequencing. Nat Rev Genet *15*, 56-62.

Robert, C., and Rassool, F. V. (2012). HDAC inhibitors: roles of DNA damage and repair. Adv Cancer Res *116*, 87-129.

Robey, R. B., and Hay, N. (2009). Is Akt the "Warburg kinase"?-Akt-energy metabolism interactions and oncogenesis. Semin Cancer Biol *19*, 25-31.

Rohren, E. M., Turkington, T. G., and Coleman, R. E. (2004). Clinical applications of PET in oncology. Radiology *231*, 305-332.

Ruf, J., Lopez Hanninen, E., Oettle, H., Plotkin, M., Pelzer, U., Stroszczynski, C., Felix, R., and Amthauer, H. (2005). Detection of recurrent pancreatic cancer: comparison of FDG-PET with CT/MRI. Pancreatology *5*, 266-272.

Sabatini, D. M. (2006). mTOR and cancer: insights into a complex relationship. Nat Rev Cancer *6*, 729-734.

Samuels, Y., Wang, Z., Bardelli, A., Silliman, N., Ptak, J., Szabo, S., Yan, H., Gazdar, A., Powell, S. M., Riggins, G. J*., et al.* (2004). High frequency of mutations of the PIK3CA gene in human cancers. Science *304*, 554.

Sancho, P., Burgos-Ramos, E., Tavera, A., Bou Kheir, T., Jagust, P., Schoenhals, M., Barneda, D., Sellers, K., Campos-Olivas, R., Grana, O*., et al.* (2015). MYC/PGC-1alpha Balance Determines the Metabolic Phenotype and Plasticity of Pancreatic Cancer Stem Cells. Cell Metab *22*, 590-605.

Sarbassov, D. D., Guertin, D. A., Ali, S. M., and Sabatini, D. M. (2005). Phosphorylation and regulation of Akt/PKB by the rictor-mTOR complex. Science *307*, 1098-1101.

Sassone-Corsi, P., Mizzen, C. A., Cheung, P., Crosio, C., Monaco, L., Jacquot, S., Hanauer, A., and Allis, C. D. (1999). Requirement of Rsk-2 for epidermal growth factor-activated phosphorylation of histone H3. Science *285*, 886-891.

Scheffzek, K., Ahmadian, M. R., Kabsch, W., Wiesmuller, L., Lautwein, A., Schmitz, F., and Wittinghofer, A. (1997). The Ras-RasGAP complex: structural basis for GTPase activation and its loss in oncogenic Ras mutants. Science *277*, 333-338.

Scheidig, A. J., Burmester, C., and Goody, R. S. (1999). The pre-hydrolysis state of p21(ras) in complex with GTP: new insights into the role of water molecules in the GTP hydrolysis reaction of ras-like proteins. Structure *7*, 1311-1324.

Schleger, C., Verbeke, C., Hildenbrand, R., Zentgraf, H., and Bleyl, U. (2002). c-MYC activation in primary and metastatic ductal adenocarcinoma of the pancreas: incidence, mechanisms, and clinical significance. Mod Pathol *15*, 462-469.

Schlessinger, J. (2002). Ligand-induced, receptor-mediated dimerization and activation of EGF receptor. Cell *110*, 669-672.

Schönhuber, N., Seidler, B., Schuck, K., Veltkamp, C., Schachtler, C., Zukowska, M., Eser, S., Feyerabend, T. B., Paul, M. C., Eser, P*., et al.* (2014). A next-generation dual-recombinase system for time- and host-specific targeting of pancreatic cancer. Nat Med.

Scialpi, M., Cagini, L., Pierotti, L., De Santis, F., Pusiol, T., Piscioli, I., Magli, M., D'Andrea, A., Brunese, L., and Rotondo, A. (2014). Detection of small (</= 2 cm) pancreatic adenocarcinoma and surrounding parenchyma: correlations between enhancement patterns at triphasic MDCT and histologic features. BMC Gastroenterol *14*, 16.

Scortegagna, M., Ruller, C., Feng, Y., Lazova, R., Kluger, H., Li, J. L., De, S. K., Rickert, R., Pellecchia, M., Bosenberg, M., and Ronai, Z. A. (2014). Genetic inactivation or pharmacological inhibition of Pdk1 delays development and inhibits metastasis of Braf(V600E)::Pten(-/-) melanoma. Oncogene *33*, 4330-4339.

Sendler, A., Avril, N., Helmberger, H., Stollfuss, J., Weber, W., Bengel, F., Schwaiger, M., Roder, J. D., and Siewert, J. R. (2000). Preoperative evaluation of pancreatic masses with positron emission tomography using 18F-fluorodeoxyglucose: diagnostic limitations. World J Surg *24*, 1121-1129.

Sharma, S. V., Lee, D. Y., Li, B., Quinlan, M. P., Takahashi, F., Maheswaran, S., McDermott, U., Azizian, N., Zou, L., Fischbach, M. A*., et al.* (2010). A chromatin-mediated reversible drug-tolerant state in cancer cell subpopulations. Cell *141*, 69-80.

Shi, C., Hong, S. M., Lim, P., Kamiyama, H., Khan, M., Anders, R. A., Goggins, M., Hruban, R. H., and Eshleman, J. R. (2009). KRAS2 mutations in human pancreatic acinar-ductal metaplastic lesions are limited to those with PanIN: implications for the human pancreatic cancer cell of origin. Mol Cancer Res *7*, 230-236.

Shim, H., Dolde, C., Lewis, B. C., Wu, C. S., Dang, G., Jungmann, R. A., Dalla-Favera, R., and Dang, C. V. (1997). c-Myc transactivation of LDH-A: implications for tumor metabolism and growth. Proc Natl Acad Sci U S A *94*, 6658-6663.

Siegel, R., Ma, J., Zou, Z., and Jemal, A. (2014). Cancer statistics, 2014. CA Cancer J Clin *64*, 9-29.

Skarnes, W. C., Rosen, B., West, A. P., Koutsourakis, M., Bushell, W., Iyer, V., Mujica, A. O., Thomas, M., Harrow, J., Cox, T.*, et al.* (2011). A conditional knockout resource for the genome-wide study of mouse gene function. Nature *474*, 337-342.

Smith, J. A., Poteet-Smith, C. E., Malarkey, K., and Sturgill, T. W. (1999). Identification of an extracellular signal-regulated kinase (ERK) docking site in ribosomal S6 kinase, a sequence critical for activation by ERK in vivo. J Biol Chem *274*, 2893-2898.

Son, J., Lyssiotis, C. A., Ying, H., Wang, X., Hua, S., Ligorio, M., Perera, R. M., Ferrone, C. R., Mullarky, E., Shyh-Chang, N.*, et al.* (2013). Glutamine supports pancreatic cancer growth through a KRAS-regulated metabolic pathway. Nature *496*, 101-105.

Sperti, C., Pasquali, C., Bissoli, S., Chierichetti, F., Liessi, G., and Pedrazzoli, S. (2010). Tumor relapse after pancreatic cancer resection is detected earlier by 18-FDG PET than by CT. J Gastrointest Surg *14*, 131-140.

Srinivasan, L., Sasaki, Y., Calado, D. P., Zhang, B., Paik, J. H., DePinho, R. A., Kutok, J. L., Kearney, J. F., Otipoby, K. L., and Rajewsky, K. (2009). PI3 kinase signals BCR-dependent mature B cell survival. Cell *139*, 573-586.

Stephens, L., Anderson, K., Stokoe, D., Erdjument-Bromage, H., Painter, G. F., Holmes, A. B., Gaffney, P. R., Reese, C. B., McCormick, F., Tempst, P.*, et al.* (1998). Protein kinase B kinases that mediate phosphatidylinositol 3,4,5-trisphosphate-dependent activation of protein kinase B. Science *279*, 710-714.

Tan, J., Li, Z., Lee, P. L., Guan, P., Aau, M. Y., Lee, S. T., Feng, M., Lim, C. Z., Lee, E. Y., Wee, Z. N.*, et al.* (2013). PDK1 signaling toward PLK1-MYC activation confers oncogenic transformation, tumor-initiating cell activation, and resistance to mTOR-targeted therapy. Cancer Discov *3*, 1156-1171.

Thomas, R. K., Baker, A. C., Debiasi, R. M., Winckler, W., Laframboise, T., Lin, W. M., Wang, M., Feng, W., Zander, T., MacConaill, L.*, et al.* (2007). High-throughput oncogene mutation profiling in human cancer. Nat Genet *39*, 347-351.

Tomimaru, Y., Takeda, Y., Tatsumi, M., Kim, T., Kobayashi, S., Marubashi, S., Eguchi, H., Tanemura, M., Kitagawa, T., Nagano, H.*, et al.* (2010). Utility of 2-[18F] fluoro-2-deoxy-D-glucose positron emission tomography in differential diagnosis of benign and malignant intraductal papillary-mucinous neoplasm of the pancreas. Oncol Rep *24*, 613-620.

Tong, W. M., Hande, M. P., Lansdorp, P. M., and Wang, Z. Q. (2001). DNA strand break-sensing molecule poly(ADP-Ribose) polymerase cooperates with p53 in telomere function, chromosome stability, and tumor suppression. Mol Cell Biol *21*, 4046-4054.

Towbin, H., Staehelin, T., and Gordon, J. (1979). Electrophoretic transfer of proteins from polyacrylamide gels to nitrocellulose sheets: procedure and some applications. Proc Natl Acad Sci U S A *76*, 4350-4354.

Trahey, M., and McCormick, F. (1987). A cytoplasmic protein stimulates normal N-ras p21 GTPase, but does not affect oncogenic mutants. Science *238*, 542-545.

Trapnell, C., Pachter, L., and Salzberg, S. L. (2009). TopHat: discovering splice junctions with RNA-Seq. Bioinformatics *25*, 1105-1111.

Trucco, C., Oliver, F. J., de Murcia, G., and Menissier-de Murcia, J. (1998). DNA repair defect in poly(ADP-ribose) polymerase-deficient cell lines. Nucleic Acids Res *26*, 2644-2649.

Van Cutsem, E., van de Velde, H., Karasek, P., Oettle, H., Vervenne, W. L., Szawlowski, A., Schoffski, P., Post, S., Verslype, C., Neumann, H*., et al.* (2004). Phase III trial of gemcitabine plus tipifarnib compared with gemcitabine plus placebo in advanced pancreatic cancer. J Clin Oncol *22*, 1430-1438.

Vander Heiden, M. G., Cantley, L. C., and Thompson, C. B. (2009). Understanding the Warburg effect: the metabolic requirements of cell proliferation. Science *324*, 1029-1033.

Vargas, R., Nino-Murcia, M., Trueblood, W., and Jeffrey, R. B., Jr. (2004). MDCT in Pancreatic adenocarcinoma: prediction of vascular invasion and resectability using a multiphasic technique with curved planar reformations. AJR Am J Roentgenol *182*, 419-425.

Vasen, H. F., Gruis, N. A., Frants, R. R., van Der Velden, P. A., Hille, E. T., and Bergman, W. (2000). Risk of developing pancreatic cancer in families with familial atypical multiple mole melanoma associated with a specific 19 deletion of p16 (p16-Leiden). Int J Cancer *87*, 809-811.

Vena, F., Li Causi, E., Rodriguez-Justo, M., Goodstal, S., Hagemann, T., Hartley, J. A., and Hochhauser, D. (2015). The MEK1/2 Inhibitor Pimasertib Enhances Gemcitabine Efficacy in Pancreatic Cancer Models by Altering Ribonucleotide Reductase Subunit-1 (RRM1). Clin Cancer Res *21*, 5563-5577.

Vojtek, A. B., Hollenberg, S. M., and Cooper, J. A. (1993). Mammalian Ras interacts directly with the serine/threonine kinase Raf. Cell *74*, 205-214.

Von Hoff, D. D., Ervin, T., Arena, F. P., Chiorean, E. G., Infante, J., Moore, M., Seay, T., Tjulandin, S. A., Ma, W. W., Saleh, M. N*., et al.* (2013). Increased survival in pancreatic cancer with nab-paclitaxel plus gemcitabine. N Engl J Med *369*, 1691-1703.

von Schulthess, G. K., Steinert, H. C., and Hany, T. F. (2006). Integrated PET/CT: current applications and future directions. Radiology *238*, 405-422.

Waddell, N., Pajic, M., Patch, A. M., Chang, D. K., Kassahn, K. S., Bailey, P., Johns, A. L., Miller, D., Nones, K., Quek, K*., et al.* (2015). Whole genomes redefine the mutational landscape of pancreatic cancer. Nature *518*, 495-501.

Walters, D. M., Lindberg, J. M., Adair, S. J., Newhook, T. E., Cowan, C. R., Stokes, J. B., Borgman, C. A., Stelow, E. B., Lowrey, B. T., Chopivsky, M. E*., et al.* (2013). Inhibition of the growth of patient-derived pancreatic cancer xenografts with the MEK inhibitor trametinib is augmented by combined treatment with the epidermal growth factor receptor/HER2 inhibitor lapatinib. Neoplasia *15*, 143-155.

Wang, X., Cunningham, M., Zhang, X., Tokarz, S., Laraway, B., Troxell, M., and Sears, R. C. (2011). Phosphorylation regulates c-Myc's oncogenic activity in the mammary gland. Cancer Res *71*, 925-936.

Warburg, O. (1956). On the origin of cancer cells. Science *123*, 309-314.

Warne, P. H., Viciana, P. R., and Downward, J. (1993). Direct interaction of Ras and the amino-terminal region of Raf-1 in vitro. Nature *364*, 352-355.

Watanabe, Y., Ueda, H., Etoh, T., Koike, E., Fujinami, N., Mitsuhashi, A., and Hoshiai, H. (2007). A change in promoter methylation of hMLH1 is a cause of acquired resistance to platinum-based chemotherapy in epithelial ovarian cancer. Anticancer Res *27*, 1449-1452.

Wieman, H. L., Wofford, J. A., and Rathmell, J. C. (2007). Cytokine stimulation promotes glucose uptake via phosphatidylinositol-3 kinase/Akt regulation of Glut1 activity and trafficking. Mol Biol Cell *18*, 1437-1446.

Witkiewicz, A. K., McMillan, E. A., Balaji, U., Baek, G., Lin, W. C., Mansour, J., Mollaee, M., Wagner, K. U., Koduru, P., Yopp, A.*, et al.* (2015). Whole-exome sequencing of pancreatic cancer defines genetic diversity and therapeutic targets. Nat Commun *6*, 6744.

Wittinghofer, A., and Pai, E. F. (1991). The structure of Ras protein: a model for a universal molecular switch. Trends Biochem Sci *16*, 382-387.

Wolfman, A., and Macara, I. G. (1990). A cytosolic protein catalyzes the release of GDP from p21ras. Science *248*, 67-69.

Wullschleger, S., Loewith, R., and Hall, M. N. (2006). TOR signaling in growth and metabolism. Cell *124*, 471-484.

Xing, J., Ginty, D. D., and Greenberg, M. E. (1996). Coupling of the RAS-MAPK pathway to gene activation by RSK2, a growth factor-regulated CREB kinase. Science *273*, 959-963.

Yang, S., Wang, X., Contino, G., Liesa, M., Sahin, E., Ying, H., Bause, A., Li, Y., Stommel, J. M., Dell'antonio, G.*, et al.* (2011). Pancreatic cancers require autophagy for tumor growth. Genes Dev *25*, 717-729.

Yang, X., Matsuda, K., Bialek, P., Jacquot, S., Masuoka, H. C., Schinke, T., Li, L., Brancorsini, S., Sassone-Corsi, P., Townes, T. M.*, et al.* (2004). ATF4 is a substrate of RSK2 and an essential regulator of osteoblast biology; implication for Coffin-Lowry Syndrome. Cell *117*, 387-398.

Ying, H., Elpek, K. G., Vinjamoori, A., Zimmerman, S. M., Chu, G. C., Yan, H., Fletcher-Sananikone, E., Zhang, H., Liu, Y., Wang, W.*, et al.* (2011). PTEN is a major tumor suppressor in pancreatic ductal adenocarcinoma and regulates an NF-kappaB-cytokine network. Cancer Discov *1*, 158-169.

Ying, H., Kimmelman, A. C., Lyssiotis, C. A., Hua, S., Chu, G. C., Fletcher-Sananikone, E., Locasale, J. W., Son, J., Zhang, H., Coloff, J. L.*, et al.* (2012). Oncogenic Kras maintains pancreatic tumors through regulation of anabolic glucose metabolism. Cell *149*, 656-670.

Zamboni, G. A., Kruskal, J. B., Vollmer, C. M., Baptista, J., Callery, M. P., and Raptopoulos, V. D. (2007). Pancreatic adenocarcinoma: value of multidetector CT angiography in preoperative evaluation. Radiology *245*, 770-778.

Zenker, M., Mayerle, J., Lerch, M. M., Tagariello, A., Zerres, K., Durie, P. R., Beier, M., Hulskamp, G., Guzman, C., Rehder, H.*, et al.* (2005). Deficiency of UBR1, a ubiquitin ligase of the N-end rule pathway, causes pancreatic dysfunction, malformations and mental retardation (Johanson-Blizzard syndrome). Nat Genet *37*, 1345-1350.

Zhang, X. F., Settleman, J., Kyriakis, J. M., Takeuchi-Suzuki, E., Elledge, S. J., Marshall, M. S., Bruder, J. T., Rapp, U. R., and Avruch, J. (1993). Normal and oncogenic p21ras proteins bind to the amino-terminal regulatory domain of c-Raf-1. Nature *364*, 308-313.

Zimmermann, G., Papke, B., Ismail, S., Vartak, N., Chandra, A., Hoffmann, M., Hahn, S. A., Triola, G., Wittinghofer, A., Bastiaens, P. I., and Waldmann, H. (2013). Small molecule inhibition of the KRAS-PDEdelta interaction impairs oncogenic KRAS signalling. Nature *497*, 638-642.

Zunder, E. R., Knight, Z. A., Houseman, B. T., Apsel, B., and Shokat, K. M. (2008). Discovery of drug-resistant and drug-sensitizing mutations in the oncogenic PI3K isoform p110 alpha. Cancer Cell *14*, 180-192.

Publications resulting from my PhD work

Maresch R, Mueller S, **Veltkamp C**, Öllinger R, Friedrich M, Heid I, Steiger K, Weber J, Engleitner T, Barenboim M, Klein S, Louzada S, Banerjee R, Strong A, Stauber T, Gross N, Geumann U, Lange S, Ringelhan M, Varela I, Unger K, Yang F, Schmid RM, Vassiliou GS, Braren R, Schneider G, Heikenwalder M, Bradley A, Saur D, Rad R. Multiplexed pancreatic genome engineering and cancer induction by transfection-based CRISPR/Cas9 delivery in mice. Nat Commun. 2016 Feb 26;7:10770.

Rad R, Rad L, Wang W, Strong A, Ponstingl H, Bronner IF, Mayho M, Steiger K, Weber J, Hieber M, **Veltkamp C**, Eser S, Geumann U, Öllinger R, Zukowska M, Barenboim M, Maresch R, Cadiñanos J, Friedrich M, Varela I, Constantino-Casas F, Sarver A, Ten Hoeve J, Prosser H, Seidler B, Bauer J, Heikenwälder M, Metzakopian E, Krug A, Ehmer U, Schneider G, Knösel T, Rümmele P, Aust D, Grützmann R, Pilarsky C, Ning Z, Wessels L, Schmid RM, Quail MA, Vassiliou G, Esposito I, Liu P, Saur D, Bradley A. A conditional piggyBac transposition system for genetic screening in mice identifies oncogenic networks in pancreatic cancer. *Nat Genet.* 2015 Jan;47(1):47-56.

Schönhuber N*, Seidler B*, Schuck K*, **Veltkamp C***, Schachtler C, Zukowska M, Eser S, Feyerabend TB, Paul MC, Eser P, Klein S, Lowy AM, Banerjee R, Yang F, Lee CL, Moding EJ, Kirsch DG, Scheideler A, Alessi DR, Varela I, Bradley A, Kind A, Schnieke AE, Rodewald HR, Rad R, Schmid RM, Schneider G, Saur D. A next-generation dual-recombinase system for time- and host-specific targeting of pancreatic cancer. *Nat Med*. 2014 Nov;20(11):1340-7. (* equal contribution)